2004

Marine geology and potential rockfish habitat in the southwestern San Juan Islands, Washington

Janet E. Tilden
California State University, Monterey Bay

Marine Geology and Potential Rockfish Habitat in the Southwestern San Juan Islands, Washington

A Thesis
Presented to the Faculty of
Cal. State University Monterey Bay
through
Moss Landing Marine Laboratories

In partial fulfillment
of the requirements for the degree
Master of Science in Marine Science

Janet E. Tilden
December 2004

APPROVED FOR MOSS LANDING MARINE LABORATORIES

Dr. H. Gary Greene, Moss Landing Marine Laboratories

Dr. Ivano Aiello, Moss Landing Marine Laboratories

Wayne A. Palsson, Washington Department of Fish & Wildlife

Dr. Gregor M. Cailliet, Moss Landing Marine Laboratories

APPROVED FOR THE UNIVERSITY

TABLE OF CONTENTS

LIST OF FIGURES

LIST OF TABLES

ABSTRACT

The San Juan Islands (SJI) region, located in Washington's seismically active northern Puget Sound, have a complicated and not yet fully understood geologic history. Due in part to the region's geology, the underwater landscape is morphologically complex and this complexity equates to habitat for a number of declining bottomfish species including rockfishes (genus *Sebastes*, family Scorpaenidae). In this study, multibeam bathymetry, multibeam backscatter, and underwater video data were collected and combined with existing geological, geophysical, and biological information to map the marine geology and identify and map potential adult rockfish habitat, specifically for copper (*Sebastes caurinus*) and quillback rockfishes (*Sebastes maliger*) in the southwestern San Juan Islands.

This study is among the first marine geologic mapping efforts within the San Juan Islands, filling an important gap in an otherwise well-studied region. Existing geologic and geophysical data were combined with interpretations of new multibeam bathymetry and backscatter seafloor imagery to construct a seamless onshore-offshore geologic map of the southwestern San Juan Islands. Simrad EM1002 (95 kHz) and Reson 8101 (240 kHz) multibeam bathymetry and backscatter data were collected between October 2000 and November 2003 within Haro Strait, northeastern Strait of Juan de Fuca, and San Juan Channel. Sun-shaded images of the processed data reveal a complex network of faulted and fractured bedrock exposures, deep glaciated channels, Pleistocene glacial sediments, and dynamic bedforms. Distinct slump morphologies in multibeam and backscatter imagery suggest active slumping of Holocene sediments at the mouth of San Juan Channel. A number of previously inferred geologic structures were extended offshore and constrained based on distinct linear bedrock features visible in the multibeam imagery.

Aeromagnetic data collected by the U.S. Geological Survey in 1997 were processed to accentuate short-wavelength, presumably shallow, magnetic sources. The resultant derivative aeromagnetic map reveals a number of areas with distinct anomaly patterns highlighting apparent structures and defining terrane boundaries. Gradients in magnetic anomalies often correspond with fault traces identified in high-resolution multibeam imagery and may reflect slight magnetic susceptibility contrasts across fault contacts. Aeromagnetic data also constrain two tectonostratigraphic terrane boundaries in the study site not identified in multibeam imagery: 1) the Buck Bay fault, which separates the Lopez Structural Complex and Decatur terrane from the underlying Constitution Formation, and 2) the Haro fault separating the Deadman Bay terrane of the San Juan Thrust system from the Wrangellia terrane on Vancouver Island.

First, marine benthic habitats were characterized within Reson 8101 survey areas according to the methods of Greene et al. (1999). Fifteen habitats were identified among the 28 km^2 surveyed. Eight of the fifteen habitats were considered potential rockfish habitats. In an attempt to identify habitat more quantitatively, seafloor complexity was characterized through spatial analysis of gridded multibeam data. Three categories of complexity; low, intermediate, and high, were distinguished based on morphologic characteristics visible in multibeam imagery. Observations of adult copper and quillback rockfishes in video from thirteen ROV dives were compared with seafloor complexity available along the dive routes. A Habitat Utilization Analysis was conducted to assess habitat use (seafloor complexity = habitat) based on available habitat. Results suggest adult copper and quillback rockfishes use high complexity habitat and to a lesser degree intermediate complexity habitat. Because high seafloor complexity alone did not

appear to adequately represent potential adult rockfish habitat, seafloor complexity data were combined with marine benthic habitat information to map the distribution of potential adult rockfish habitats. The seafloor complexity map and benthic habitat maps presented in this study together will provide important baseline information for rockfish conservation and regional planning for marine protected areas (MPAs).

1. INTRODUCTION

The San Juan Islands (SJI), located in northern Puget Sound (Figure 1.1), are a popular tourist destination in northwestern Washington State largely because of their unique natural beauty. The rugged rocky shorelines, occasional sandy pocket beaches, prevalent marine bedrock outcrops, and deep marine channels exist as a result of the islands' complex tectonic and glacial history. Prior to this study no marine geologic map existed for the San Juan Islands. The complicated onland geology of the islands has been thoroughly investigated since the first reconnaissance mapping by McClellan (1927). Geologic structures, including faults and folds, have been mapped onland, but remain inferred at best in the marine environment. With over 35% of the land in the SJI underwater (Russell, 1975), a good portion of the regions' geology remains unknown and unmapped.

The types and distribution of marine benthic habitats, which support a diverse assemblage of marine fishes and invertebrates, are largely defined by the marine geology in the southwestern SJI. The lithologies of seafloor substrates and the degree to which those substrates are eroded and deformed affect the complexity, or roughness, of the seafloor surface. For the purposes of this study, seafloor complexity describes an area of seafloor as represented by gridded multibeam bathymetric data. Complexity is defined by the ratio of surface area to planar area of a given neighborhood of cells in the bathymetry grid. Seafloor complexity creates refugia for marine species, including many rockfishes. The link between seafloor geology and marine benthic habitat is well illustrated in the seafloor classification of Greene et al. (1999). Pre-Tertiary bedrock is exposed over large areas of the seafloor among the SJI as a result of regional uplift associated with Mid-Cretaceous thrusting, glacial scouring that occurred throughout the Pleistocene, and strong tidal flushing that occurs today, potentially providing valuable information on bedrock geology, neotectonics, and benthic habitat distribution.

1.1. OBJECTIVES

The goal of this study is to characterize and map the seafloor in the southwestern SJI for the purpose of describing the marine geology and potential adult rockfish habitats in the region by 1) creating a seamless (onshore/offshore) geologic map, linking onshore geology with surficial, bedrock, and structural marine geology, 2) providing evidence that constrains the

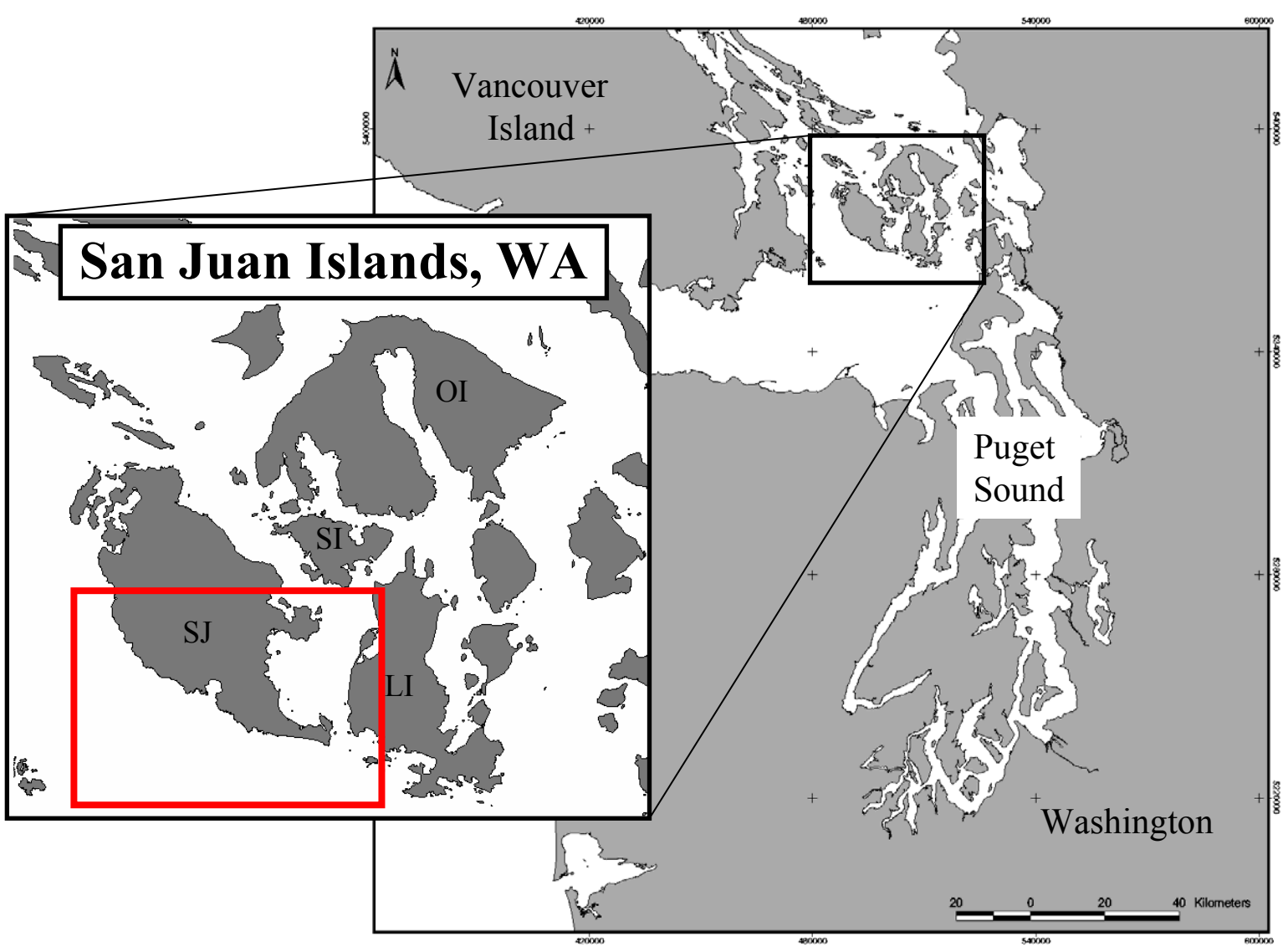

Figure 1.1. Map showing the location of the San Juan Islands in northern Puget Sound just east of Vancouver Island, British Columbia, Canada. The study site is outlined in red. OI = Orcas Island, LI = Lopez Island, SI = Shaw Island, and SJ = San Juan Island.

surface expression of two tectonostratigraphic[1] terrane boundaries located offshore, 3) mapping marine benthic habitats, 4) devising a quantitative method for characterizing seafloor complexity aimed at identifying potential adult rockfish habitat, 5) describing the relationship between seafloor complexity and the occurrence of adult rockfishes, and 6) predicting potential adult rockfish habitat within the study site. To complete the objectives listed above; existing geological, geophysical, and fisheries information were synthesized and integrated with analyses of new high-resolution multibeam bathymetry, multibeam backscatter, and underwater video data collected between October 2000 and November 2002 (Plate 1, Inset C). All data were geo-referenced and imported into ArcView® 3.2.a and ArcView® 3.3 for visualization and analysis within a GIS framework.

1.2. GEOHAZARDS AND TERRANE BOUNDARIES

Considering the potential for large magnitude earthquakes and devastating tsunamis in the heavily populated Puget Sound region (Atwater, 1992; Mathewes and Clague, 1994; Johnson, 1999, 2001; Blais-Stevens and Clague, 2001), any information pertaining to the surficial and/or structural geology in the region could be of great value for seismic hazard assessment. The discovery of Quaternary activity along the >125 kilometer long Devils Mountain fault (DMF) and associated structures (Figure 1.2; Johnson et al., 2001), located just south of the SJI, highlighted a need for high-resolution bathymetric imagery to help identify and characterize fault morphology on the seafloor. Seismic activity along the DMF could potentially reactivate other fault systems in the area. Detailed mapping of the fault systems surrounding the DMF, including the San Juan thrust system, is thus critical for regional earthquake hazard assessment.

The southwestern San Juan Islands include San Juan and Lopez Islands. San Juan and Lopez Islands are part of the larger San Juan thrust system (Figure 1.3), which is a folded system of thrust faults composed of mainly Paleozoic and Mesozoic volcanic arc rocks, clastic accretionary units, and metamorphic oceanic rocks that make up a series of terranes. The folds are likely Tertiary in age and plunge gently to the southeast with limbs that dip steeply between

[1]A tectonostratigraphic terrane, according to Jones et al. (1983), is a fault-bounded block composed of one or more related rock units that have a distinct geologic history indicating that the block is far traveled with respect to adjacent terranes. From this point forward, the word “terrane” referes to a tectonostratigraphic terrane unless otherwise noted.

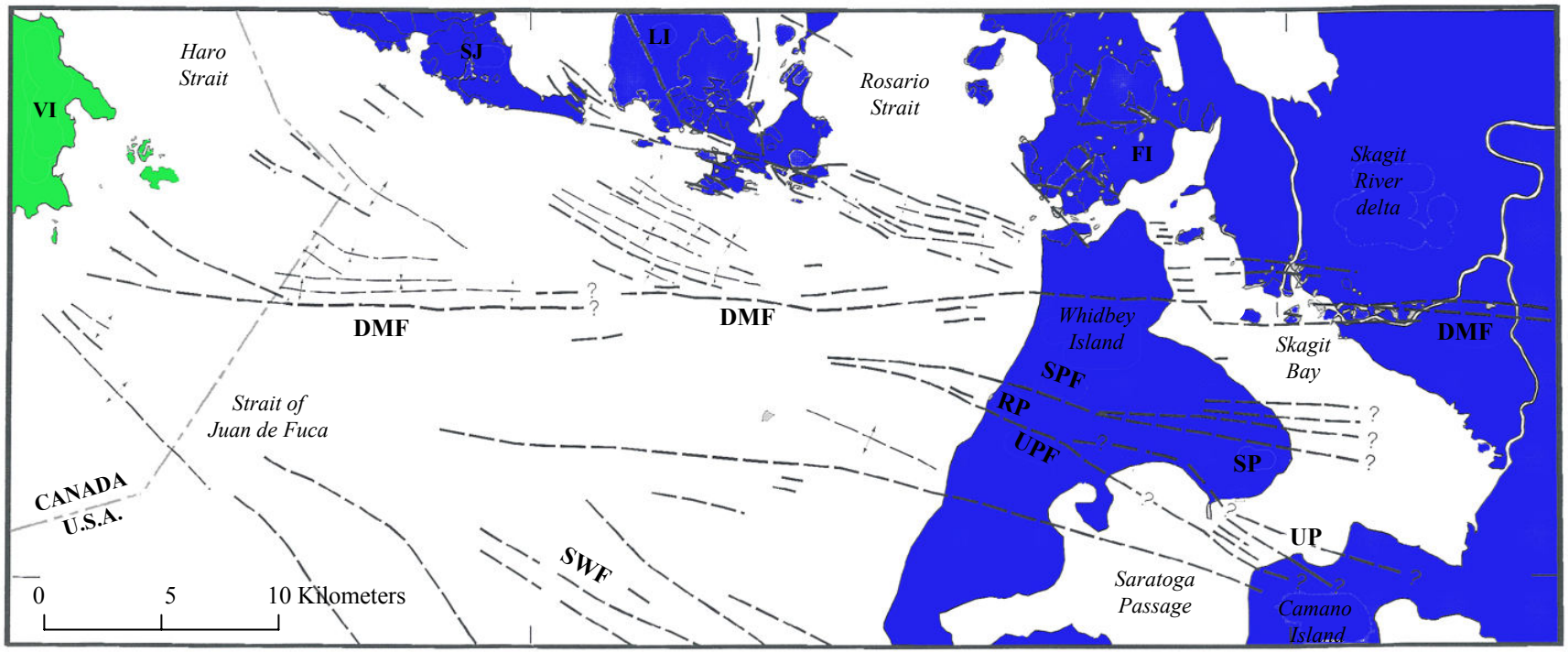

Figure 1.2. Regional map of the Devils Moutain Fault Zone in the northern Puget Lowland. DMF = Devils Mountain fault main trace, SPF = Strawberry Point Fault, SWF = southern Widbey Island Fault, UPF = Utsalady Point Fault, FI = Fidalgo Island, LI = Lopez Island, RP = Rocky Point, SJ = San Juan Island, SP = Strawberry Point, UP = Utsalady Point, and VI = Vancouver Island, Blue = U.S., and Green = Canada, (modified after Johnson et al., 2001).

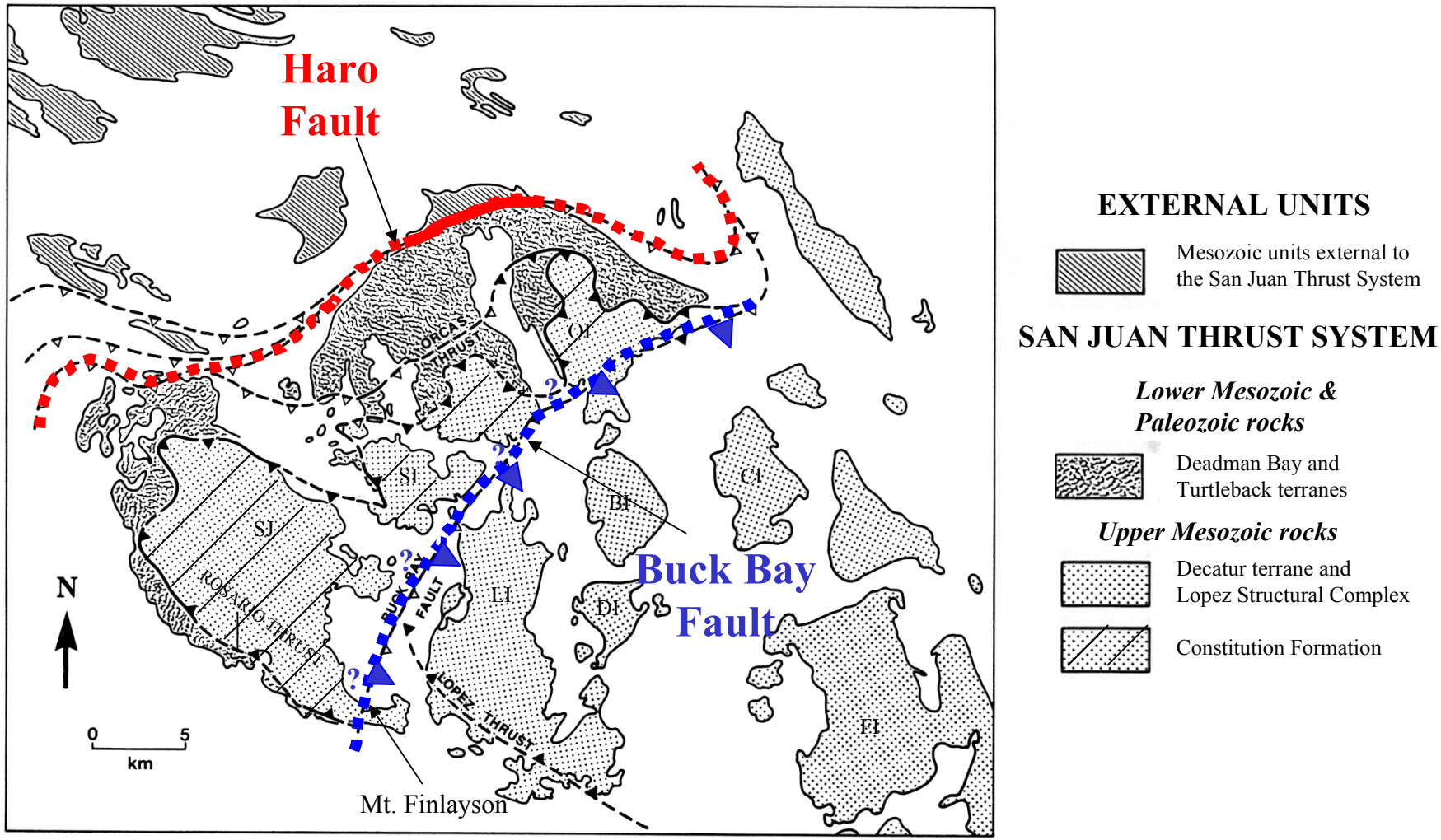

Figure 1.3. Regional Geology of the San Juan Islands, with the Haro fault (red) marking the boundary between the San Juan Thrust system and the external units of the Wrangellia terrane. The Buck Bay fault (blue) marks the boundary between the Decatur terrane and the underlying Constitution Formation (Modified after Bergh, 2002). BI = Blakely Is., CI = Cypress Is., DI = Decatur Is., FI = FIdalgo Is., LI = Lopez Is., OI = Orcas Is., SI = Shaw Is., and SJ = San Juan Is.

45º and 60º (Brandon et al., 1988). The Haro fault marks the northwestern boundary of the San Juan thrust system. Rocks north of the Haro Fault are un-metamorphosed, well-stratified Mesozoic units belonging to the Late Triassic Haro Formation, the Late Jurassic Spieden Group, and the Upper Cretaceous Nanaimo Group. Rocks south of the Haro Fault are part of a series of metamorphosed, highly deformed, and imbricated units ranging in age from Lower Paleozoic to Early Cretaceous. The geologic nomenclature for the San Juan thrust system adopted for this study is that of Brandon et al. (1988). According to Brandon et al. (1988), the San Juan thrust system is composed of four terranes, one clastic-linking[2] sequence, and a Late Cretaceous imbricate fault zone (Figure 1.4). Listed structurally from bottom to top, the San Juan thrust system includes the Turtleback terrane, Garrison terrane, Deadman Bay terrane, Constitution Formation, Lopez Structural Complex, and the Decatur terrane (Figure 1.5).

The locations and geometries of two terrane boundaries within the SJI remain unclear. One marks the boundary between the Deadman Bay terrane and the Wrangellia terrane offshore western San Juan Island. This boundary is recognized as the Haro Fault to the north and east crossing Orcas Island. The identification of the Haro fault in Haro Strait is important in understanding the collisional history of Wrangellia with respect to the San Juan thrust system and the North Cascades. For instance, Danner (1977) argued that there are distinct differences between the marine faunal assemblages of the East Sound Group within the Turtleback terrane on Orcas Island and the Sicker Group of Vancouver Island, supporting the idea that Wrangellia does not extend into the San Juan Islands.

[2] Brandon et al. (1988) uses the term clastic-linking sequence to refer to a clastic unit(s) that contains clasts derived from a lithologically diverse source region. Provenance studies can then link that clastic unit to a specifc source region(s).

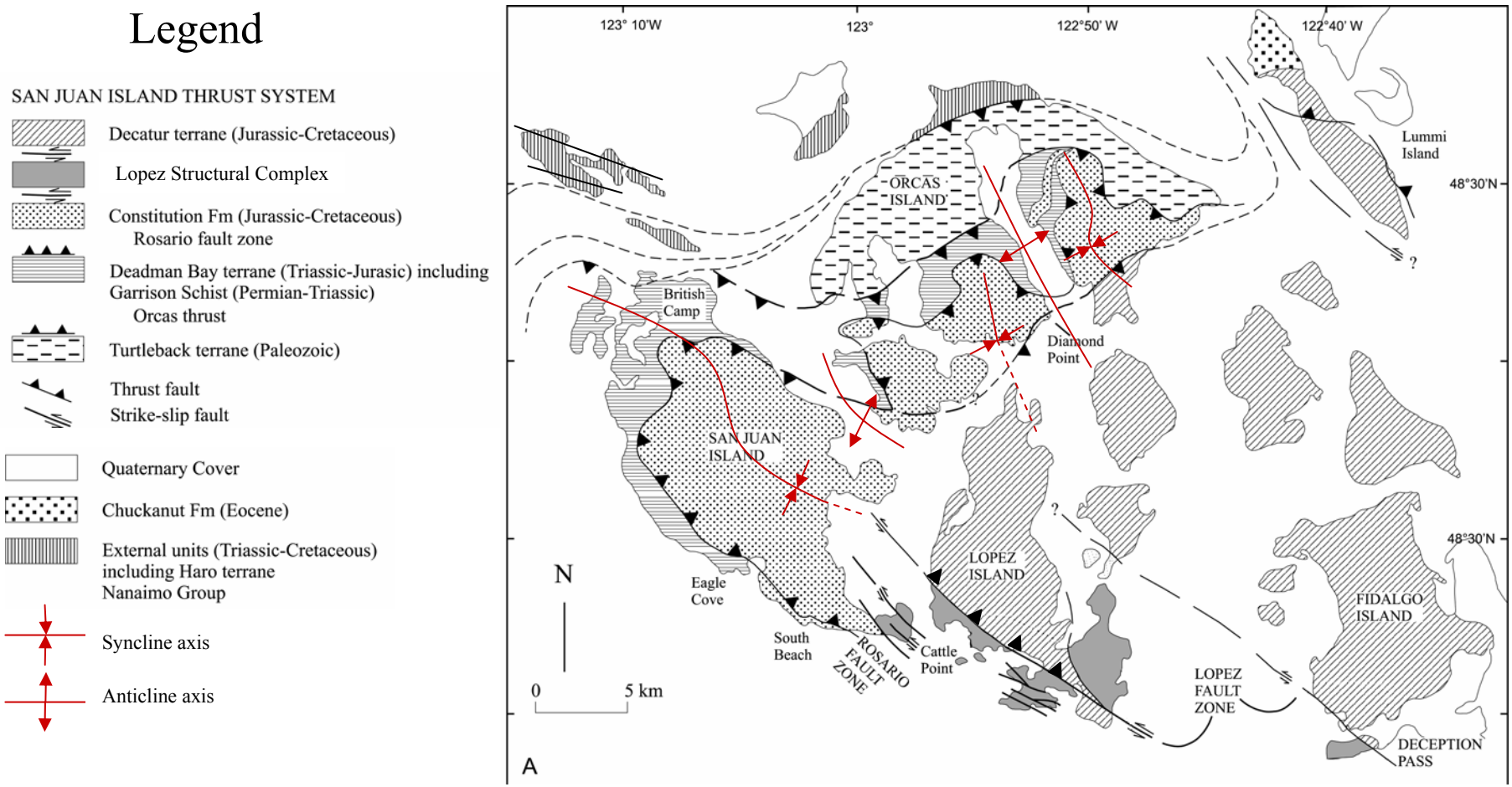

Figure 1.4. Overview of the San Juan thrust system showing the different terranes, clastic-linking sequence, and structural complex of Brandon et al. (1988) and the terrane bounding fault zones according to Bergh (2002). Note that Bergh (2002) shows the Lopez Structural Complex as a strik-slip fault zone as opposed to an imbricate thrust fault zone, as described by Brandon et al. (1988). Also, the Garrison Schist is included in the Deadman Bay terrane according to Bergh (2002). The units external to the San Juan thrust system include the Chuckanut Formation, the Haro terrane, and the Nanaimo Group. Faults modified after Bergh (2002) and Brandon et al. (1988). Folds (red) after Vance (1977).

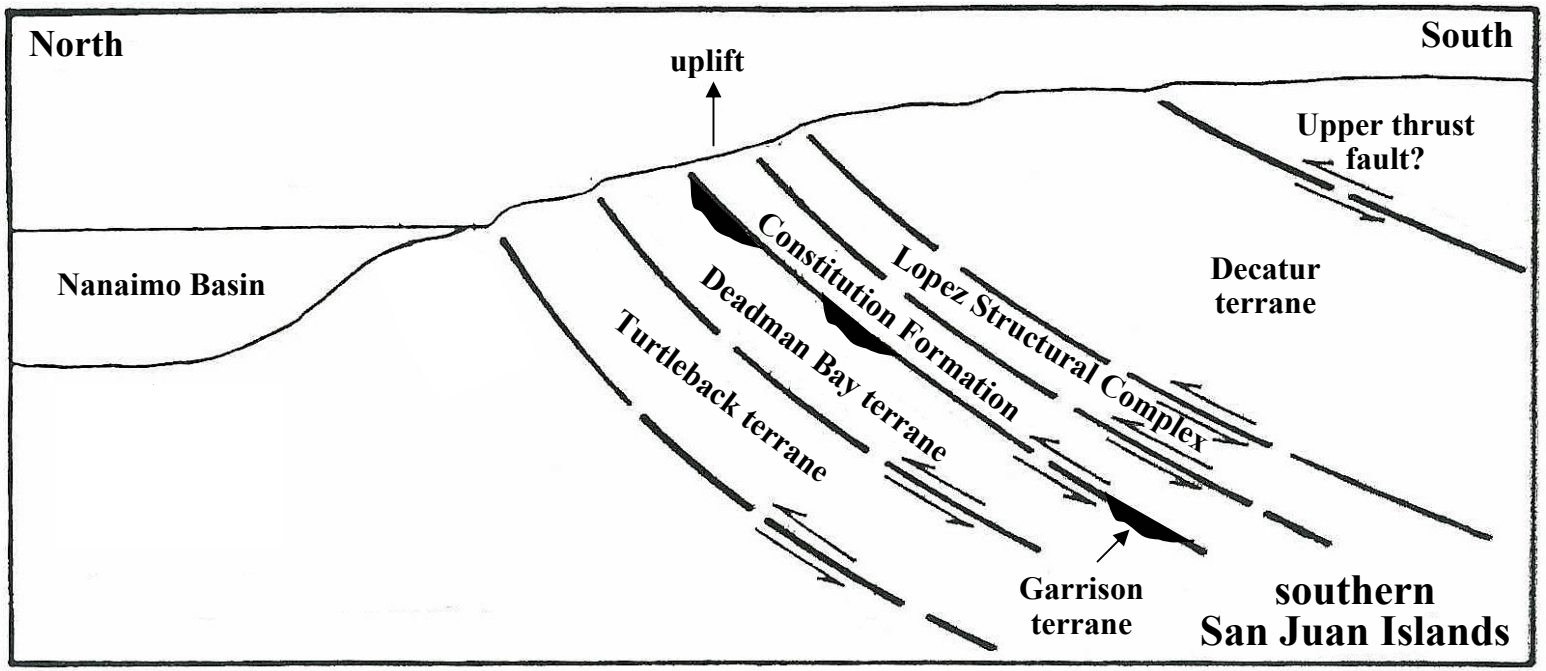

Figure 1.5. Schematic cross-section of the San Juan Thrust System illustrating the general stacking order of the thrust sheets based on Johnson et al. (1986) and Brandon et al. (1988).

Muller (1980), on the other hand, argues that Wrangellia extends into the SJI based on geologic similarities between the East Sound Group and the Sicker Group (Figure 1.6).

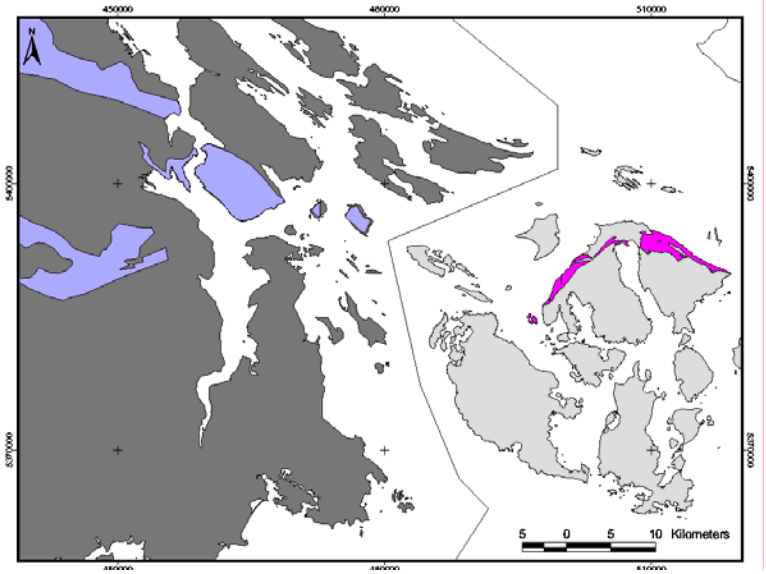

Figure 1.6. Map showing the extents of the Sicker Group (purple) as mapped by Muller (1983) on Vancouver Island (dark grey) and the East Sound Group (pink) as mapped by Schuster (2000) in the San Juan Islands (light grey).

Another major terrane boundary that needs to be better constrained offshore separates the Constitution Formation from the overlying Decatur terrane. This boundary is marked by the Buck Bay fault (Figure 1.3), which was mapped as a shallow southeastern-dipping structure onshore southeastern Orcas Island by Vance (1977), and extended to the southwest through Griffin Bay based on speculation by Brandon (1980). Both of the unconstrained terrane boundaries mentioned above represent zones of weakness within the crust where stress created by continuing oblique left-lateral motion along the Devils Mountain fault zone to the south can be transferred and released.

1.3. POTENTIAL ADULT ROCKFISH HABITATS

Along the west coast of the U.S. and in northern Puget Sound, many bottomfish populations are in decline due to a number of factors, including overfishing, pollution, and climatic perturbations (Puget Sound Water Quality Action Team, 2000; Pacific Fishery Management Council, 1999; West et al., 1997). Copper rockfish (*Sebastes caurinus*) and quillback rockfish (*Sebastes maliger*) are among those in decline (Figure 1.7) and listed

under the Washington Department of Fish and Wildlife's (WDFW) "Priority Habitats and Species List" (Palsson et al., 1998).

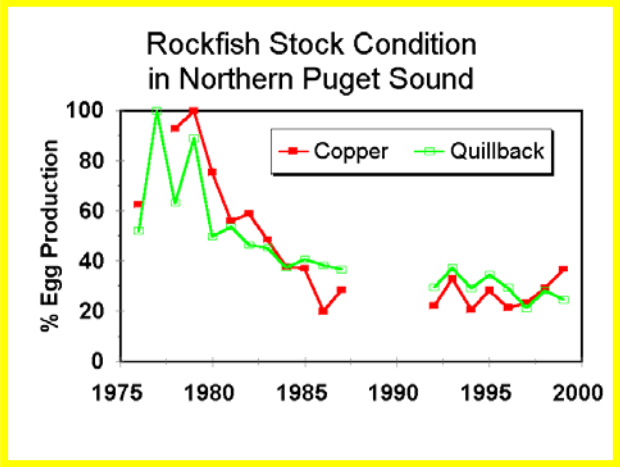

Figure 1.7. Graph showing the declining stocks of Copper and Quillback rockfish based on % egg production (Palsson, written commun., 2000)

Copper and quillback rockfishes are sedentary, structure-oriented, marine benthic species (Hart, 1973). The two species are morphologically similar, but differ in coloration. They occur sympatrically in Puget Sound (Matthews, 1990a). Both copper and quillback rockfish can be found in water depths ranging from 10 to 183 m, however, quillback rockfish can be found as deep as 274 m (Eschmeyer et al., 1983).

A clear understanding of the marine geology in the SJI will not only provide valuable information on regional geology and geohazards, but will also provide detailed lithologic and textural information about the seafloor that can be used to identify and map marine benthic habitats. Identifying potential adult rockfish habitats is fundamental to regional conservation and fisheries management efforts, such as the Northwest Straits Initiative and the Bottomfish Recovery Program created by the San Juan County Marine Resource Committee (San Juan Nature Institute, 1998). In addition, identifying potential adult rockfish habitats on a regional scale and knowing how these habitats are distributed spatially throughout the islands are important steps towards establishing and evaluating an effective network of marine protected areas (MPAs) in the SJI.

As a result of tectonic uplift, glacial scouring, and daily tidal flushing in the SJI, rugged bedrock is often exposed on the seafloor; effecting nutrient supply through increased upwelling

and providing refuge from predators for numerous marine species. Adult rockfishes, specifically copper and quillback rockfishes (*Unless otherwise noted, "adult rockfishes" refers to copper and quillback rockfishes*), utilize areas of complex (convoluted) high relief rocky seafloor in Puget Sound and the Georgia Basin (Matthews, 1990a, b; Pacunski and Palsson, 2001). Based on the assumption that adult rockfishes inhabit high complexity areas, characterizing the seafloor according to its complexity is a necessary part of identifying potential rockfish habitats. A wide variety of marine benthic habitats has been identified and characterized along the east and west coasts of the United States (O'Connell and Carlile, 1993; Greene et al., 1995; Todd et al., 2002; Yoklavich et al., 2000, 2002, 2003), using human interpretation of remote sensing imagery. While this form of habitat characterization involves first-hand expert knowledge of geologic and remote sensing principles and can be used to identify a wide variety of meso (10's of meters to 1 km) and macro-habitat (1 m–10 m) types, this method does not allow for standardized assessment of seafloor complexity. The human eye cannot calculate surface area to planar area ratios from two-dimensional seafloor imagery. For scientists and resource managers to quantitatively compare habitat parameters such as complexity among different sites within the SJI, the habitat data and methodology must be quantitative, standardized, and thus reproducible. In this study, a quantitative, standardized method will be presented for characterizing the complexity of the seafloor to more accurately identify and map potential adult rockfish habitats on a regional scale.

The terms "complex" or "high relief" and the scale at which these parameters are measured and/or described are often poorly defined in fish habitat studies. For instance, seafloor relief has previously been defined in the z direction (Matthews, 1990 a, b; O'Connell and Carlisle, 1993), without a clear explanation of the two dimensional horizontal extent (area) of that relief. The problem being, both a pinnacle with <3 m horizontal extent and a bedrock outcrop with >10 m horizontal extent could have the same "relief" as defined by the authors listed above. By including a horizontal component to the measure of relief, the ambiguity of the term is lessened. This study uses rugosity, which takes into account both the vertical and horizontal component of "relief", as a measure of complexity. Rugosity is defined as the ratio of surface area to planar area. Commonly, SCUBA surveys measure rugosity by draping a chain over the seafloor and measuring the ratio of line length to transect length (García-Charton, 2001). For this study, complexity describes an area of seafloor (2 m x 2 m) in map view (macro-habitat

scale) within a specified range of rugosity values as measured from gridded multibeam bathymetry data. It must be noted that the nature of multibeam data and the fact that these data are gridded at 2 m horizontal resolution (one sounding per 2 m x 2 m cell) means these data cannot resolve features that are less than 2 m (horizontal), small crevices or holes (void spaces), and overhanging structures. Therefore, complexity is inherently being underestimated at the micro-habitat (<1 m) scale.

To conserve habitat for rockfishes, habitat must not only be identified and mapped, but also protected. MPAs are becoming increasingly important for environmental conservation and fisheries management around the world, including Puget Sound. According to Presidential Executive Order 13158, an MPA is "any area of the marine environment that has been reserved by federal, state, territorial, tribal, or local laws or has regulations to provide lasting protection for part or all of the natural and cultural resources within". In the San Juan Islands specific types of marine protected areas have been designated by organizations such as the WDFW and the San Juan County Marine Resource Committee. In addition, over 83 islands in the San Juan Archipelago are part of the San Juan Islands National Wildlife Refuge. These MPAs have been selected for various reasons, most of which were not scientifically based. A goal of the Northwest Straits Marine Conservation Initiative is to identify an effective network of MPAs in northern Puget Sound using sound science as a basis for decision-making.

Evaluations of both the WDFW's marine preserves and the San Juan County Marine Resource Committee's voluntary no-take bottomfish recovery areas within the SJI have shown increases in species abundance, size, and reproductive potential (Palsson and Pacunski, 1995; Eisenhardt, 2003). It must be mentioned that a "positive reserve effect" may take ten's of years to detect. A study comparing rockfish densities and sizes inside and outside the 3.5 year-old Big Creek Ecological Reserve in Big Sur (Yoklavich et al., 2002) found no differences between reserve and non-reserve areas. The seafloor complexity maps presented in this study will help provide a regional view of the distribution of potential adult rockfish habitat, which can be used in designation and evaluation of a system of MPAs.

2. GEOLOGIC SETTING

2.1. TECTONIC HISTORY

The SJI represent the western portion of a series of metamorphic nappes, or thrust sheets, that make up what Bergh (2002) termed the Northwest Cascades orogen, which is synonymous with the San Juan-Cascade Nappes of Brandon et al. (1988) and the Northwest Cascade System of Brown (1987). The Northwest Cascades orogen represents a boundary zone between the Insular superterrane[3] on the west and the Intermontane superterrane on the east (Figure 2.1). North of 49ºN the boundary between these superterranes is obscured by the Coast Plutonic Complex, which represents Mid-cretaceous to Eocene subduction volcanism. To the south, the two superterranes are separated by the north Cascades crystalline core. The Insular and Intermontane superterranes represent the two largest allochthonous blocks in North America. The Intermontane superterrane was accreted to North America during the Mid-Jurassic, and represented the western margin of the continent during the Cretaceous (Monger et al., 1982). The Insular superterrane includes the Wrangellia terrane and is parallel to and west of the Intermontane superterrane. The entire boundary zone extends for approximately 1200 km from southern southeast Alaska to northern Washington. The SJI, which are associated with the Coast Plutonic Complex, can be divided into two main blocks separated by the Haro Fault (Figure 1.3). The highly metamorphosed rocks of the San Juan thrust system are exposed south of the fault, while the primarily un-metamorphosed units external to the San Juan thrust system are found north of the fault.

The tectonic origin of the SJI remains an unresolved scientific issue. The idea that the SJI underwent a fairly rapid period of thrusting and uplift between 100 Ma and 84 Ma (Brandon et al., 1988) is broadly accepted, however, there is widespread disagreement as to the direction and mechanism by which the SJI were amalgamated as well as the paleo-latitude of this region during the mid-Late Cretaceous. The existing theories on the direction and mechanism of mid-Late Cretaceous thrusting can be summarized by three models: 1) the *contractional model* in which the SJI formed due to SW-NE accretion in a zone of shortening between Wrangellia and North America (Brandon et al., 1983, 1988, 1993; Rubin et al., 1990; McGroder, 1991; Feehan

[3] The term superterrane refers to a fault-bounded package including multiple smaller tectonostratigraphic terranes.

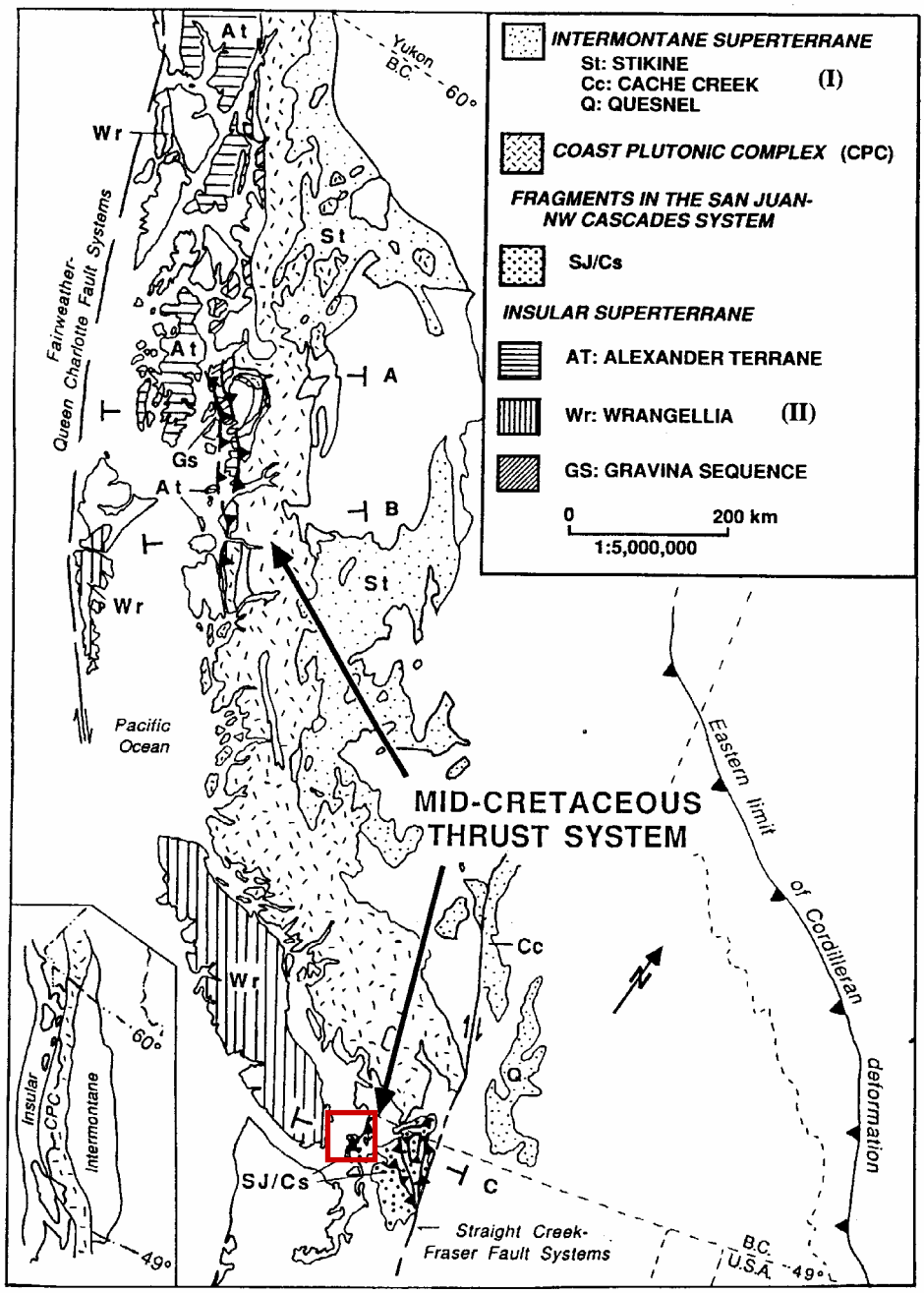

Figure 2.1. Shows the extent of the Intermontane and Insular superterranes, the Coast Plutonic Complex, the Northwest Cascades Orogen of Bergh (2002), and the distribution of the Mid-Cretaceous thrust system in the U.S. and Canada including the San Juan Island shown in the red box (after Rubin et al., 1990).

and Brandon, 1999; Figure 2.2A), and 2) the *northward transport model* in which a dextral transform fault zone along the North America subduction margin transports accreted terranes and clastic sequences northward until reaching a bend in the coastline where northwest-directed thrusting commences (Vance, 1977; Vance et al., 1980; Maekawa and Brown, 1991, 1993) (Figure 2.2B), and 3) the *combination model* in which early SW-NE contraction is followed by northwest directed thrusting and sinistral coast-parallel transport as suggested by a left-lateral fault zone in the Lopez Structural Complex (Bergh, 2002) (Figure 2.2C). A growing pool of paleomagnetic data suggests there has been between 1,000 – 3,000 km of northward transport of the Insular superterrane, the Coast Plutonic Complex, and by association the SJI since 90 Mya with minimal tilting (Irving, 1985; Housen and Beck, 1999; and Bogue et al., 1989). In addition, Burmester et al. (2000) recognized widespread remagnetization during the Cretaceous normal superchron in rocks of the eastern SJI. These magnetizations were consistently dipping steeply down to the southeast, suggesting a combination of tilting and clockwise rotation since terrane accretion. Some geologists argue that <1,000 km of northward translation has occurred between the Insular and Intermontane superterranes, based primarily on the absence of evidence of a fault system that could have accommodated more than 1,000 km of slip (Price and Charmichael, 1986; Mahoney et al., 1999).

At present, the regional tectonic setting of northwestern Washington involves the oblique convergence of the North American and Juan de Fuca Plates. Currently, the Juan de Fuca Plate is moving northeastward in a reference frame fixed to North America and is being subducted at a rate of approximately 45 mm/yr (Wilson, 2002). The Cascadia subduction zone defines this active Plate boundary. According to GPS velocity data along the Cascadia subduction zone (Mazzotti et al., 2002); the northwestern Washington/Southwestern British Columbia region is currently shortening in a N-S direction at ~3–3.5 mm/yr, with long term shortening estimated at 5–6 mm/yr. According to Wells et al. (2002), this shortening is linked to the dextral translation of the Sierra Nevada block in California. The convergence of the Sierra Nevada block with the Oregon forearc near the Mendocino triple junction has resulted in the clockwise rotation of the Oregon forearc, which in turn drives the Washington forearc northward against the Canadian Coast Mountains (Wells et al., 2002; Figure 2.3).

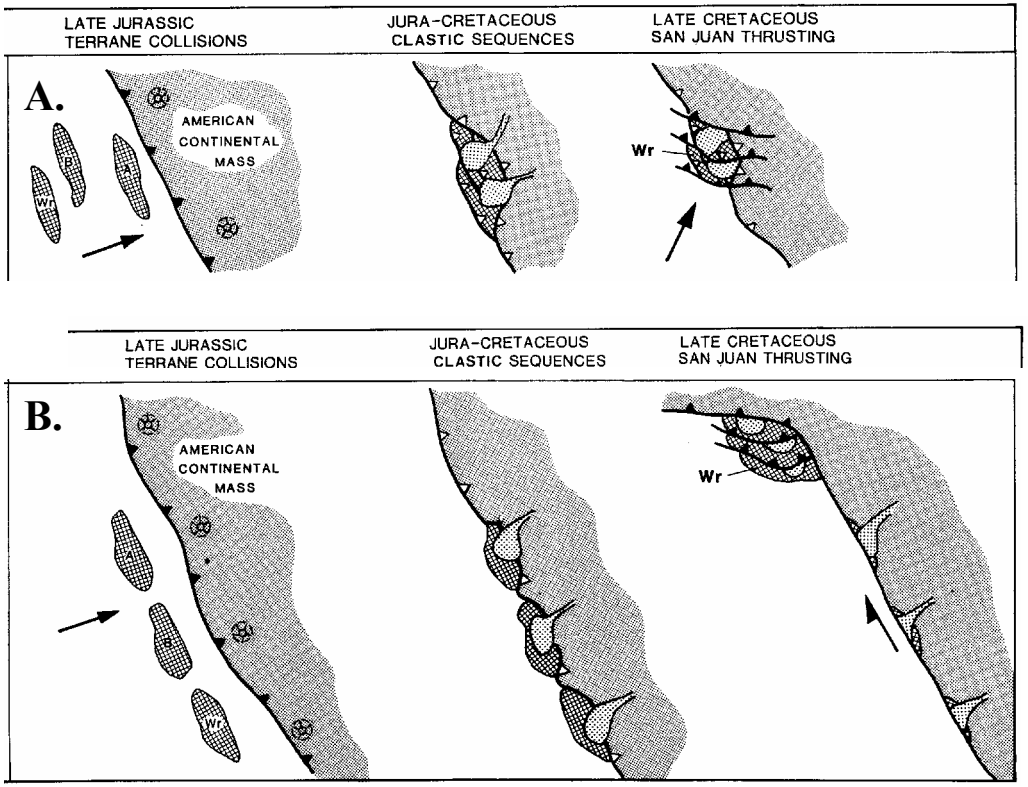

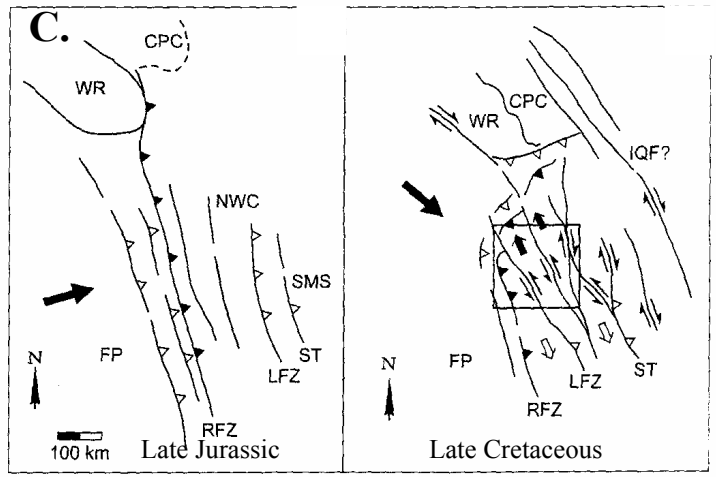

Figure 2.2. Three models for the accretionary history of the San Juan Island and surrounding terranes. All models agree that the terranes were accreted to the American continent by latest Jurassic. The *contractional model* (A.) shows SW-NE accretion of the SJI and Wrangellia terranes. Wr = Wrangellia. B. illustrates the *northward transport model*, in which the SJI and Wrangellia were accreted to North America south of their present location and transported northward along coast-parallel strike-slip faults until reaching a re-entrant in the margin, where NE-SW directed thrusting occurred. C. demonstrates the *combination model*, in which early SW-NE contration along a subduction margin changed to northwest-directed thrusting and northward transport along sinistral strike-slip faults. CPC = Coast Plutonic Complex, IQF = Intra-Quesnellia Fault, FP = Farallon Plate, RFZ = Rosario Fault Zone, LFZ = Lopez Fault Zone, ST = Strait Creek Fault (A. & B. after Brandon et al., (1988) and C. after Bergh (2002).

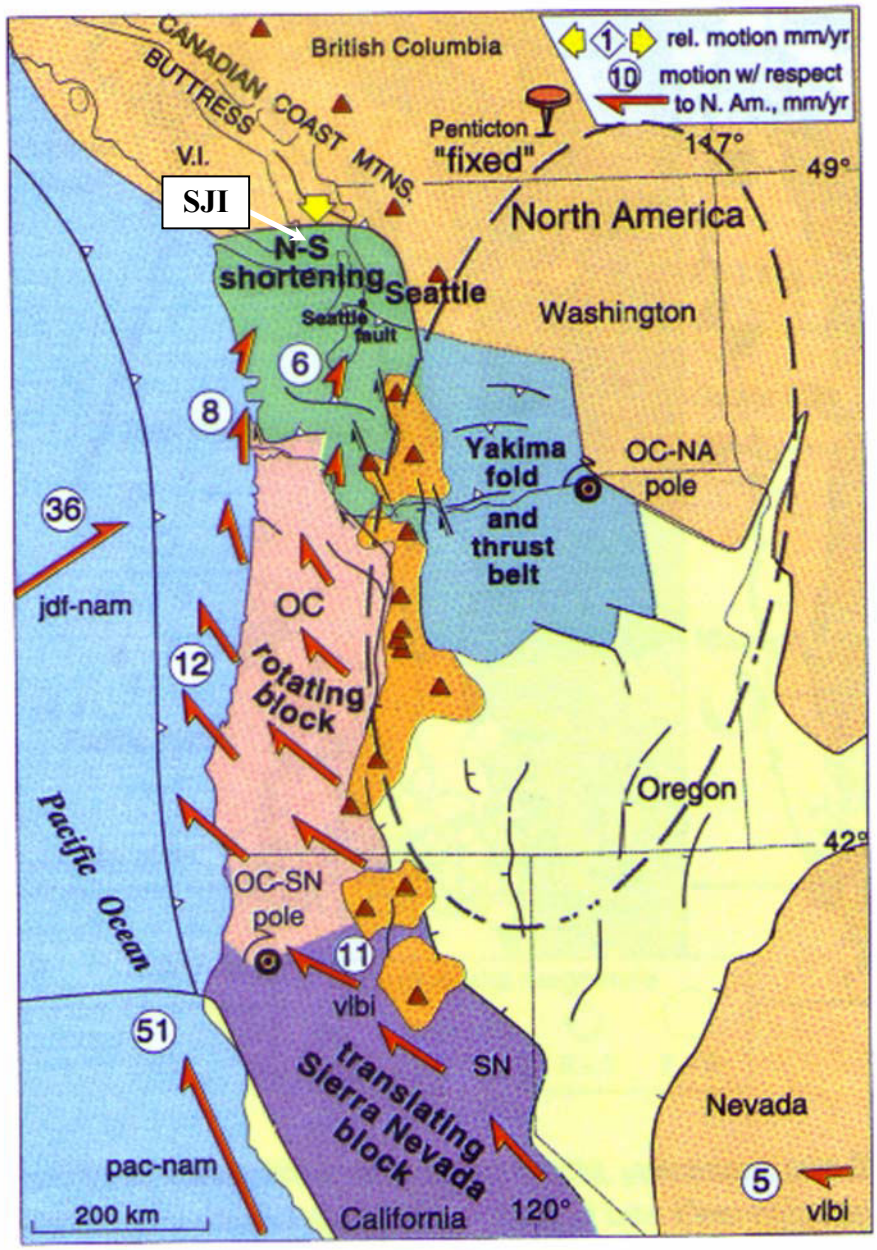

Figure 2.3. Velocity field for Oregon forearc microplate with reference to the OC-NA pole. The Oregon block (OC) is rotating clockwise due to northward movement of the Sierra Nevada (SN) block in the Klamath Mountains. The north end of the Oregon block deforms the Washington forearc against Canada, causing north-south compression. Jdf = Juan de Fuca plate, nam = North American plate, pac = Pacific plate, and vibi = rates from very long baseline interferometry (modified after Wells et al., 2002).

2.2. REGIONAL SEISMICITY

The San Juan Islands are located within the seismically active Puget Lowland. Earthquakes that occur in the region can be divided into crustal earthquakes that occur within the upper ~37 km (Ramachandran, 2003), subduction earthquakes that occur at the interface between the North American and subducting Juan de Fuca Plate at intermediate depths, and deep earthquakes within the Juan de Fuca Plate (Figure 2.4). This study will focus on crustal earthquakes because crustal earthquakes record movement on faults within the crust and these faults may have surface expression on the seafloor. Crustal earthquakes in the Puget Sound region occur primarily as a result of N-S compressive stresses taking place along the northern Washington forearc. While large earthquakes with magnitudes greater than 4 are rare in the SJI, smaller earthquakes are prevalent and can aid in outlining active fault planes and/or zones of active deformation within the crust. Figure 2.5 shows the distribution of earthquakes within the upper 35 km in the southwestern SJI region. There appears to be a cluster of seismic activity directly offshore southwestern San Juan Island, however, the surrounding areas appear relatively inactive.

2.3. MAJOR FAULT ZONES

2.4.1. Lopez and Rosario Fault Zones

Two of the most prominent fault zones in the SJI, the Lopez Fault Zone [referred to as the Lopez Structural Complex by Brandon (1988)] and the Rosario Fault Zone, comprise a mixture of deformed igneous, sedimentary, and metamorphic rocks that were emplaced during Late Cretaceous terrane accretion in the San Juan thrust system (Figure 1.4). Bergh (2002) conducted a detailed analysis of mesoscopic structures (folds, axial-planar cleavage, and stretching lineations) along these two fault zones and concluded that the rocks of both fault zones were affected by two Late Cretaceous deformational events, referred to as D1 and D2 (Figure 2.6). Based on this fabric analysis, Bergh (2002) deduced that the D1 fabrics are related to southwest-northeast shortening that occurred during initial subduction-related accretion of the nappes, while the D2 fabrics are the result of combined orogen-parallel strike-slip motion and

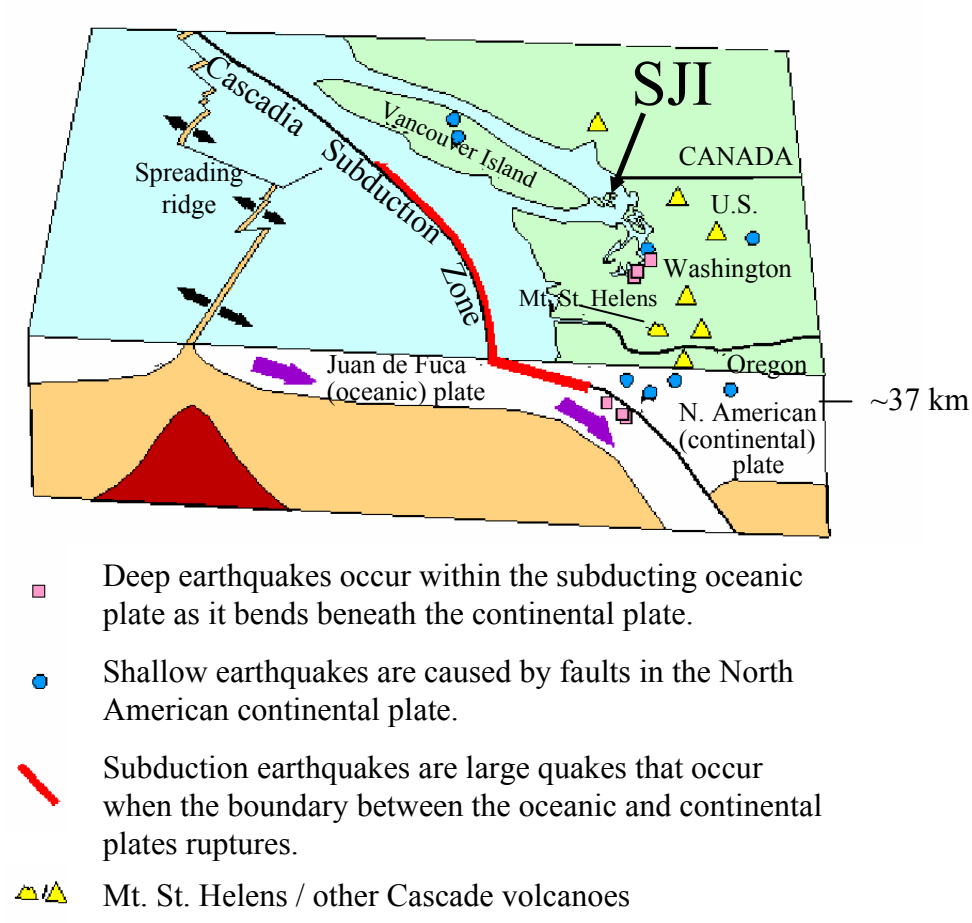

Figure 2.4. Schematic cross-section of the Cascadia Subduction Zone, showing the different types of earthquakes and where they occur in map view and in cross section (modified after http://www.pnsn.org/INFO_GENERAL/eqhazards.html website, 2004).

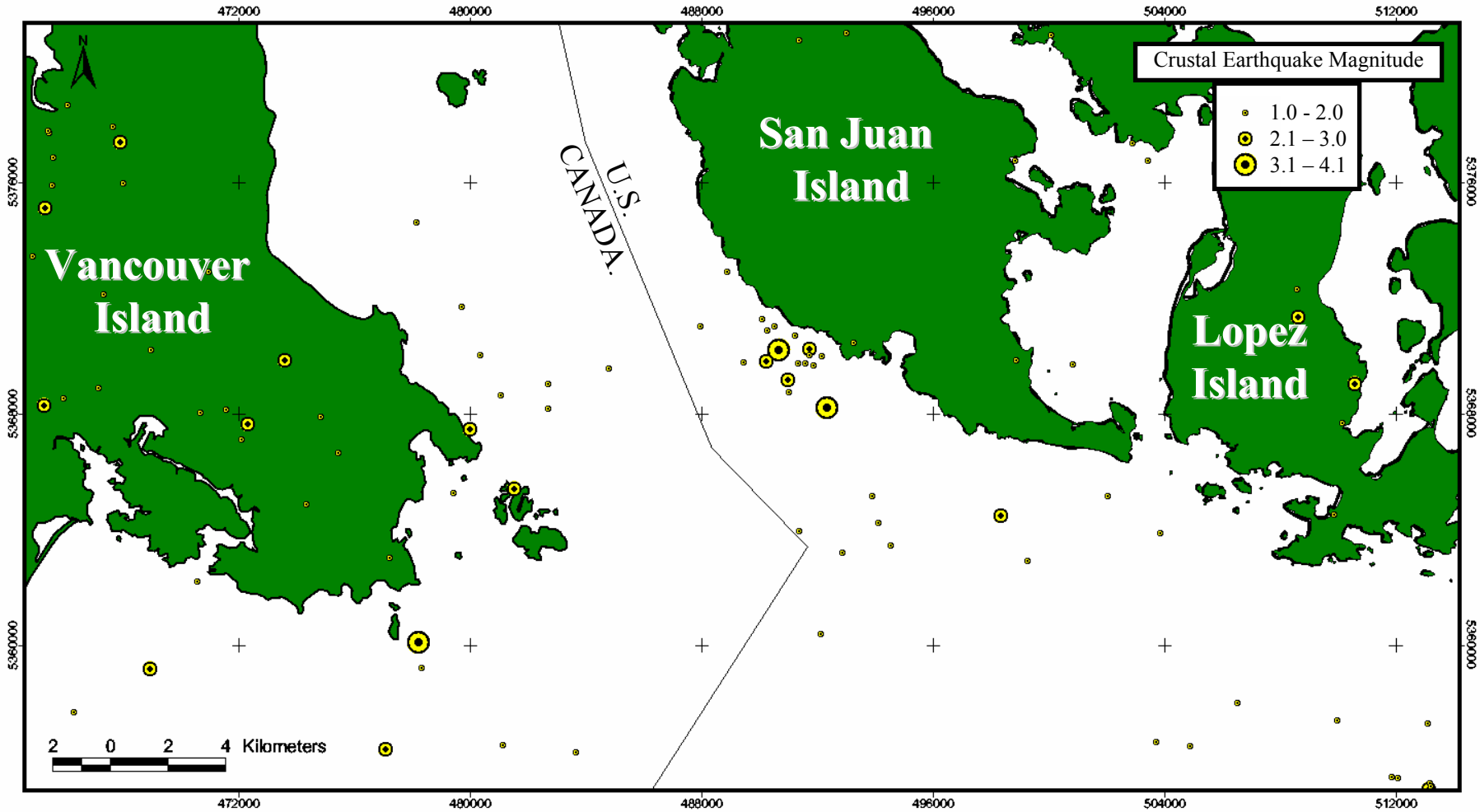

Figure 2.5. Map showing crustal (<35 km depth) earthquake epicenters plotted by magnitude in the southwestern San Juan Islands and southeastern Vancouver Island region (earthquake data downloaded on 6/15/04 from <http://quake.geo.berkeley.edu/anss/catalog-search.html>, the search includes earthquakes between Jan 1, 1981 and June 15, 2004).

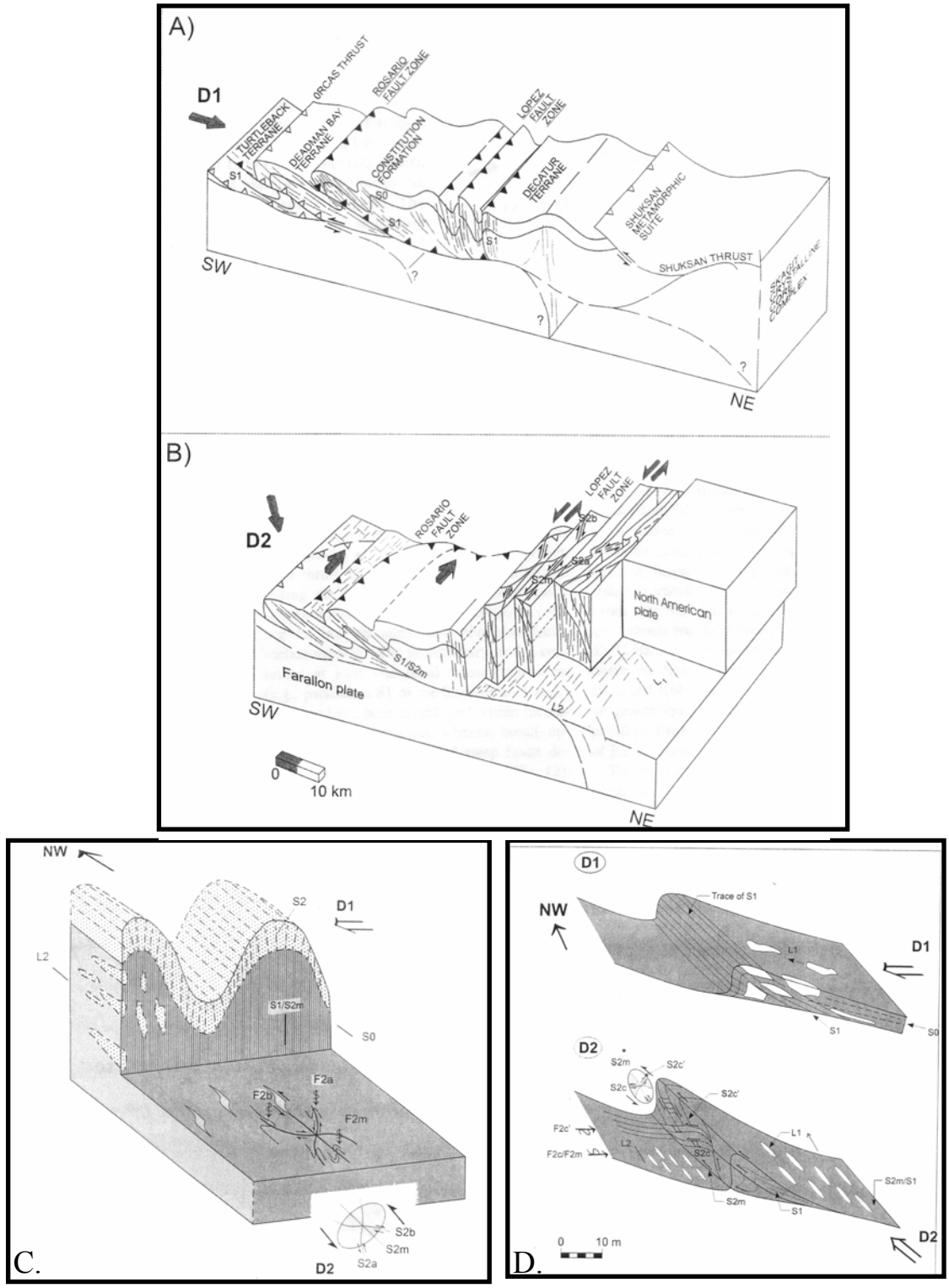

Figure 2.6. (A & B) Sketch showing a two-stage (D1 & D2) kinematic model for the Lopez (LFZ) and Rosario fault zones (RFZ). (A) D1 orogen-normal shortening and juxtaposition of terranes, followed by accretion. (B) D2 oblique convergence involving linked northwest-directed thrusting (RFZ) and strike-slip translation (LFZ). (C & D) Schematic cross-sections of the LFZ (C) and the RFZ (D), showing D1 and D2 fabric elements and kinematic relationships. Arrows indicate shortening directions. Modified after Bergh (2002).

northwest-directed thrusting associated with oblique convergence (Figure 2.6A, B). Both fault zones trend northwest-southeast in the southern SJI.

According to Bergh (2002), the LFZ is a 3 km wide system of steep to subvertical en echelon sinistral strike-slip faults bounded by the Decatur terrane and the Constitution Formation (Figure 1.4). In the LFZ D1 produced symmetric upright folds (F1) with steep to subvertical axial-planar S1 cleavage, while D2 produced subvertical strike-slip shear zones striking northwestward that either parallel or are conjugate to S1 (Figure 2.6C). Steeply plunging F2 drag folds accompanied this D2 fabric. Bergh (2002) speculates that the high-angle LFZ was located above a thrust detachment represented by the RFZ that allowed for orogen-parallel translation.

The RFZ can be traced from the southern tip of San Juan Island north and eastward across Orcas Island (Figure 1.4). This 1 km wide gently dipping fault zone is comprised of strongly foliated mudstone mélange containing ribbon chert, schist, and metavolcanic rocks derived from the footwall (Deadman Bay terrane) and metasandstone from the headwall (Constitution Formation). D1 in the RFZ produced asymmetric northwest-trending F1 folds and S1 foliation that dips gently to the northeast in the south (Figure 2.6 D) and to the southeast on Orcas Island (Bergh, 2002). This change in dip likely reflects the regional-scale folding of the San Juan thrust system (Brandon et al., 1988, 1993). Unlike the LFZ, D2 produced shallow northeast-dipping S2 shear zones and associated gently plunging F2 drag folds in the RFZ (Figure 2.6D) (Bergh, 2002). The seismic potential in both the LFZ and the RFZ is low, however, the possibility of re-activation of structures in these fault zones due to recent activity along the DMF cannot be ignored. Prior to this study, the offshore traces of the LFZ and RFZ were not well constrained.

2.4.2. Buck Bay Fault

Brandon (1980) described the Buck Bay fault as a low angle thrust juxtaposing the Lopez Structural complex and Decatur terrane with the Constitution Formation and older terranes (Figure 1.3). The Buck Bay fault is part of the Mid-Cretaceous San Juan Thrust system. The fault is only exposed on southeast Orcas Island. Brandon (1980) extended the Buck Bay fault to the southwest based on the need for a fault to explain the truncation of the Lopez Structural Complex in southern San Juan Channel. The faults of the Lopez Structural Complex are not

exposed along the shoreline of Griffin Bay, and therefore Brandon (1980) drew the fault through San Juan Channel and across the glacial deposits on Mt. Finlayson (Figure 1.3).

2.4.3. Devils Mountain Fault Zone

The Devils Mountain Fault, first named by Lovseth (1975), and associated structures make up the Devils Mountain Fault Zone (Figure 1.2). The Devils Mountain Fault Zone is a west-northwest-striking 125 km long oblique-slip transpressional deformation zone that extends westward from the Cascade Range foothills across the eastern Strait of Juan de Fuca to Vancouver Island (Johnson et al., 2001), where it may join the Leech River Fault and/or the San Juan fault (Figure 2.7). The oldest rocks offset by the DMF are Oligocene in age, marking the lower age limit of faulting. Onshore and offshore geophysical and geologic data indicate left-lateral and/or vertical displacement of Quaternary sediments at numerous locations along the 125 km DMF, indicating high seismic potential for this fault zone (Johnson et al., 2001 and Oldow, 2000). Possible segment boundaries in the fault were recognized east of Whidbey Island in Skagit Bay and south of southeastern San Juan Island (Figure 1.2). The dip of the DMF was estimated based on crossing seismic-reflection profiles to be 61° ± 10° to the north with the steepest dips in the east near the western shore of Whidbey Island (Johnson et al., 2001). The map-view geometry of the DMF and its associated structures is similar to left-lateral, oblique-slip wrench fault zones (Wilcox et al., 1973) with the DMF acting as the "master fault" within a wide zone of deformation (Johnson et al., 2001). Mapping of these northwest-trending structures offshore False Bay on San Juan Island was limited because of incomplete coverage of seismic-reflection profiles. However, additional seismic reflection profiles have been collected offshore southwestern San Juan Island by the Canadian Geological Survey. These data are currently being processed, but were not available for this study.

2.4. BEDROCK GEOLOGY OF SAN JUAN AND LOPEZ ISLANDS

According to Brandon et al. (1988), the San Juan thrust system is composed of four terranes, one clastic-linking sequence, and a Late Cretaceous imbricate fault zone. Listed structurally from bottom to top, the San Juan thrust system includes the Turtleback terrane, Garrison terrane, Deadman Bay terrane, Constitution Formation, Lopez Structural Complex, and the Decatur terrane. Each of the terranes is composed of one or more stratigraphic units

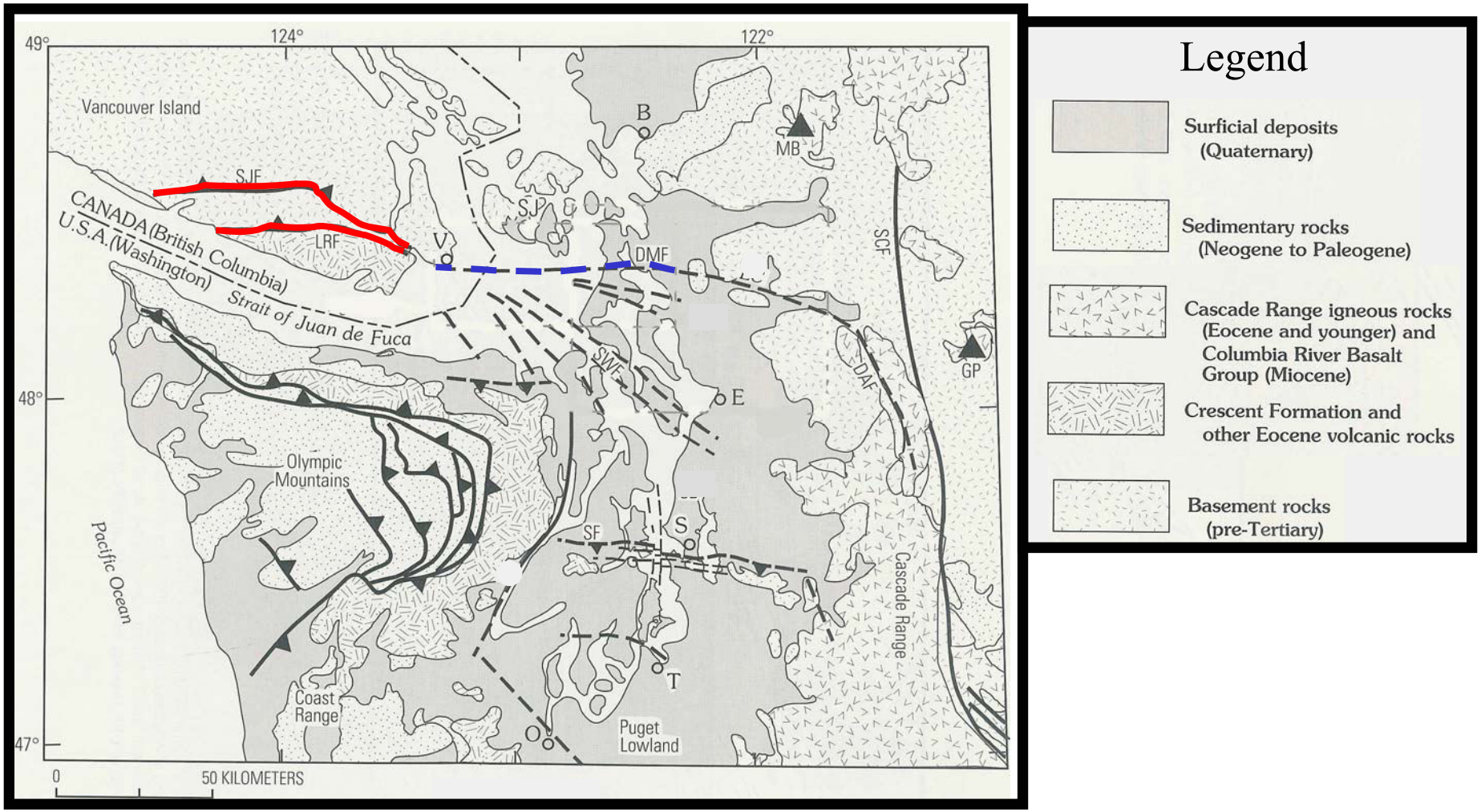

Figure 2.7. Generalized geologic map of the region highlighting the trace of the Devils Mountain Fault (dashed blue) across the Strait of Juan de Fuca, where it joins the Leech River and/or San Juan Fault (red). B, Bellingham; E, Everett; O, Olympia; S, Seattle; T, Tacoma; V, Victoria; Heavy line, fault; dashed where inferred, teeth on upper plate of thrust fault. Triangle, modern Cascade volcano. DAF, Darrington fault; DMF, Devils Mountain fault; GP, Glacier Peak; LRF, Leech River fault; MB, Mount Baker; SCF, Strait Creek fault; SF, Seattle fault; SJ, San Juan Islands; SJF, San Juan fault; SWF, southern Widbey Island fault. (modified after Johnson et al., 2001).

(Table 2.1). The map extent of the nappes in the San Juan thrust system is illustrated in Figure 1.4. Each of these units has distinctive petrologic, stratigraphic, and metamorphic characteristics, however, a common mineral assemblage of lawsonite and aragonite are found throughout the SJI (Vance, 1968; Glassley et al., 1976) indicates all the rocks of the San Juan thrust system underwent a period of very low-temperature and high-pressure metamorphism likely during thrust-related burial to depths of about 20 km (Brandon et al., 1988). The bedrock geology of the study site, including southern San Juan and southwestern Lopez Islands includes rocks from the following stratigraphic units: the Deadman Bay Volcanics (early Permian – Triassic) and Orcas Chert (Triassic and early Jurassic) of the Deadman Bay terrane, the Garrison Schist of the Garrison terrane (Permian – early Triassic metamorphic age), the Constitution Formation (Jurassic or early Cretaceous), the Lopez Structural Complex (late Jurassic – early Cretaceous), and the Fidalgo Igneous Complex (middle and late Jurassic) and Lummi Formation (late Jurassic and early Cretaceous) of the Decatur terrane (Table 2.1). In the following paragraphs I will discuss the geology of each of these stratigraphic units within the terranes they compose.

2.3.1. Deadman Bay terrane (*early Permian – early Jurassic*)

The Permian to Triassic Deadman Bay Volcanics and the Triassic to early Jurassic Orcas Chert are related stratigraphic units that comprise the Deadman Bay terrane (Figure 1.4). The Deadman Bay volcanics occur as discontinuous fault slices intermixed with the Orcas Chert. The Deadman Bay unit consists of pillow basalt and pillow breccia interbedded with massive limestone and ribbon chert. The limestones are unique in that they contain late Permian fusulinids that are characteristic of the Asiatic fusulinid province "Tethyan", a faunal province exotic to North America. The presence of these fusulinids represents one line of evidence in support of the Baja British Columbia hypothesis, which states that 90 Ma a large segment of the western edge of northern North America was situated about 2,400 km to the south adjacent to California and northern Mexico (Irving, 1985; Housen and Beck, 1999). The Orcas Chert is composed primarily of grayish ribbon chert with minor sequences of mudstone, pillow basalt, basaltic tuff, and limestone. The ribbon cherts are commonly folded and distorted, but where interbedded with mudstone and tuff the bedding becomes more chaotic. Trace-element compositions indicate the basalts of both the Orcas Chert and Deadman Bay Volcanics are

Stratigraphic Nomenclature for the rocks of the San Juan Thrust System (Unitslisted in their relative structural position, from bottom to top)		
Stratigraphic Names (ages)	***Lithologic Description***	***Terrane Names***
Turtleback Complex (*pre-Devonian*)	A plutonic complex consisting of tonalite and subordinate gabbro. Inferred to be basement for the East Sound Group.	Turtleback terrane
East Sound Group (*early Devonian -early Permian*)	An arc-volcanic sequence with minor interbedded limestone. Fusulinids from these limestones are non-Tethyan.	
Deadman Bay Volcanics (*early Permian - Triassic*)	Pillow basalt with minor interbedded Tethyan-fusulinid limestone and ribbon chert.	Deadman Bay terrane
Orcas Chert (*Triassic & early Jurassic*)	Ribbon chert and minor pillow basalt and limestone. Inferred to be stratigraphically related to the Deadman Bay Volcanics. Locally imbricated with slices of Turtleback Complex.	
Garrison schist (*Permian - early Triassic metamorphic age*)	High-pressure metamorphic rocks composed of mafic schist with minor quartz-mica schist. Ranges from greenschist to albite-epidote amphibolite facies. Occurs only in small fault slices along the Rosario thrust.	Garrison terrane
Constitution Formation (*Jurassic or early Cretaceous*)	A clastic sequence containing massive volcaniclastic sandstone, with interbedded mudstone, ribbon chert, pillow lava, and green tuff.	clastic-linking sequence
Lopez Structural Complex (*late Jurassic - middle Cretaceous*)	An imbricate fault zone containing fault slices of Jura-Cretaceous sandstone, pebbly mudstone, pillow lava, and chert; and mid-Cretaceous pillow basalt and Turtleback tonalite.	imbricate fault zone
Fidalgo Igneous Complex (*middle & late Jurassic*)	An ophiolite with a younger, super-imposed volcanic arc.	Decatur terrane
Lummi Formation (*late Jurassic & early Cretaceous*)	A clastic marine sequence overlying the Fidalgo Complex.	

Table 2.1. List of stratigraphic names, lithologic descriptions, and related terranes for rock units within the San Juan thrust system (modified after Brandon et al. (1988).

comparable to tholeiitic and alkalic basalts of modern ocean volcanic islands (Brandon et al., 1988).

2.3.2. Garrison terrane (*Permian – early Triassic metamorphic age*)

The Garrison terrane is a metamorphic unit made up of both greenschist and amphibolite. This unit exists as a series of discontinuous fault slices along the Rosario Fault Zone (RFZ), which separates the Deadman Bay terrane from the overlying Constitution Formation (Figure 2.8).

Figure 2.8. Map showing the distribution of the Garrison Schist (solid black pattern), which occurs as exotic fault slices along the Rosario Fault zone. The size of the exposures is greatly exaggerated (after Brandon et al., 1988).

The existence of a well-developed schistosity in the Garrison Schist indicates these rocks are more highly metamorphosed than the adjacent Orcas Chert and Constitution Formation rocks. The Garrison rocks are highly fractured and brecciated likely as the result of thrust emplacement (Brandon et al., 1988). The Garrison rocks were metamorphosed before thrusting because the age of metamorphism (Permian to early Triassic) is older than the adjacent rocks units. Furthermore, there are metamorphic clasts of Garrison Schist in the overlying Constitution Formation. However, the exact mechanism of emplacement of the Garrison Schist is still being debated. The precursor rocks of the Garrison Schist most likely originated from a sequence of

submarine basalts with minor chert and limestone along a divergent Plate boundary (Brandon et al., 1988).

2.3.3. Constitution Formation (*Jurassic – early Cretaceous*)

This Formation represents a sequence of upper Mesozoic volcaniclastic sandstone, black mudstone, ribbon chert, green tuff, and minor pillow lava. The Constitution Formation is made up of three informal units as described by Brandon (1980) (Figure 2.9A). The lower unit, which occurs primarily within the Rosario Fault zone separating the Constitution Formation from the lower Orcas Chert, contains black mudstone, green tuff, ribbon chert, and minor volcaniclastic sandstone. This unit has not been confidently linked to either the Constitution Formation or the Orcas Chert, but Brandon et al. (1988) includes it with the Constitution Formation based on the existence of volcaniclastic sandstone, which is not typical of the Orcas Chert. The middle unit is comprised of massive volcaniclastic sandstone with minor conglomerate. The upper unit contains thinly interbedded black mudstone and cherty sandstone, with minor pebbly mudstone, massive sandstone, ribbon chert, and basalt and dacite pillow lavas. Unlike the lower unit, the middle and upper units are relatively intact with no evidence of exotic fault slices. The clastic rocks of the middle and upper units were likely deposited within a submarine fan system with the mud-rich upper member representing a slope or base of slope setting and the massive sandstones and conglomerate of the middle unit representing channel deposits. According to Brandon et al. (1988), the dacite pillow lavas of the upper unit appear to represent submarine slide blocks derived from an older unit, possibly the mid to late Jurassic Fidalgo Igneous Complex. While the Constitution Formation is entirely fault bounded and therefore not stratigraphically related to the surrounding units, the provenance of the clastic rocks indicates the Constitution Formation was deposited adjacent to a volcanic-arc terrane and uplifted assemblage of older rock containing mafic schists similar to those in the Garrison terrane. The Constitution Formation has been correlated with other Jurassic-Lower Cretaceous units on southern and western Vancouver Island such as the Pandora Peak unit and the Pacific Rim Complex, which Brandon (1985) considers to be displaced pieces of the San Juan thrust system that were moved northwestward by transform faulting during the early Cenozoic.

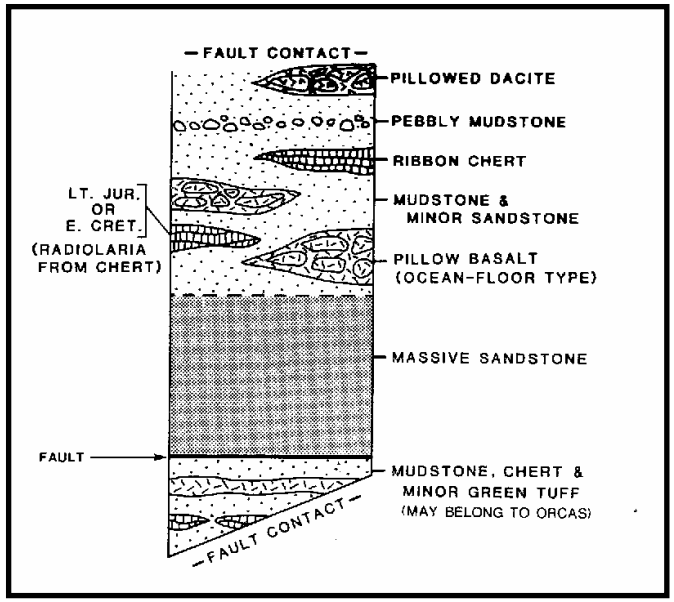

A. Generalized stratigraphic column of the Constitution Formation as it exists on San Juan Island, after Brandon (1988).

B. Generalized stratigraphic column of the Decatur terrane as it exists on Lopez Island, after Brandon (1988)

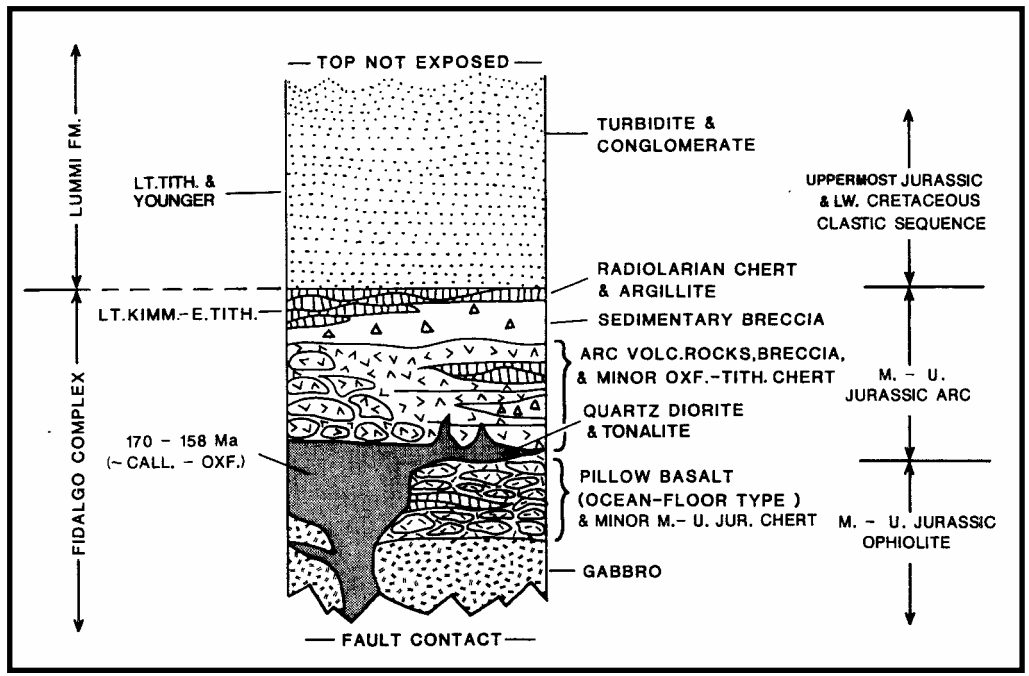

Figure 2.9. Generalized stratigraphic columns of the Constitution Foramtion (A.) as it has been mapped on San Juan Island and the Decatur terrane (B.), as it is mapped on Lopez Island (after Brandon et al., 1988).

2.3.4. Lopez Structural Complex (*late Jurassic – middle Cretaceous*)

The Lopez Structural Complex was first described by Brandon (1980) as a late Cretaceous imbricate fault zone exposed onshore along the coast of southern Lopez Island and on the southeast tip of San Juan Island. Recently, detailed analysis of rock fabric (Bergh, 2002) has revealed that the Lopez Structural Complex is a steep to subvertical strike-slip fault zone rather than a series of imbricate thrust faults. The most common rock unit in the Lopez Structural Complex contains Jurassic-Cretaceous turbidite sandstone, interbedded mudstone, and conglomerate likely derived from the Decatur terrane. Other rocks derived from the Decatur terrane include Jurassic pillow basalt of ocean-floor affinity and brecciated gabbro. The Lopez Structural Complex also contains Jurassic-Cretaceous pebbly mudstone and sandstone with interbedded chert, green tuff, and basalt that are lithologically similar to the Constitution Formation. There are two exotic rock units within the Lopez Structural Complex, one of which has only been found within the Complex itself. The first unit includes small slices of early Paleozoic quartz diorite, or tonalite, similar in age and geochemisty to the Turtleback Complex. The second exotic rock unit is made up of mid-Cretaceous vesicular pillow basalts, pillow breccia, and related diabase and gabbro that are only found near the town of Richardson (Figure 2.10). Trace element composition indicates the basalts in this mid-Cretaceous unit may be oceanic-island basalts. The Lopez Structural Complex is separated from the Decatur terrane by the moderately northeast-dipping Lopez Fault (Brandon et al., 1988) (Figure 1.3). Structural details of the Lopez Structural Complex are discussed later, where it is referred to as the Lopez Fault Zone (LFZ) by Bergh (2002).

2.3.5. Decatur terrane (*middle Jurassic – early Cretaceous*)

The Decatur terrane represents an upper Mesozoic ophiolite, arc, and clastic sequence exposed in the eastern SJI (Figure 1.4). This terrane is made up of two stratigraphically related units: the Fidalgo Complex, and the overlying Lummi Formation (Brandon et al., 1988) (Figure 2.9B). The Fidalgo Complex is a middle to upper Jurassic ophiolite and superimposed volcanic-arc sequence. Geochemical analyses conducted by Brandon et al. (1988) suggest the Fidalgo Complex contains igneous rocks formed in two different volcanic-tectonic settings. The pillow basalt-chert unit exposed on Lummi and Lopez Islands was likely formed in a mid-ocean ridge

Figure 2.10. SPOT multi-spectral satellite image of the SJI highlighting important place names. The SPOT image contains three bands: Red, Green, and Near IR. BL = Blakely Is., DC = Decatur Is., LP = Lopez Is., OR = Orcas Is., SH = Shaw Island, SJ = San Juan Is., SP = Speiden Is., ST = Stuart Is., TI = Turn Is., and WA = Waldron Is.

setting, whereas the volcanic-sedimentary sequence on Fidalgo Island (Figure 1.3) represents a younger volcanic-arc sequence. The late Jurassic to early Cretaceous Lummi Formation is a 2 km thick sequence of well-bedded turbidite sandstone, mudstone, and conglomerate that overlies the Fidalgo Complex. Like the Constitution Formation, the Lummi Formation represents a clastic-linking sequence that contains clastic rocks from a lithologically diverse source area including clasts of pyroxenite and gabbro from the underlying Fidalgo Complex. However, the Lummi Formation must have been adjacent to terranes other than the Decatur during Jurassic and Cretaceous time because the Lummi Formation contains late Jurassic and early Cretaceous clastic material that could not have been derived from the Decatur terrane (Brandon et al., 1988). The Decatur terrane has been compared to other Jurassic ophiolitic units located further south, such as the Coast Range ophiolite and overlying Great Valley Group in California (Brandon et al., 1988).

2.5. GLACIAL HISTORY

The northern Puget Lowland, where the San Juan Islands are located, is an extensive topographic N-S trough bounded in the west by Vancouver Island and in the east by the Cascade Mountains (Figure 2.11). The Cordilleran Ice Sheet advanced into and retreated from western Washington six times or more during the Pleistocene (Easterbrook, 1992, 1994). In the central and northern Puget Lowland only deposits of the three youngest glaciations are exposed; the Double Bluff, the Possession, and the Fraser glaciations (Easterbrook, 1992). Of these, only the deposits of the Fraser glaciation (18 – 10 ka) are exposed within the southwestern SJI. The Fraser Glaciation has been divided into two distinct Stades, or periods of ice advance and retreat and one Interstade (Kovanen and Easterbrook, 2001). From oldest to youngest, they are the Vashon Stade, the Everson Interstade, and the Sumas Stade (Table 2.2).

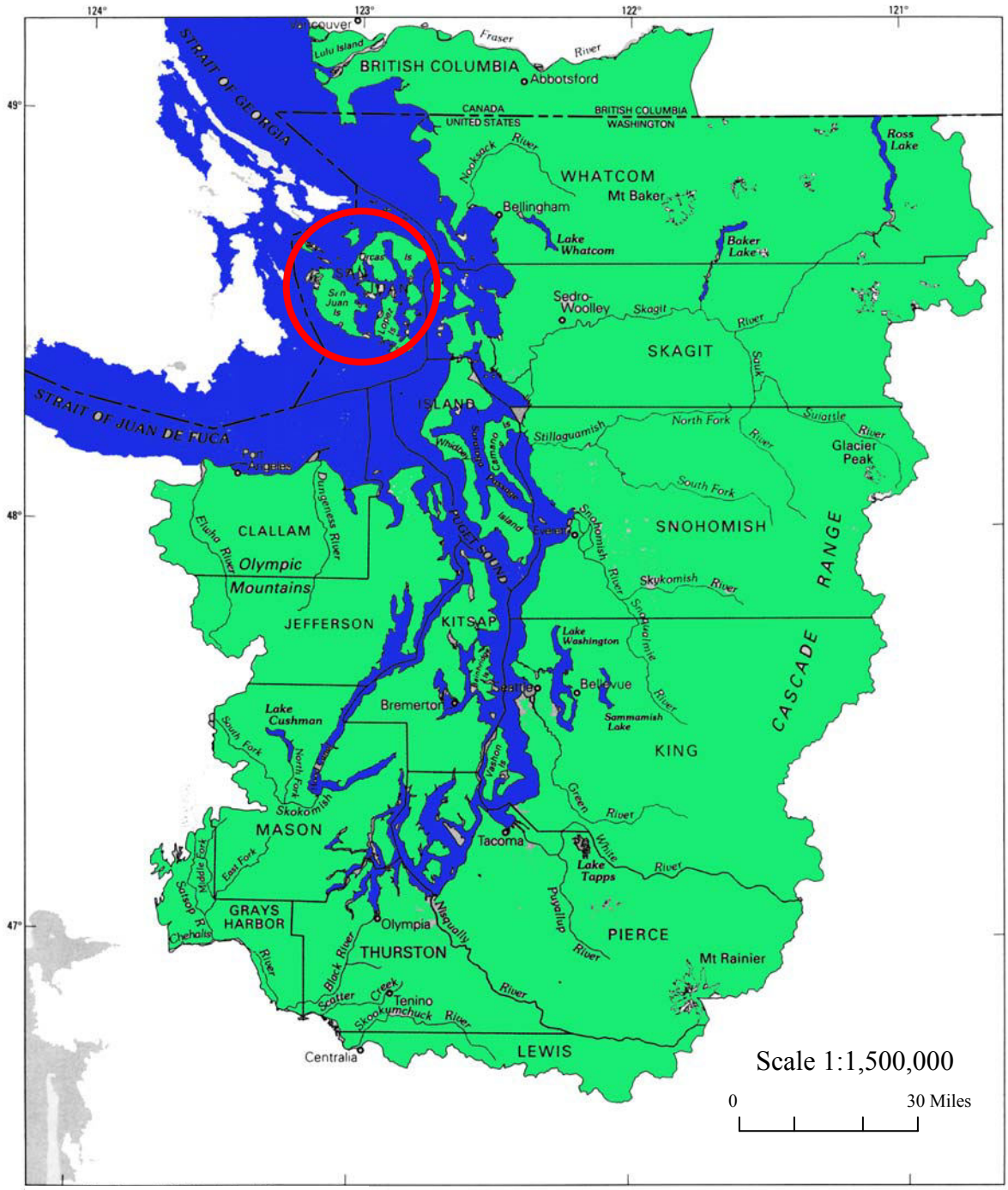

Figure 2.11. Map showing the extent of the Puget Lowland (green) (modified after Jones, 1999). San Juan Islands located within the red circle.

Geologic Climate Units of the Fraser Glaciation	Lithostratigraphic Units of the northern Puget Lowland	Time (^{14}C-yrs B.P. x 10^3)
Sumas Stade	Sumas Drift	10.0 11.3
Everson Interstade	Everson Glaciomarine Drift	13.6
Vashon Stade	Vashon till	
	Esperance Sand	18.0

Table 2.2. Lithostratigraphic and geologic climate units for the Fraser Glaciation in the northern Puget Lowland (after Dethier et al., 1995; Kovanen and Easterbrook, 2001).

Since deposits of the Sumas Stade lie well to the north of the study site, (Kovanen and Easterbrook, 1997) the following discussion will focus on the Vashon Stade and the Everson Interstade. The Vashon Stade represents the maximum advance of the Cordilleran Ice Sheet. The Vashon Stade began around 18 ka and can be identified by the presence of sand and gravel sediment called the Esperance Sand in the Puget Lowland. This sediment was deposited by melt water in front of the advancing glacier, and is therefore termed advance outwash sediment. In the San Juan Islands, the largest volume of Esperance Sand can be found on Lopez Island. When Fraser ice reached the Strait of Juan de Fuca, the ice margin split into two lobes: the Juan de Fuca, which spread westward, and the Puget, which continued south (Figure 2.12). Based on radiocarbon age constraints, Porter and Swanson (1998) estimated that the Cordilleran ice reached its southernmost limit just south of Olympia by ~16,950 years ago, and after only about 100 years began to retreat northward. Maximum ice thickness in the San Juan Islands was around 1500 m, based on the maximum elevation of glacial erratics (Thorson, 1980; Easterbrook, 1992; Kovanen and Easterbrook, 2001).

During retreat of the Fraser ice, rapid glacio-isostatic rebound commenced (Thorson, 1989). According to Dethier et al. (1995), the local uplift rate at Davis Bay was 10 cm/yr. As the ice retreated, marine waters poured in from the Strait of Juan de Fuca eventually creating calving margins on both lobes in northern Puget Sound. According to Dethier et al. (1995), the marine

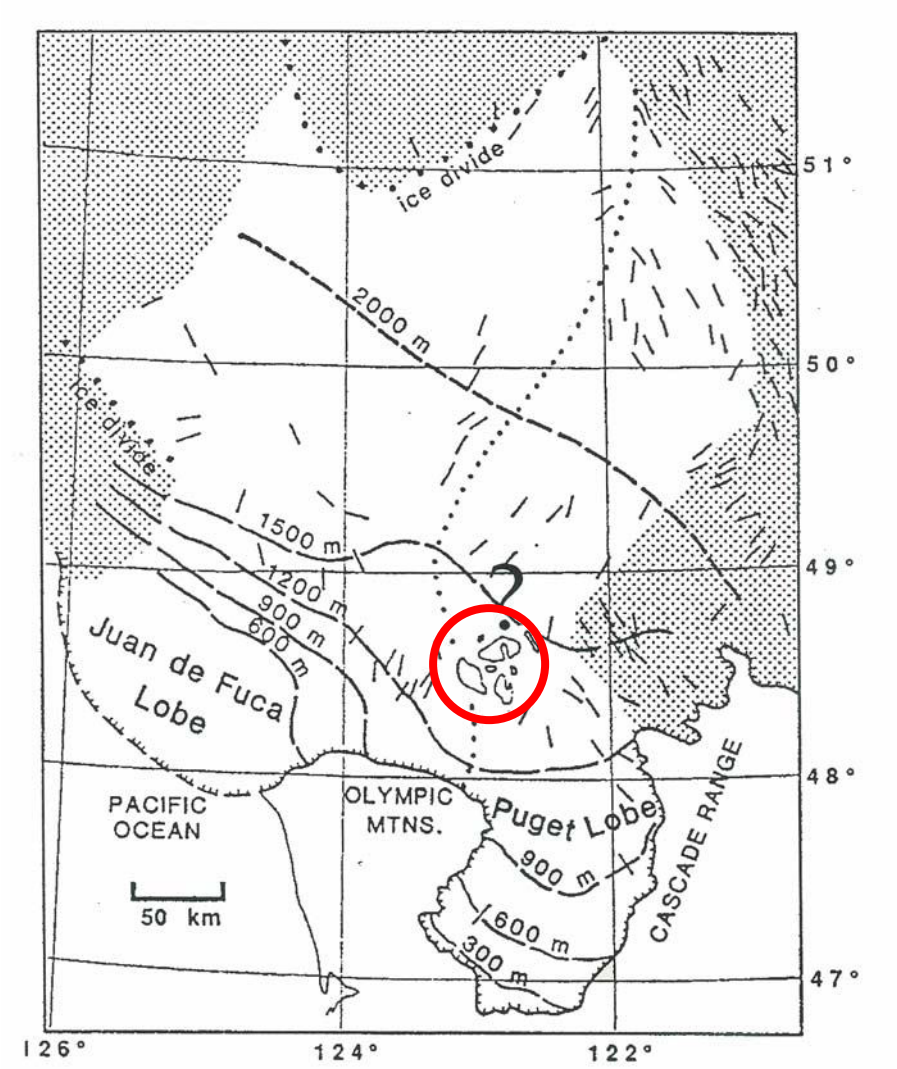

Figure 2.12. Map showing the glacial maxima of both the Juan de Fuca and Puget Lobes, including ice surface elevation contours (dashed lines) and an ice flow divide (dotted line). The short solid lines indicate areas where ice flow directions were measured (modified after Morgan, 1996). San Juan Islands located within red circle. Stippled area represents areas not covered by the Puget and Juan de Fuca ice lobes.

incursion began before 13.6 ka and ended with emergence before 11.0 ka. The maximum marine limit within the SJI was between 90 m in the south and 125 m in the north (Figure 2.13). This period of partial ice retreat resulted in the deposition of glaciomarine sediments called the Everson Glaciomarine Drift. The numerous emerged glaciomarine fans and deltas and submerged banks in the eastern Strait of Juan de Fuca mark grounding line positions of the ice during calving at the time of retreat (Dethier et al., 1995). The ice likely stalled near these deposits due to topographic highs in underlying bedrock, such as were imaged at Salmon Bank by Hirshfield (1996) using seismic reflection profiling. Three of these submerged banks are located within my study site, Middle Bank, Salmon Bank, and McArthur Bank (Figure 2.14). Morgan (1996) speculates that McArthur Bank is an interlobate moraine based on paleoflow indicators showing ice was flowing westward east of the bank and also flowing southwestward within San Juan Channel (Figure 2.14). Part of this study will focus on constraining the present-day surface extents of these banks using multibeam and backscatter data.

3. METHODS

3.1. DATA COLLECTION/PROCESSING

Multibeam bathymetry, multibeam backscatter, and ROV data were collected during three separate research cruises between 2000 and 2002. Both a Reson 8101 240 kHz shallow-water system and a Simrad EM1002 95 kHz deep-water system were used to map the seafloor in the southwestern SJI. Areas within the study site that were not covered by the multibeam surveys mentioned above are represented by NOAA singlebeam data that were gridded to 30 m by Norman Maher. An Hd2 Phantom ROV was deployed in areas where Reson 8101 data had been collected and processed, and these transects provided the basis to verify benthic habitat interpretations and to statistically compare adult rockfish occurrence with seafloor complexity.

3.1.1. Reson 8101 Multibeam bathymetry data

During October 2000, multibeam bathymetry and backscatter data were collected in southern San Juan Channel, southeastern Haro Strait, and the northeastern Strait of Juan de Fuca (Plate 1, Inset C). From here forward the three Reson 8101 survey areas will be referred to as Turn Island, Cattle Pass, and Pile Point. These data were collected using a pole-mounted Reson

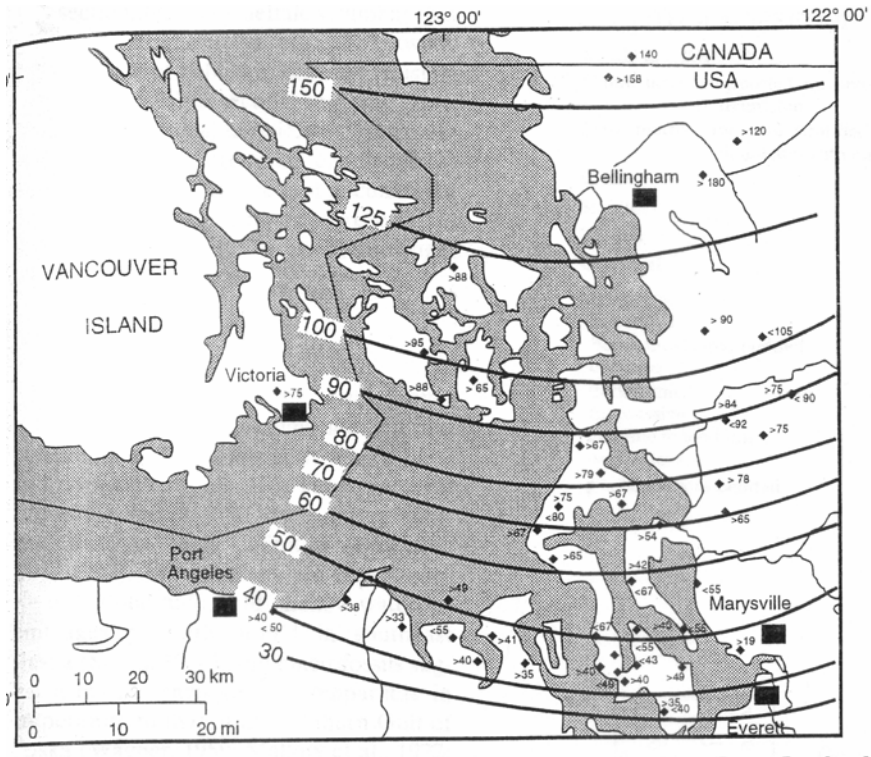

Figure 2.13. Map showing the altitude of the marine limit in the northern Puget Lowland. Contour interval = 10 m south of the SJI and 25 m north of the SJI. Notice marine waters reached between 90 m and 125 m in the SJI (after Hirshfeld, 1996).

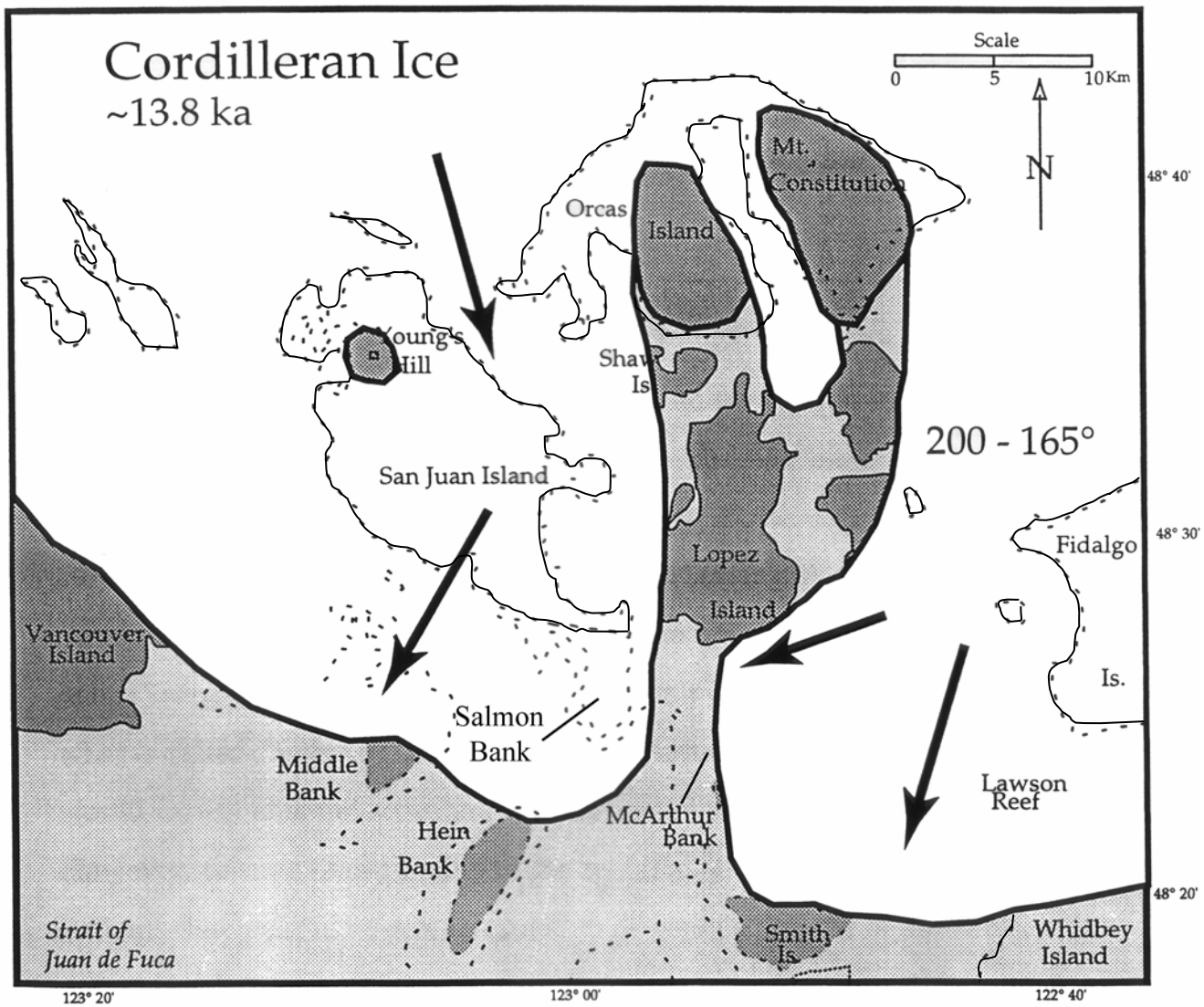

Figure 2.14. Reconstruction of the retreating ice margin ~13.8 ka, showing locations of present-day submerged banks (dashed black lines). McArthur Bank is shown as an interlobate moraine with ice flowing 270° from the east while Salmon Bank and San Juan Channel remain under ice. Middle bank was partially covered by ice at this time. Thin black lines show present island shorelines. Dark grey shading indicates ice-free land areas. The banks were paritally above sea-level at this time. Dotted lines are bathymetric contours. Arrows indicate ice-flow directions (modified after Morgan, 1996).

8101 (240 kHz) echo sounder with 150° swath coverage on the *R/V MacGinitie* of the Seafloor Mapping Lab at California State University (CSU), Monterey Bay. The purpose of these surveys was to collect detailed bathymetric information for further geologic and biologic investigations. Survey depths ranged from 3 m in the nearshore to 300 m in Haro Strait. However, the shallow-water Reson system was only able to collect quality data to approximately 200 m.

The boat's position was accurately recorded using differential geographic positioning system (DGPS) and the attitude information, such as heave, pitch, and roll, were also recorded using a heading motion sensor (HDMS). The data acquisition system logged and integrated data from the sensor components using Triton Elics International (TEI) ISIS® and Coastal Oceanographics Hypack® software. Water column sound velocity profiles were collected daily at each site using an AML SV+ sound velocity profiler. In addition, tidal information was obtained from local tide stations. Data acquisition was maximized for collection of accurate bathymetry rather than backscatter because for identifying geologic structures and complex rock habitats accurate bathymetric information is more important than backscatter intensity. As a result, the quality of the backscatter data was substandard and the data were therefore unusable.

Bathymetric data were processed using CARIS HIPS® hydrographic data cleaning software. Soundings were corrected for vessel motion and water column sound velocity. All soundings were adjusted to mean lower low water (MLLW) using predicted tides for the San Juan Islands. Erroneous soundings were removed in CARIS HIPS® through both automated filtering and manual editing. After processing of all lines for each survey site was complete, the data were exported from CARIS as a geo-referenced sun-shaded (from the NW[4]) images, and as a binned (2 m) ASCII text (xyz) files. Finally, 2 m ArcView ASCII raster (.asc) grids were created from the xyz data using Fledermaus®, a 3D imaging software.

3.1.2. Simrad EM1002 Multibeam bathymetry/backscatter data

During the fall of 2002, additional multibeam/backscatter data were collected through a cooperative agreement between the Geological Survey of Canada, the Canadian Hydrographic Service, and the Center for Habitat Studies at Moss Landing Marine Laboratories. These data were collected in the Canadian and U.S. waters of Haro Strait, northern Strait of Juan de Fuca,

[4] For this study the standard for sun-shaded images was to shade from the NW (~ 315°).

and southern San Juan Channel aboard the Canadian Coast Guard vessel, R/V *Vector,* using a 95 kHz hull-mounted Simrad EM1002 system (Plate 1, Inset C). The ship's position was tracked using DGPS and the attitude information was recorded using Pos-MV® software. This deep water system collected data in water depths ranging from 10 meters along steep shorelines to over 300 meters in Haro Strait.

The EM1002 multibeam bathymetry data used for this study were partially processed onboard-ship. The Simrad system automatically integrated the sound velocity information during data collection. The navigation was checked for errors, and the attitude information was analyzed for anomalies. A depth spike filter was applied to the soundings to remove spurious data and swath editing was performed to manually remove additional erroneous and/or anomalous soundings. Once on land, the data were processed further at the Geological Survey of Canada. This processing included applying a tidal correction based on tide data from two tide stations within the survey area and soundings were adjusted to MLLW. The data were then merged, refraction editing was done, and the data were binned for export in xyz (ASCII) format. Finally, an ArcView ASCII raster (.asc) 10 m grid and a sun-shaded image were supplied for interpretation and post-processing. Gridded NOAA single-beam bathymetry was used for interpretation in the remainder of the study site not covered by either the Reson 8101 or the Simrad EM1002 surveys. The 2-m-gridded Reson 8101, 10-m-gridded Simrad EM1002, and 30-m-gridded NOAA single-beam data were combined to create the sun-shaded image in Figure 3.1.

Processing of the Simrad EM1002 backscatter data was done at the Center for Habitat Studies in Moss Landing using TEI ISIS® software. First, raw Simrad files were converted to .xtf files for compatibility with the ISIS® software. Backscatter data were processed in ISIS® line-by-line, and exported as 0.2 m pixel images. Individual line images were imported into MicroImages TNTmips®, where lines were edited and mosaiced into a single geo-referenced image (Figure 3.2).

3.1.3. ROV Survey

During October of 2002 a 7-day underwater video survey was carried out in southern San Juan Channel and the northern Strait of Juan de Fuca (Figure 3.3) using an Hd2 Phantom ROV, which is owned and operated by the University of Washington's, Friday Harbor Laboratories. This ROV survey was funded in part by NOAA's West Coast and Polar Region's National

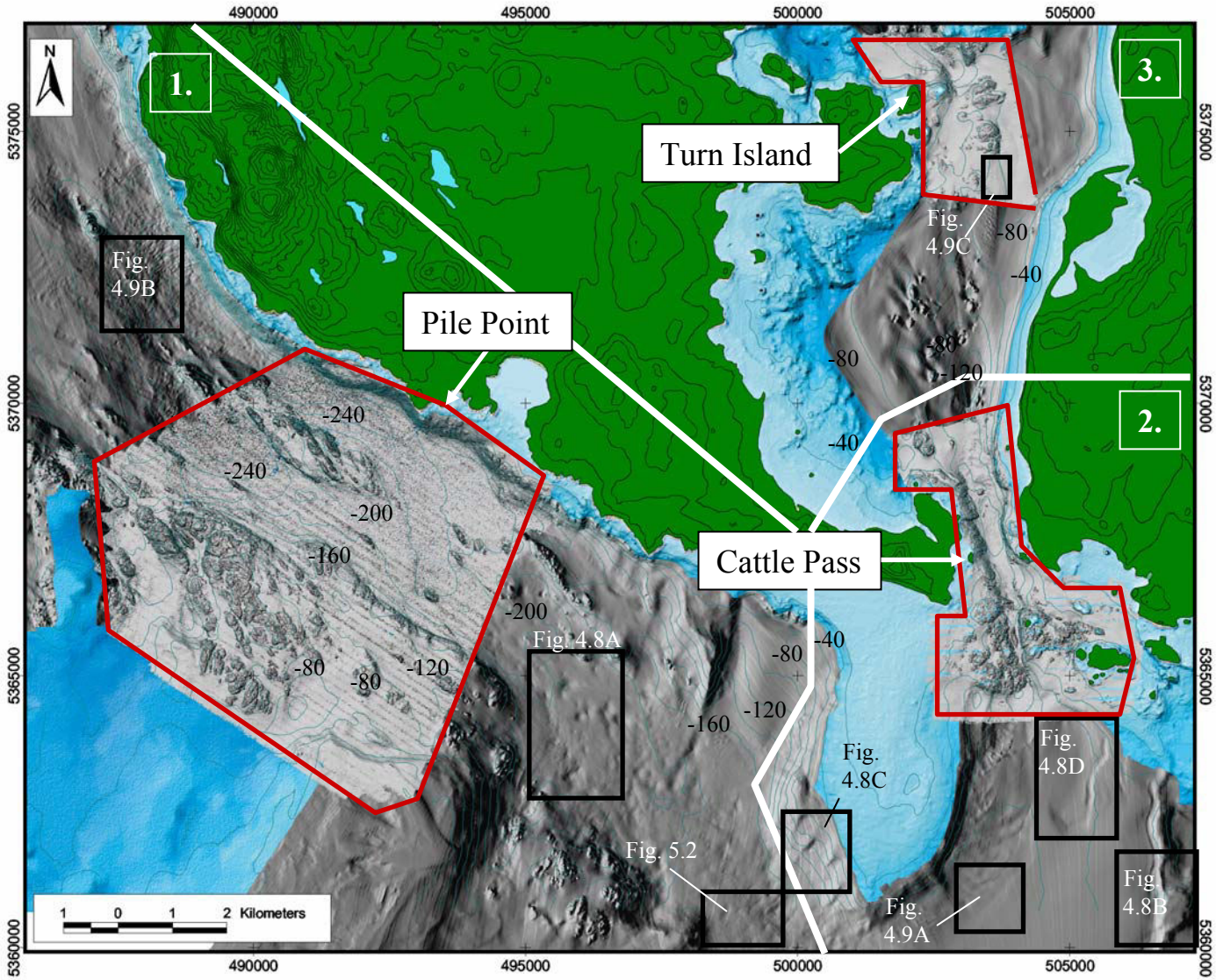

Figure 3.1. Map of Reson 8101 (red outline), Simrad EM1002 multibeam bathymetry (darker grey images), and NOAA single-beam imagery (shaded blue) within the study site. Bathymetry and topographic contour intervals = 20 m. The three Reson 8101 survey areas are referred to as Turn Island, Cattle Pass, and Pile Point in the text. The thick white line denotes the boundaries of Areas 1, 2, & 3 in the discussion.

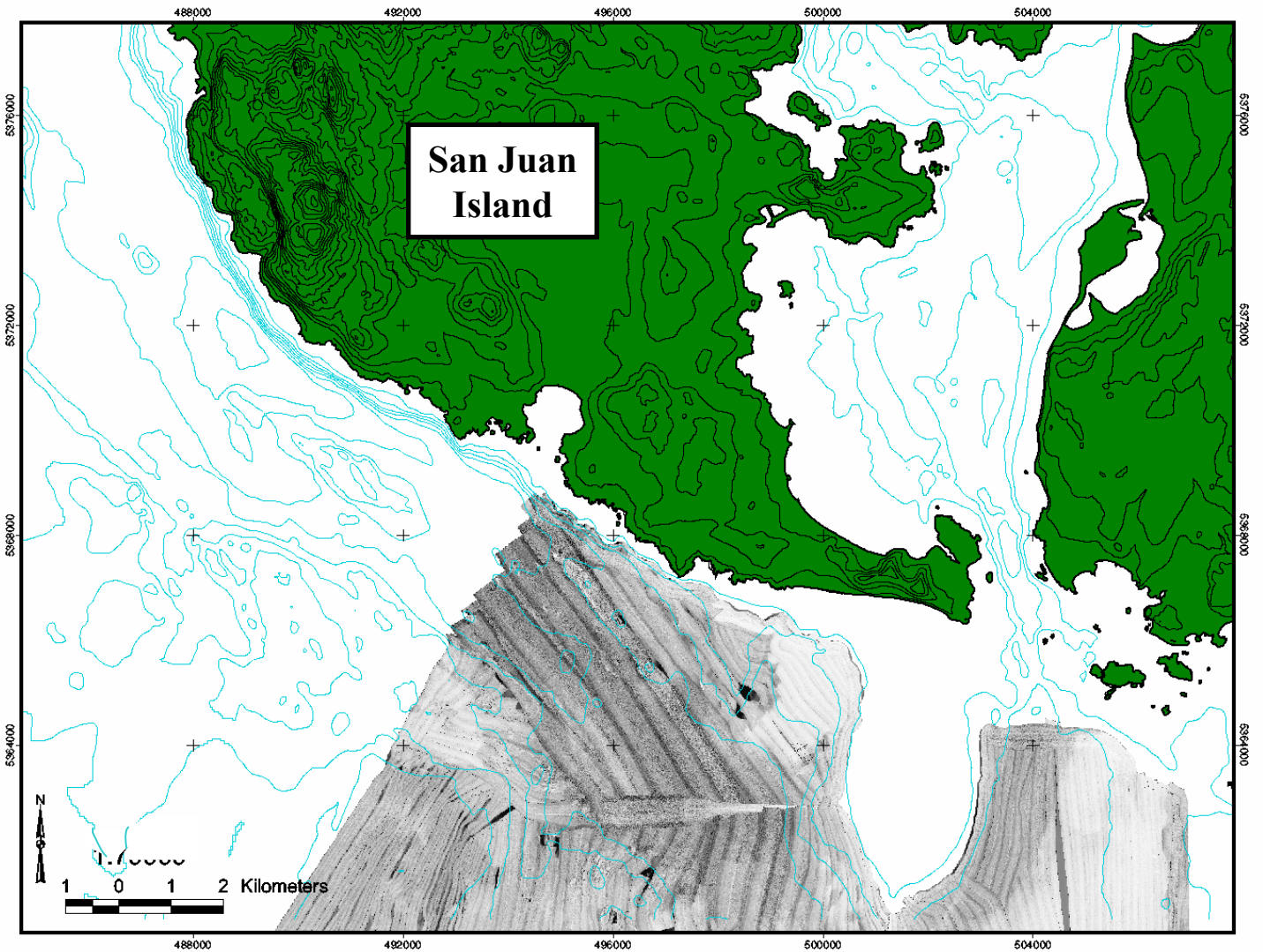

Figure 3.2. Map showing the extent of mosaiced Simrad EM1002 multibeam backscatter data south of San Juan Island. Bathymetric and topographic contour interval = 20 m.

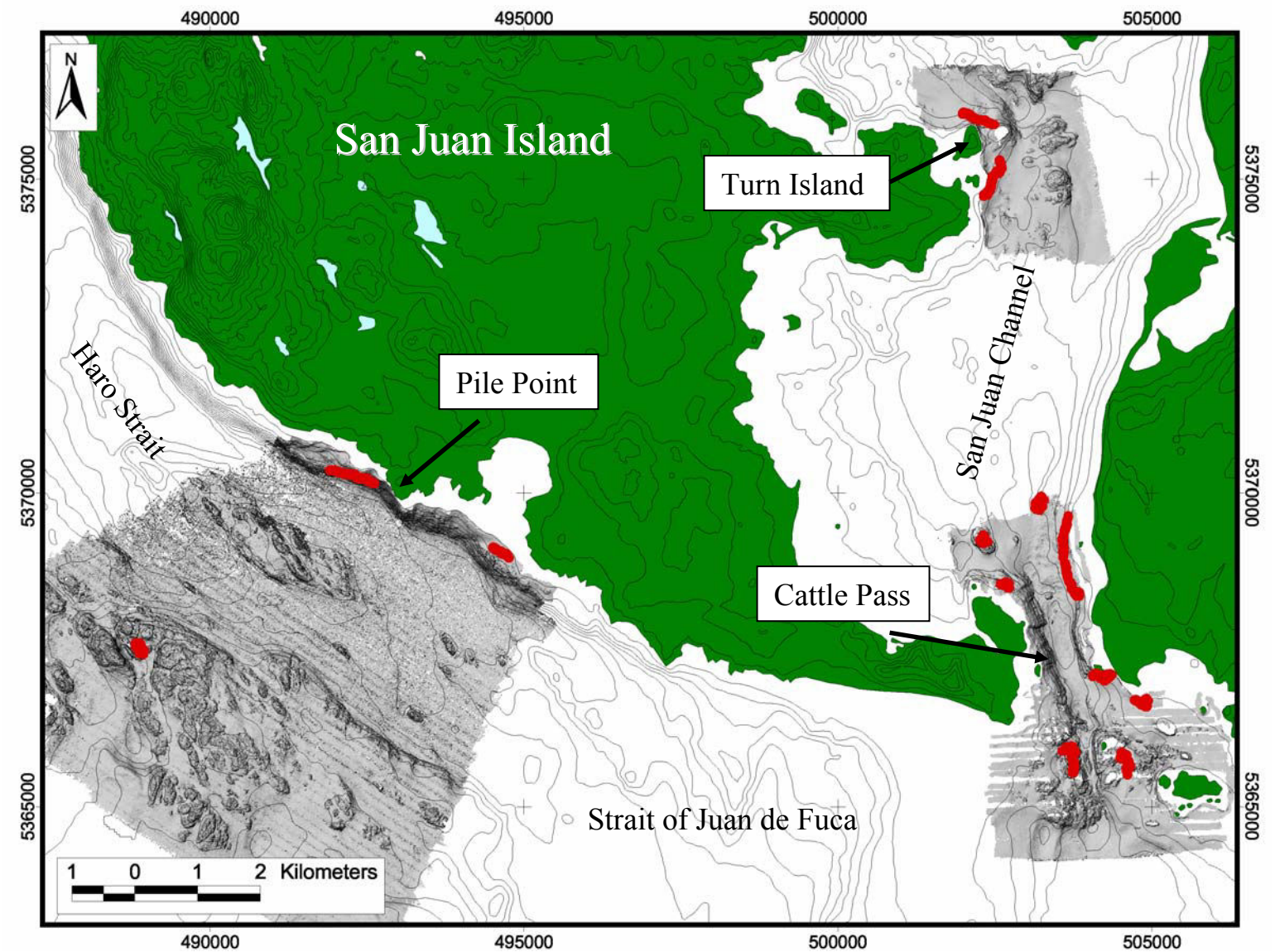

Figure 3.3. Map of three Reson 8101 multibeam bathymetry survey areas, showing where underwater video (ROV) data were collected (Red = transect location). Notice the majority of the transects are in Cattle Pass. Contour interval = 20 m.

Undersea Research Program (NURP) at the University of Alaska, Fairbanks. The ROV was launched from the WDFW vessel, *R/V Molluscan*. This survey was a pilot study to test the capabilities of a small, under-powered ROV for habitat and marine ecological research in the San Juan Islands. As part of my thesis research, the ROV video data were used for groundtruthing marine benthic habitat maps and for describing the general relationship between seafloor complexity and common adult rockfish occurrence to map potential rockfish habitat. Rather than a statistically sound survey design (i.e. random or stratified random), sites were chosen based upon geology, habitat type and diversity, depth, tidal current regime, and MPA boundaries. Dives were made at bottom depths ranging from 13 to 94 m. Each dive was documented on Mini DV digital videocassette and verbally annotated with descriptions of the seafloor and fish identifications. Each dive recorded approximately 50 minutes of video along the seafloor. Two parallel lasers were mounted 10 cm apart on the front of the ROV. These lasers were used to determine the relative sizes of fishes and substrates for general description.

Many of the planned dives were altered and/or abandoned due to the limited ability of the ROV to maneuver in or against tidal currents. Even at slack tide, ~2 knot surface currents in San Juan Channel were observed. To compensate for the lack of thrusting power in the ROV and maximize maneuverability in high currents, the "downweight method" was employed. This method involves attaching a weight (in this case 240 lb. of clump weights in the form of lead balls) at a specified distance along the ROV's tether, allowing the ROV to operate without pulling the entire weight of its tether. This allows the majority of the ROV power to be used for maneuvering in high currents. The ROV's position was recorded using a differential GPS (dGPS) and acoustic Trackpoint® system. Location and time were displayed in real-time on videotape. The horizontal accuracy of the ROV Trackpoint® system was estimated to be approximately 12.5 ft based on the combined accuracy of Trackpoint® and differential GPS (Lance Horn, personal commun., 2002). When the ROV's roll or pitch attitude exceeded the gimbal limits of the compass, which often occurred when the ROV was fighting the current and/or was at the end of the clump-weight tether, the compass would malfunction making navigation along flat bottom or through open water extremely difficult. Based on the results of this pilot study, more rigorous sampling protocols suited to more quantitative and comparative research goals are being employed as part of a joint Moss Landing Marine Laboratories, Center

for Habitat Studies and University of Washington, Friday Harbor Laboratories project funded by Washinton State SeaGrant Program.

3.2. DATA ANALYSIS/INTERPRETATION

3.2.1. Incorporating Existing Data into GIS

Prior to conducting further analysis or interpretation; existing geologic, geophysical, and satellite data were incorporated into ArcView. The existing geologic and geophysical data included the following: onshore bedrock and surficial geology, offshore surficial geology, and regional aeromagnetic data. Table 3.1 provides a detailed list of geologic and geophysical maps and datasets used in this study and Figure 3.4 shows the coverage areas for the existing geologic and geophysical datasets. Onshore bedrock geology and surficial geology information was compiled from digital 1:100,000 scale geologic maps of the Roche Harbor, Bellingham, Port Angeles, and Port Townsend quadrangles (Schuster, 2000) and from a hardcopy geologic map of Victoria, British Columbia (Muller, 1983). Offshore surficial geology information was obtained from a digital map published by Hewitt and Mosher (2001), which had been created based on interpretations of seismic reflection data collected in the eastern Strait of Juan de Fuca (southern portion of my study area). Geologic structures (fault and folds) were acquired from both digital and hardcopy sources. Digital sources included the onshore 1:100,000 geologic maps of Schuster (2000) and the offshore structure map by Johnson et al. (2000). Faults and fold axes mapped by Gower (1985) and Brandon (1988) were compiled from hardcopy maps. Finally, orientations of bedding and/or foliation were obtained from the hardcopy geologic maps of Muller (1980) and Lapen (2000). Information from hardcopy maps was integrated into an ArcView project either as a scanned geo-referenced image, or as digitized features from a scanned geo-referenced image of the original map.

The crustal magnetic anomaly and residual, or shallow-focused, magnetic anomaly data were provided by the USGS (R.J. Blakely, written commun. 2003) and imported into ArcView as geo-referenced sun-shaded images and as grids. Aeromagnetic surveys record the magnitude of the total magnetic field near the earth's surface. The total field, or crustal, anomaly characterizes the magnetic field from the earth's surface to either the crust-mantle boundary or the Curie-temperature isotherm. The crustal anomaly is calculated by subtracting the magnetic

Data Type	Map Scale	Grid Scale	Data Source	Author Citation	Comments
Geologic					
Digital Geology of Washinton	1: 100,000	N/A	WDNR	Schuster, 2000	Compilation of Roche Harbor, Bellingham, Port Townsend, and Port Angeles 1:100,000 quadrangles
Geologic Map of the Bellingham Quadrangle, Washington	1:100,000	N/A	WDNR	Lapen, 2000	Used for bedding / foliation information not supplied in the digital geology map (above)
Geology of Victoria, British Columbia, Canada	1:100,000	N/A	GSC	Muller, 1980	Used digitized structures from this publication
Surficial Geology of the eastern Juan de Fuca Strait	N/A	N/A	GSC / USGS	Hewitt and Mosher, 2001	No Map Scale provided
Tertiary and Quaternary structures of the eastern Juan de Fuca Strait	N/A	N/A	GSC / USGS	Johnson et al., 2000	No Map Scale provided
Seismotectonic map of the Puget Sound region	1:250,000	N/A	USGS	Gower et al., 1985	Used digitized structures from this publication
Late Cretaceous San Juan Thrust System				Brandon et al., 1988	Used digitized structures from this publication
Aeromagnetic					
Puget Sound Aeromagnetic maps	N/A	N/A	USGS	Blakely et al., 2000	Flight lines = 0.25 mile spacing at ~800 feet above the ground (1997 survey)
Bathymetric					
Single beam bathymetry	N/A	30 m	NOAA	N/A	Used both grids and sunshaded images
Reson 8101 multibeam bathymetry	N/A	2 m	MLML / CSUMB	N/A	Used both grids and sunshaded images
Simrad EM1002 multibeam bathymetry	N/A	10 m	MLML / GSC	N/A	Used both grids and sunshaded images
Simrad EM1002 multibeam backscatter	N/A	0.2 m	MLML / GSC	N/A	Used both grids and sunshaded images
Marine Benthic Habitat					
Marine Benthic Habitats of the San Juan Islands	1:12,000	*2 m	MLML	Greene and Tilden, 2002	*Maps created from interpretation of 2 m gridded bathymetry

Table 3.1. This table illustrates the variety of scales and data types used to compile the seamless geologic

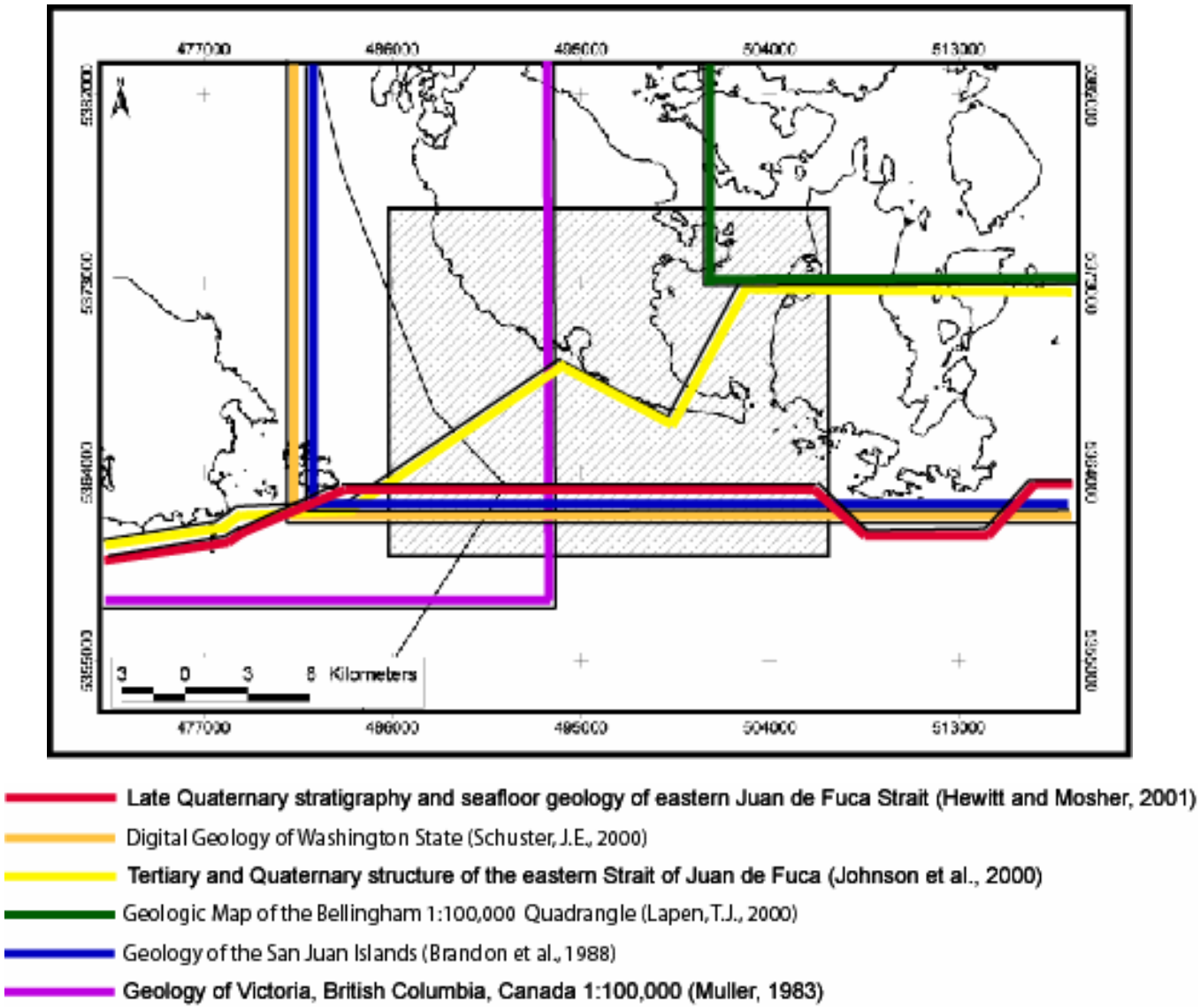

Figure 3.4. Map of existing data coverage used to construct the geologic map in Plate 1. The hatched box outlines the study area. The colored lines indicate the extent of the data coverage (colored line on inside of data area).

field of the earth's core, known as the International Geomagnetic Reference Field (IGRF), from total field measurements (Figure 3.5; Blakely, 1996). The strength of the magnetic field is related to the magnetization of the rocks below the aircraft, which is in turn related to the concentration of magnetic minerals (mainly magnetite) in those rocks (Beaumont and Foster, 1989). In general, mafic rocks contain more magnetic minerals, and are therefore more magnetic, than felsic rocks. The 1997 aeromagnetic survey was flown at an altitude of approximately 800 ft. Flight lines were flown in an EW direction and lines were spaced 0.25 miles apart. To highlight anomalies in the near surface for identifying shallow crustal structures, the total field magnetic data were transformed in a two-step process (R.J. Blakely, written commun. 2003). First, the total field data were continued to a surface 100 m above the original flight path. This process, known as upward continuation, transforms the potential field to that which would be measured on another surface further from the magnetic source. As a result, the shorter wavelength, presumably shallower, anomalies are attenuated and the longer wavelength, presumably deeper, anomalies are emphasized. Because the shallow, short-wavelength, anomalies were of more interest in this study, an additional step was taken. The long-wavelength (upward continued) field was subtracted from the total field, resulting in a short-wavelength shallow-focused dataset. In addition, these data were reduced to the magnetic pole to remove the shadow-effect of a non-vertical dipole. (Figure 3.6).

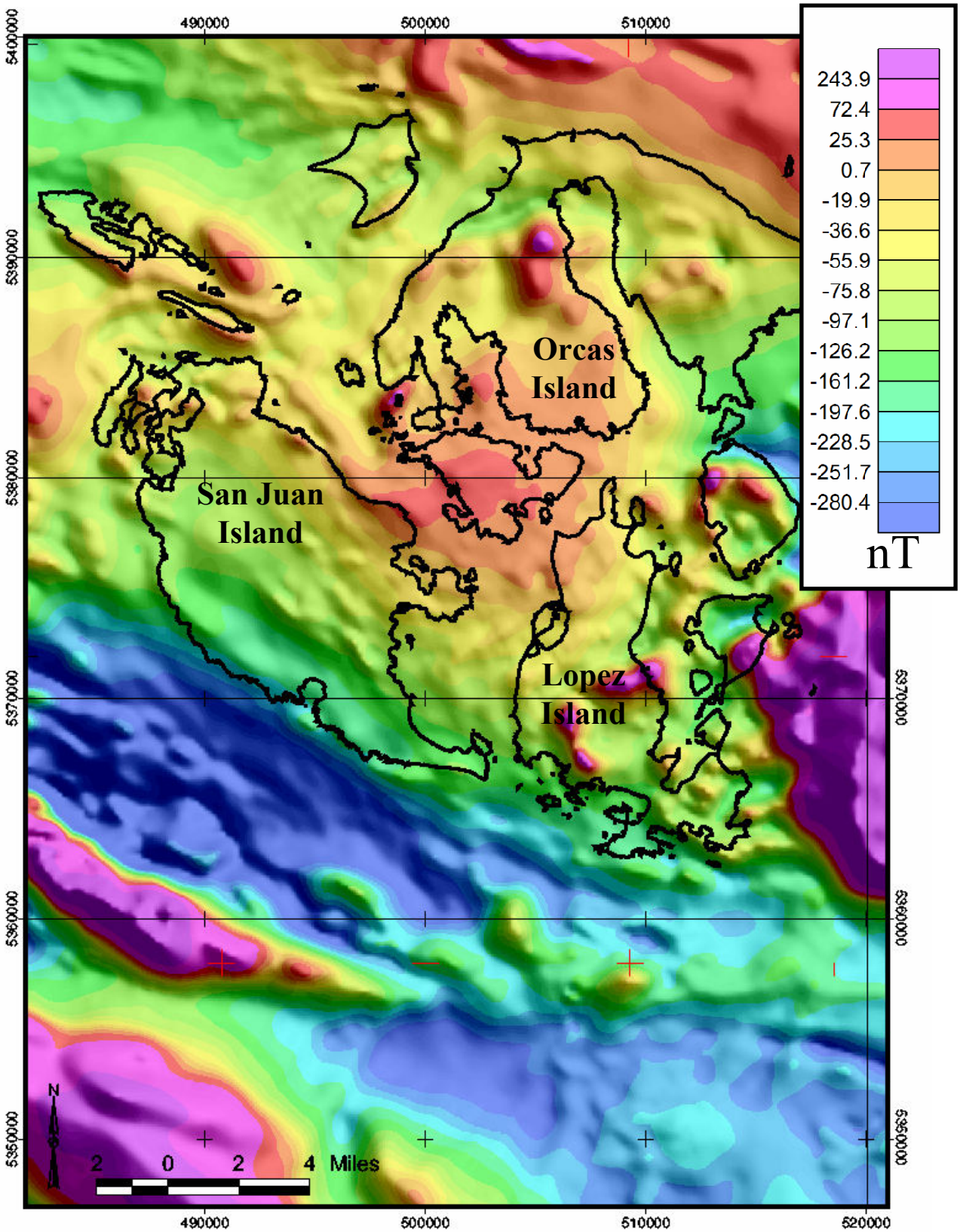

Figure 3.5. Total aeromagnetic anomaly map for the SJI region (R.J. Blakely, written commun., 2003). Islands outlined in black.

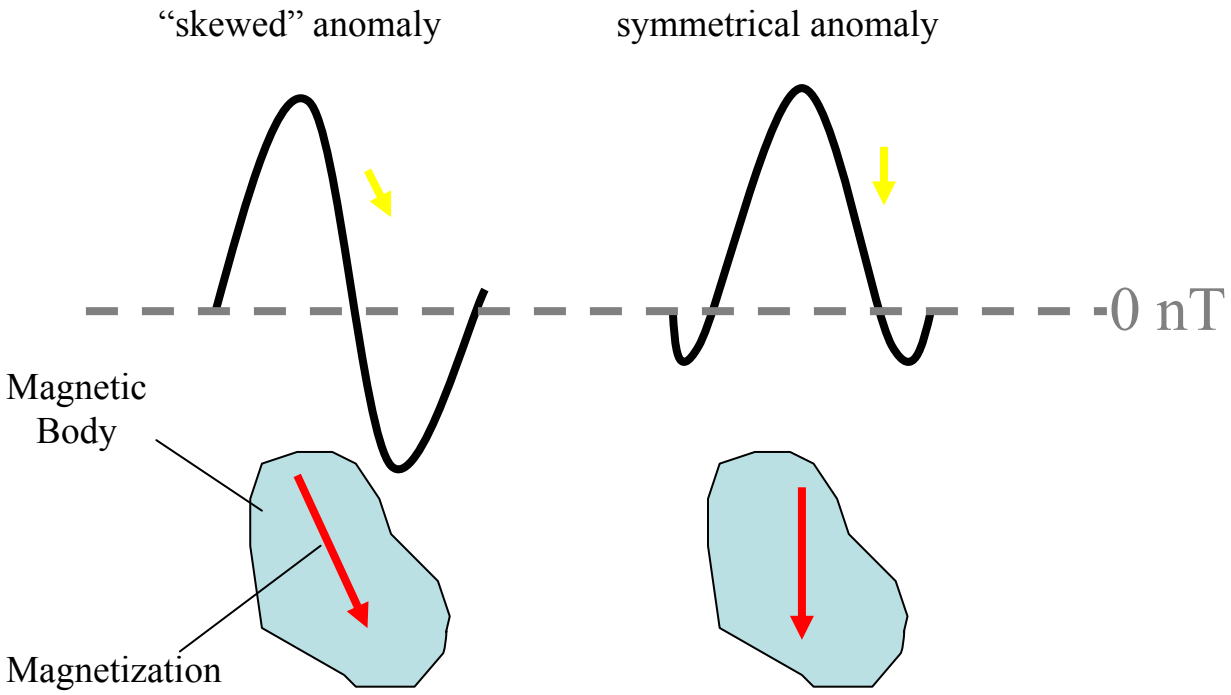

Figure 3.6. Illustration of how a magnetic anomaly is reduced to the pole. The skewed anomaly is recalculated based on the latitude of the survey to be more symmetrical, so that the magnetic source is directly below the magnetic anomaly.

The amount of offset of the positive magnetic anomaly from the source is dependent on latitude. This gridded dataset was artificially sun-shaded from the northwest to highlight anomaly gradients (Figure 3.7). The Buck Bay fault and the boundary between Wrangellia and the San Juan thrust system supposedly juxtapose rock units of different magnetic susceptibilities and of unique structural character. These differences should be reflected in the gradient and pattern of shallow-focused aeromagnetic anomalies and allow for identification of these terrane boundaries.

In addition, a SPOT 4 multi-spectral image was acquired for the SJI and used to identify linear fault-related features on land within the study site (Figure 2.10). The SPOT image contains three color bands; Red, Green, and Near-Infrared (IR). Fault-related features were identified based on the existence of either an abrupt linear change in vegetation or an offset in drainage patterns. Changes in vegetation pattern are interpreted as abrupt changes in coloration of the land surface. Vegetation patterns are linked to soil type, which is related to bedrock lithology, if

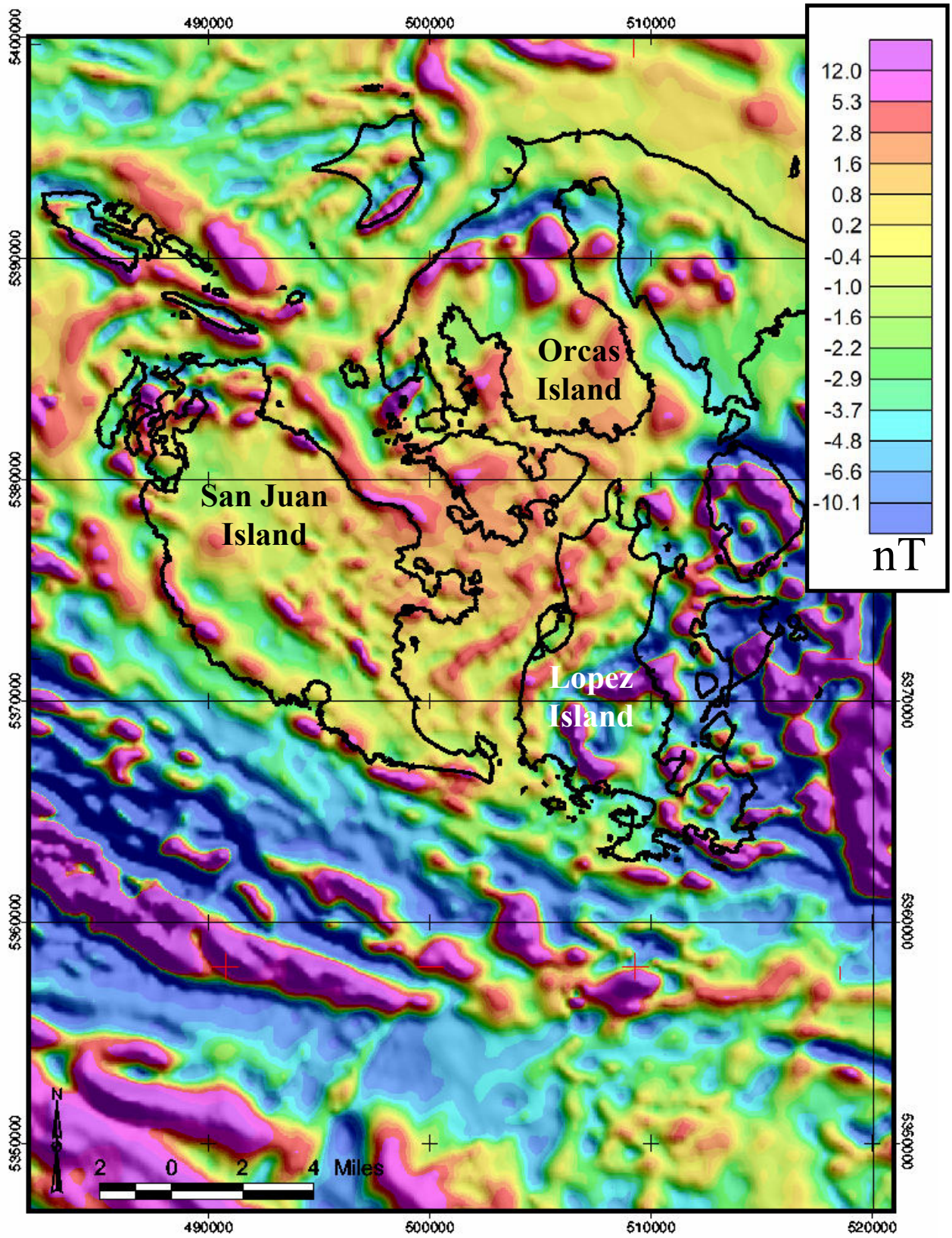

Figure 3.7. Residual (shallow-focused) aeromagnetic anomaly map of the SJI region (R.J. Blakely, written commun., 2003). SJI outlined with black line.

bedrock is close to the surface. Therefore a linear change in vegetation pattern may signify an abrupt change in bedrock lithology across a fault boundary.

3.2.2. Linear Feature Analysis

Structural linear feature analyses were conducted offshore using Reson 8101 data. The purpose of these analyses was to identify and distinguish structural patterns within and among multibeam survey areas and identify faults. For instance, if the Buck Bay fault extension passes through southern San Juan Channel, high-resolution multibeam imagery may provide morphological evidence of its existence in the form of linear seafloor feature(s). Each of the three Reson 8101 survey areas was analyzed separately. Linear features (lineations) within sun-shaded multibeam imagery were digitized manually on-screen in ArcView. For the purpose of this study, a lineation is defined as any linear bedrock or feature that has a length of 100 meters or longer. This length cut-off was chosen because after conducting the lineation analysis multiple times for each site, the repeatability of digitizing the lineations became poor with linear features with lengths shorter than 100 meters. Lineations were identified for each site in a systematic fashion as to reduce human bias and error. At each site lineations were digitized at a number of scales beginning with the scale at which the entire site could be viewed on the screen (Figure 3.8). The coarsest scale of analysis was 1:53,000 for Pile point, 1:37,000 for Cattle Pass, and 1:21,000 for Turn Island. At each finer scale, lineations were digitized while systematically panning across the image until the entire image had been viewed. The finest scale at which analysis was performed was 1:2,000, which was the scale at which the image started to become pixelated. All survey areas became pixilated at this scale because they were all gridded to the same 2 m resolution. Each site was completely analyzed at least three times at a range of scales. Finally, lineations <100 m in length were removed from the datasets using the querying function in ArcView.

After lineations had been identified and digitized, length and azimuth were calculated for each lineation using the ArcView extension XTools and the data were plotted on rose diagrams using GEOrient© software. Linear feature orientations were plotted with length-azimuth overlying frequency-azimuth rose diagrams. A frequency-azimuth rose diagram plots data frequency against azimuth direction, whereas a length-azimuth rose diagram plots cumulative length against azimuth direction. The latter emphasizes longer lineations. The following statistics

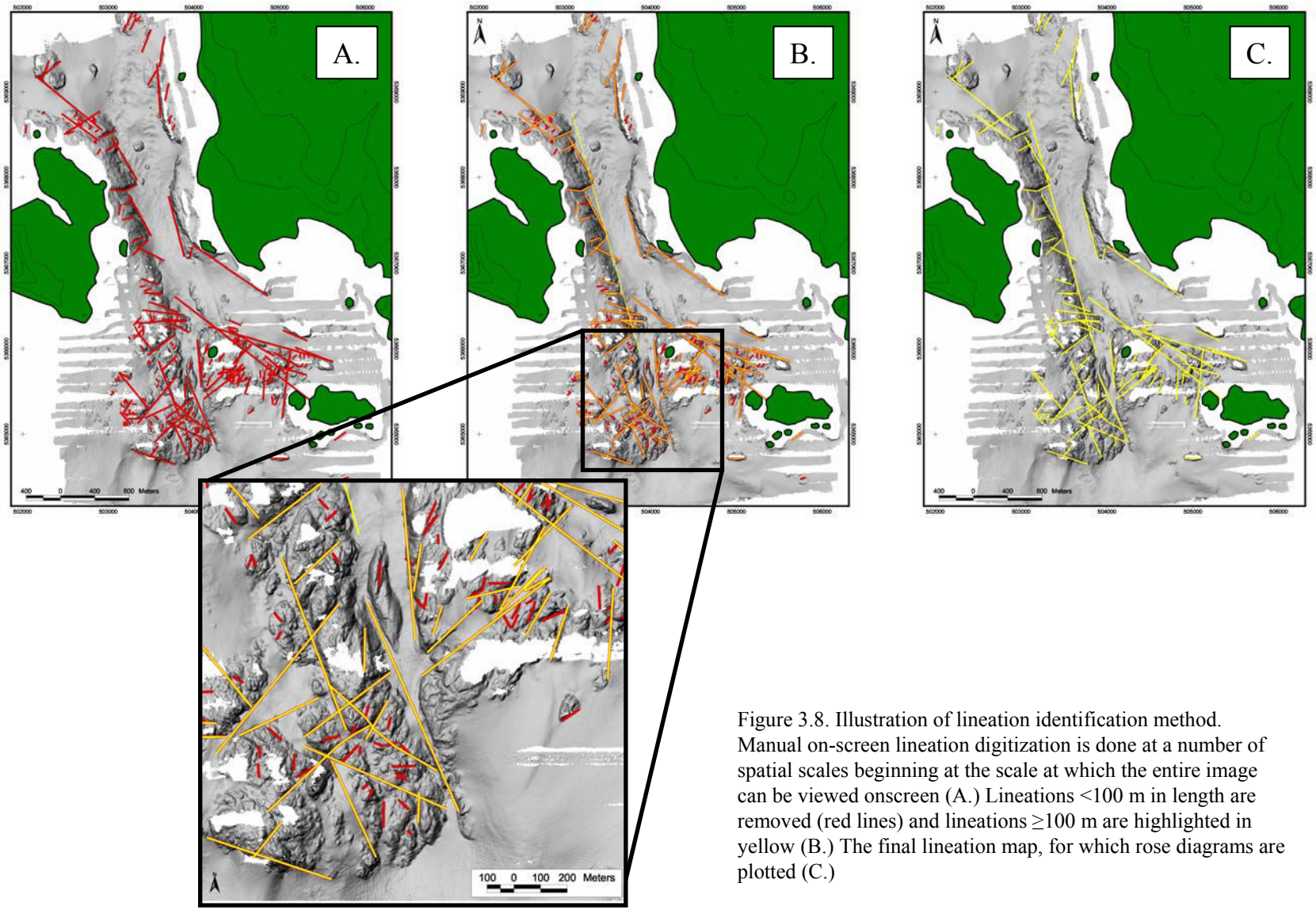

Figure 3.8. Illustration of lineation identification method. Manual on-screen lineation digitization is done at a number of spatial scales beginning at the scale at which the entire image can be viewed onscreen (A.) Lineations <100 m in length are removed (red lines) and lineations ≥100 m are highlighted in yellow (B.) The final lineation map, for which rose diagrams are plotted (C.)

were generated by GEOrient for the length-azimuth rose diagrams: maximum linear feature length, total length of all features, mean resultant direction, and the 95% confidence interval for the mean resultant direction.

3.2.3. Seafloor Textural and Morphologic Characterization

Sun-shaded Reson 8101 multibeam data and observational data from the ROV were used to visually classify the seafloor into benthic habitats according to the modified Greene et al. (1999) habitat classification scheme (*Appendix A*). Interpretations were sketched on clear mylar sheets overlain on sun-shaded multibeam imagery at a scale of 1:6,000 for the Turn Island site and at a scale of 1:12,000 for both the Davis Pt. and Pile Pt sites. The mylar sheets were scanned, geo-referenced and vectorized using TNTmips®. The vector interpretation files were edited and then exported as polygon shapefiles for further processing in ArcView. In ArcView the individual polygons were assigned a GIS habitat code (modified after Greene et al., 1999, *Appendix A*). A habitat map is very similar to a surficial geologic map, but different in some respects. For one, a surficial geologic map focuses on lithostratigraphy rather than on texture and grain size.

Reson 8101 multibeam bathymetry, Simrad EM1002 multibeam bathymetry, Simrad EM1002 multibeam backscatter, and NOAA single-beam imagery, were used in conjunction with the marine benthic habitat maps to classify the seafloor into surficial geologic units. Marine benthic habitat maps were compiled only for the three Reson 8101 survey areas. Marine benthic habitat polygons were modified and combined with the surficial geology information of Hewitt and Mosher (2001), to compile the marine geology polygons at Turn Island, Cattle Pass, and Pile Point. The remaining seafloor within the study site was classified into surficial geologic units using on-screen digitizing of polygons. On-screen interpretation of both the 10 m resolution Simrad EM1002 multibeam bathymetry data and the 30 m resolution NOAA single-beam data was done at a scale of 1:30,000. The Simrad EM1002 multibeam backscatter data were interpreted using an on-screen resolution of 1:6,000, keeping in mind each pixel in the multibeam backscatter imagery represents 0.2 m. To create the final seamless map, the Reson 8101 interpretations were merged with the on-screen interpretations by editing and merging adjacent polygons within ArcView.

The seafloor was characterized based on surface texture and morphology visible in the sun-shaded multibeam bathymetry and multibeam backscatter imagery where available. First, bedrock outcrops were distinguished from areas of unconsolidated sediment. Bedrock outcrops were assigned a formation name when direct onshore comparisons could be made. When no direct onshore comparison could be made, bedrock outcrops were distinguished based on differences in linear feature pattern(s) within outcrops and related to a particular formation. Unconsolidated sediments are classified into surficial deposits based on multibeam backscatter intensity, surface texture and morphology visible in sun-shaded multibeam bathymetry images and the mapping of Hewitt and Mosher (2001).

3.2.4. Index of Complexity

Three objectives were established to quantitatively identify potential adult copper and quillback rockfish habitats. The first involved characterizing the seafloor with an index of complexity in a manner that highlights potential rockfish habitat. The second objective was to use video observations from the ROV survey to assess the usefulness of such a complexity index to predict potential adult rockfish habitats (refer to section 3.2.5 below). Based on the results of the second objective, the third objective involved integrating the qualitative marine benthic habitat maps created for this study to improve the predictive capabilities of the more quantitative method.

A seafloor complexity index was created from analyses of 2 m bathymetric grids (1 sounding every 2 m horizontal), modified after Fox et al. (1999). An ArcView extension called "Surface Areas and Ratios from Elevation Grid" (Jenness, 2001) was used to measure seafloor rugosity, which is the parameter used as a proxy for complexity. More specifically, this extension calculated a ratio of surface area to planimetric area for a given neighborhood (group of cells) in the bathymetry grid. For this study, a 3 x 3 cell area was used, which translates to 36 m^2 (6 m x 6 m). This was the smallest neighborhood of cells that could be analyzed using this technique. The program first connects the center points of each bathymetry grid cell in the neighborhood to create an artificial surface. The center 2 m x 2 m area is then extracted from that artificial surface and the surface area to planar area ratio of that 2 m x 2 m cell is calculated (Figure 3.9). Finally, the program creates a 2 m grid with each cell having a rugosity value assigned to it. The higher the value, the more rugose and thus complex is the seafloor in that

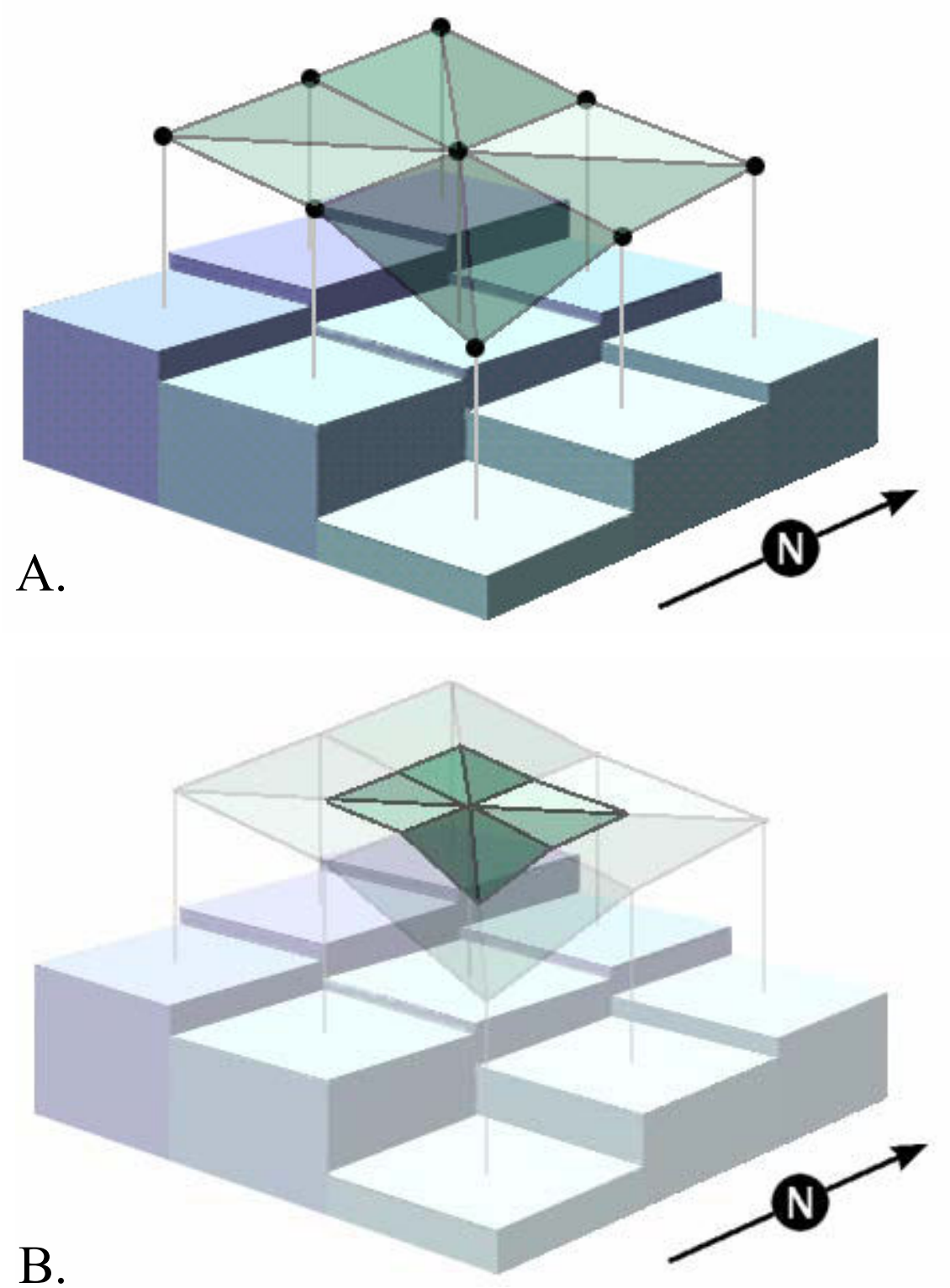

Figure 3.9. Illustration of how the ArcView extension "Surface Areas and Ratios from Elevation Grids" calculates a rugosity value for each 2 m cell. First, an artificial surface is created by connecting the center points of 9 adjacent cells (A) and then that surface is truncated to 2 m x 2 m (B) before the ratio is calculated (Jenness, 2001).

area. The index values are not independent of each other because the rugosity value of one cell is dependent on the depth values of adjacent cells. This is an inherent problem in the surface analysis program used in this study.

Initially, the rugosity grids from each survey area were analyzed in ArcMap 8.3® using natural breaks statistical analysis to try and identify complexity categories objectively. Unfortunately, the results of these analyses were greatly affected by the "noise" in the data and did not adequately distinguish rock from non-rock substrate as interpreted from multibeam imagery. On the other hand, the natural breaks statistical analysis consistently broke the rugosity datasets into three categories, which lead to the decision to arbitrarily define three categories of seafloor complexity. Ultimately, rugosity ratios were grouped into three categories (low, intermediate, and high) based on the following criteria. The low complexity category encompassed a range of rugosity ratios that corresponded to areas of seafloor that appeared flat and featureless on the multibeam sun-shaded imagery. The lower limit of the intermediate category was defined by the appearance of a hummocky seafloor and/or the existence of bedforms (sand waves), whether on a slope or on flat seafloor (Figure 3.10A). The intermediate complexity category also consistently highlighted intermittent role error in the multibeam data (Figure 3.10B). Only areas mapped as bedrock in the qualitative marine benthic habitat maps were included in the high complexity category (Figure 3.11).

3.2.5. Habitat Utilization Analysis

Prior to collecting the ROV video data, I explored the relationships between seafloor complexity and adult rockfishes using underwater video data provided by the WDFW (W.A. Palsson written comm., 2000). These data had been collected over a five-year period during the summer months of 1993 to 1997 using a non-baited drop camera system. Drop camera locations where adult copper and quillback rockfishes were identified were overlaid on the seafloor complexity maps to evaluate the relationship between rockfish occurrence and seafloor complexity. Of the adult rockfishes observed, 83% were on seafloor characterized as high complexity (Figure 3.12). These drop camera data were sparsely distributed throughout our study area and insufficient for further statistical analysis

ROV video data collected offshore southern San Juan Island were analyzed to assess the utilization of seafloor complexity by adult rockfishes. As part of this habitat utilization analysis,

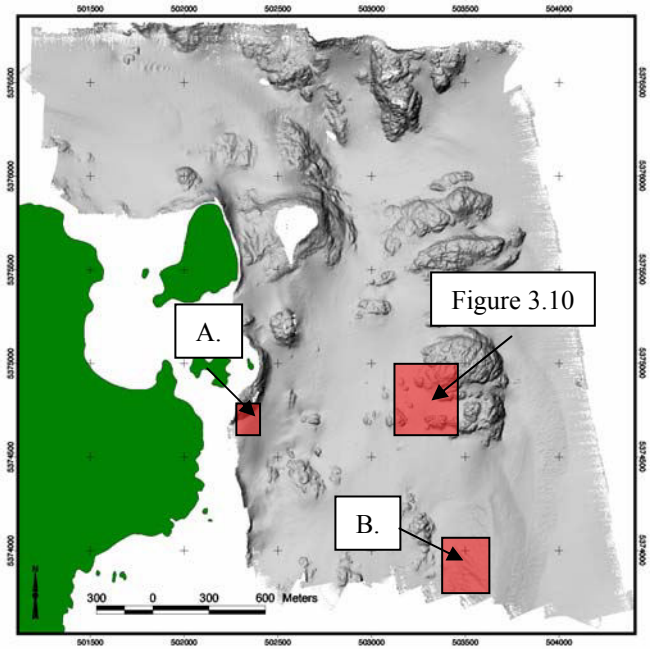

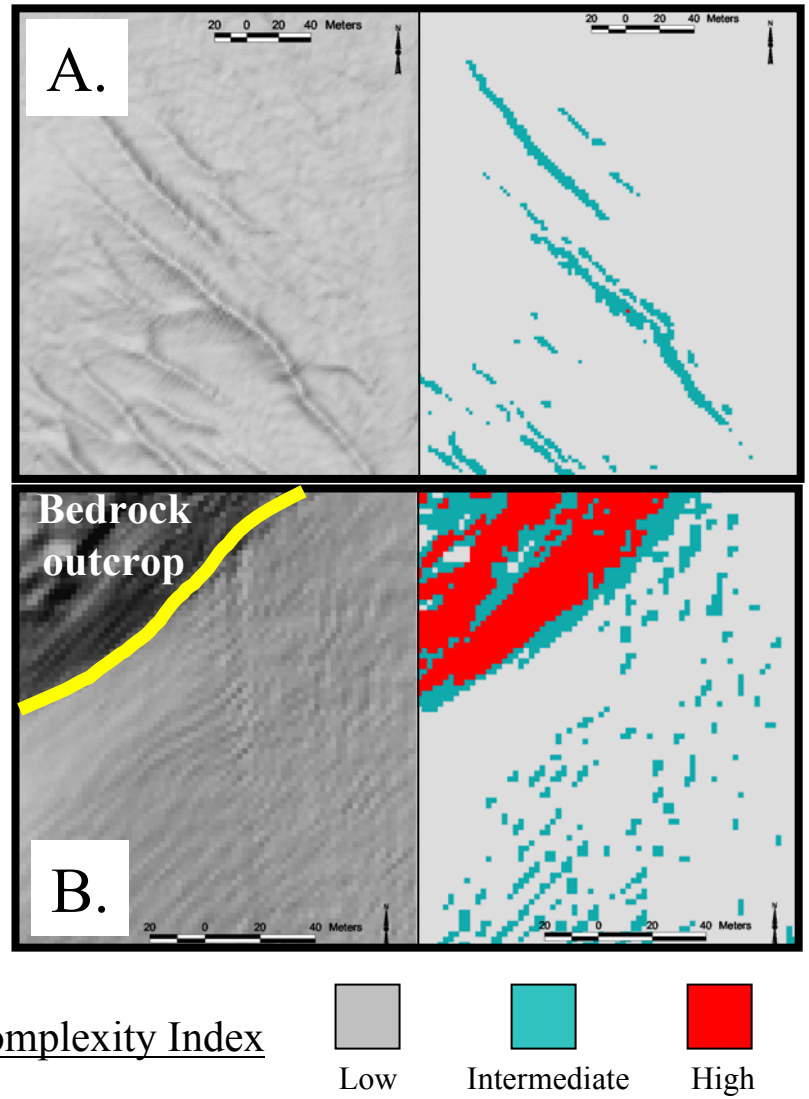

Complexity Index

Low Intermediate High

Figure 3.10. Examples of multibeam imagery and the corresponding seafloor complexity map for areas within the Turn Island multibeam survey area (above). The lower limit of intermediate complexity was determined based on the existence of visible bedforms and/or hummocky seafloor (A.). (B.) illustrates the existence of role error in the multibeam data (left below yellow line) corresponding to the intermediate complexity seafloor (right).

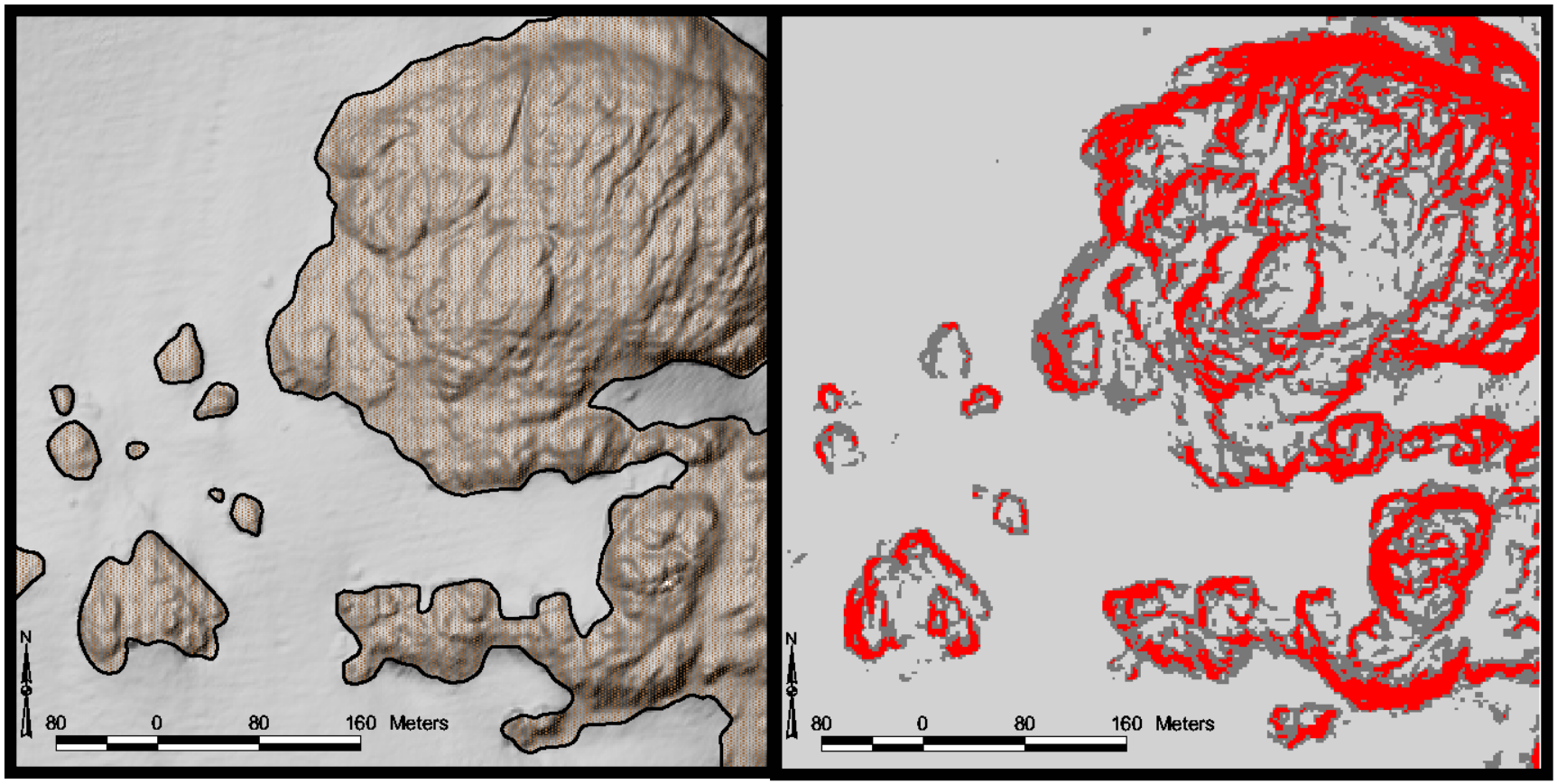

Figure 3.11. Sun-shaded multibeam image showing seafloor mapped as rock habitat on the left (hatched) and the corresponding seafloor complexity map (right). Red = high complexity, dark gray = intermediate complexity, and light gray = low complexity.

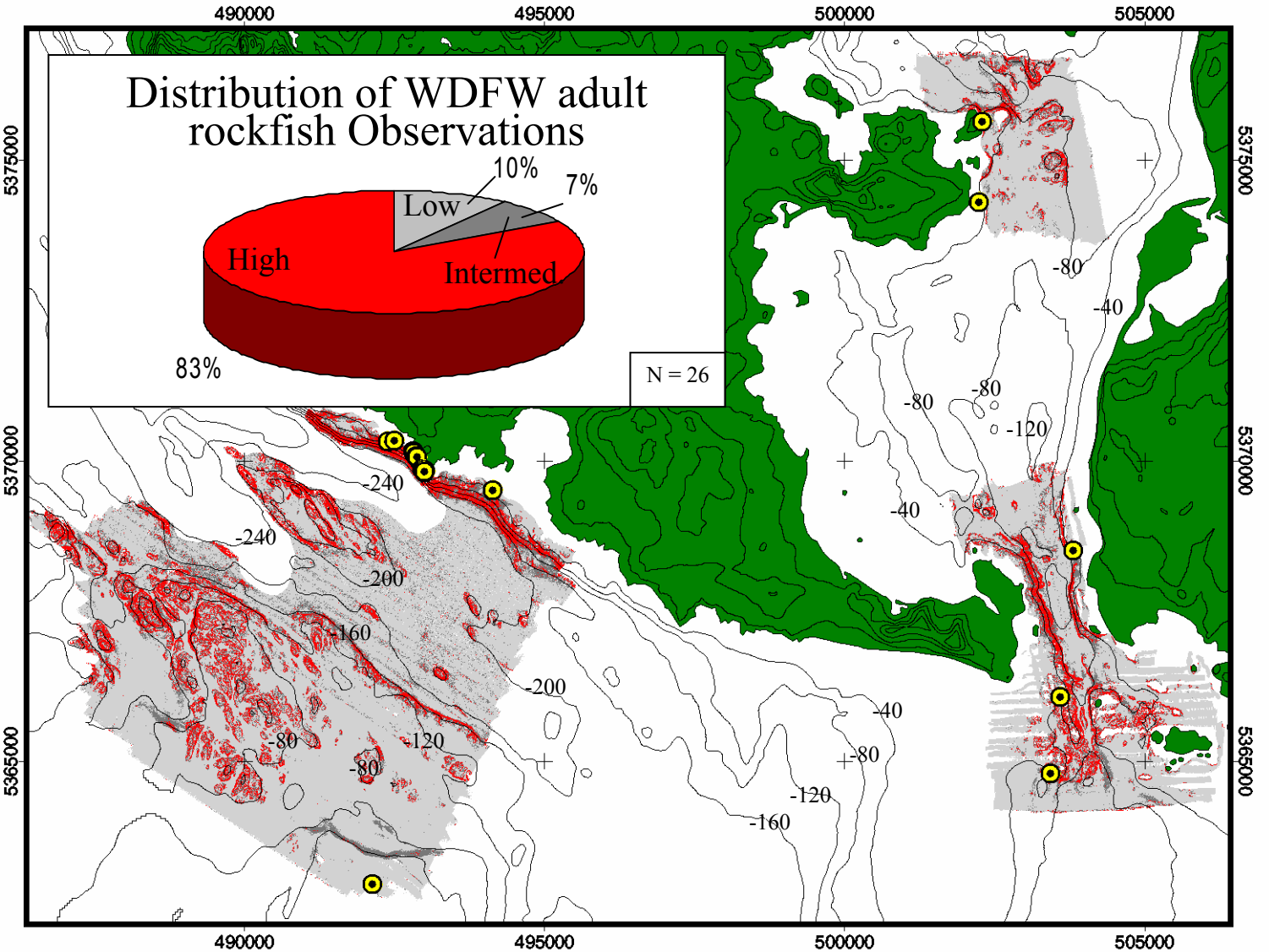

Figure 3.12. Pie chart and map showing the locations of adult copper and quillback rockfish (yellow circles) observed by WDFW drop cameras on low, intermediate, and high complexity seafloor as measured from multibeam bathymetry. Bathymetry contour interval = 40 m and topographic contour interval = 20 m.

the following null hypothesis was tested: adult rockfish occurrence is independent of seafloor complexity as measured using multibeam bathymetry data. Locations of adult copper and quillback rockfishes were recorded only when fish were observed in a stationary position. Locations were reported in decimal minutes, as the ROV passed over the position where an individual fish was initially observed. Following completion of video analysis, the locations of copper and quillback rockfish were first transformed to Universal Transverse Mercator (UTM) grid coordinates using TNTmips and then plotted in ArcView atop the complexity data (2 m grids). Each of the three categories of complexity were assigned an integer value (Low = 1, Intermediate = 2, and High = 3).

Locations of adult rockfishes were matched with the complexity value in the grid cell directly underneath using Grid Analyst, an ArcView extension which extracts x, y, z grid information for an overlying point theme. The z value represents complexity (surface area to planar area ratio). The same was done with points from the navigation file of the ROV, collected every two seconds, to estimate the total availability of seafloor complexities. The navigation files were edited so that only locations where the ROV was on bottom were analyzed. It should be noted that the ROV speed and distance above the seafloor were not constant; therefore area swept could not be calculated. Data from thirteen dives were utilized during analysis. Since dives could not be considered independent samples, the entire dive survey was considered a sample of the population. Treating each dive as a sample did not make sense given the small number of rockfishes observed. Individual fish occurrences along each transect were assumed to be independent.

To assess habitat use (in this case habitat = complexity) of adult rockfishes, I conducted a habitat utilization analysis by combining and modifying the methods of Manly et al. (2002) and Neu et al. (1974). First, Manly's α (alpha) was used to create a habitat selection index (Manly et al., 2002; Krebs, 1999). Selection is a process in which an animal chooses a resource. An animal is considered selective if it uses a resource disproportionately to the availability of that resource (Johnson, 1980). This resource selection index is often used to establish an animal's utilization of a particular resource (in this case rockfishes' utilization of benthic habitats). It was assumed that fish were sampled randomly, the fishes' utilization of complexity was independent of utilizations by other animals, and seafloor complexities were equally available to all fish (Manly et al., 2002). The formula for estimating α is the following:

$$\alpha_i = r_i/n_i \ (1/\Sigma \ (r_j/n_j))$$

where;

α_i = Manly's α (utilization index) for complexity category i

r_i , r_j = Proportion of complexity i or j inhabited (i and j = 1,2,3,…m)

n_i, n_j = Proportion of complexity i or j available

m = Number of complexity categories

When complexity utilization occurs, $\alpha_I = 1/m$. If α_I is greater than $1/m$, then complexity category i is utilized. On the other hand, if α_I is less than $1/m$, then complexity i is not utilized. For this study an alpha value of 0.333 (1/3 categories of complexity) or higher indicates utilization. The resultant alpha values measure the probability that an individual seafloor complexity is selected when all complexity categories are equally available.

To assess the validity of Manly's index, two additional statistical tests comparing expected and observed proportions of fish in each category were conducted. This analysis was modified after Neu et al. (1974) by using a log-likelihood test with a G statistic instead of a χ^2 analysis because expected values were small and G is likely to result in a more powerful test (Zar, 1996). A log-likelihood test using a G statistic was used to test whether adult rockfish distributions were proportional to complexity distributions.

$$G = 4.60517 * (\Sigma f_i \log_{10} fi/Fi)$$

where;

f_i = the observed frequency of fish in each category of complexity

and;

Fi = the expected frequency of fish in each category of complexity

To determine the statistical significance of utilization for each seafloor complexity category, individual confidence intervals were calculated for the proportion of fish observed to determine whether expected values were within the range of significance for observed proportions. Confidence intervals were generated using Bonferroni normal statistics (Neu et al., 1974).

$$p_i - Z_{(1-\alpha/2k)} * [(p_i(1-p_i)/N)]^{-2} \leq p_i \leq p_i + Z_{(1-\alpha/2k)} * [(p_i(1-p_i)/N)]^{-2}$$

Where;

$Z_{(1-\alpha/2k)}$ = Bonferroni statistic ($\alpha = 0.05$, k = the number of categories)

p_i = theoretical proportion of fish expected in the *i*th complexity category

N = the total number fish observed

4. RESULTS

4.1. SPOT IMAGERY

The location of inferred fault trace "**A**" in Figure 4.1 is based on a distinct lineation visible in a SPOT satellite image of San Juan Island. The lineation runs through Trout Lake south to a valley just north and west of Pile Point. The fault appears to offset the Rosario fault zone right-laterally by approximately 0.6 km. The fault also appears to continue to the shoreline, but the surface trace is difficult to distinguish between the valley and the shoreline. Inferred fault trace "**A'**" offshore False Bay appears to connect to trace "**A**" onshore, giving an inferred fault length of approximately 8 km. Based on the apparent offset of the Rosario fault zone, the inferred fault must be late Cretaceous or younger.

4.2. ROSE DIAGRAMS

A total of 430 linear features were analyzed among all three Reson 8101 survey areas with 96 at Turn Island, 101 at Cattle Pass, and 233 at Pile Point. Linear features and corresponding rose diagrams are displayed in Figure 4.2. Lineations were plotted by frequency (blue outline) and by length-weighted frequency (red). The length-weighted plots helped constrain the linear feature distribution for each site, particularly for Pile Point and Cattle Pass, where the frequency plots had widely dispersed directions.

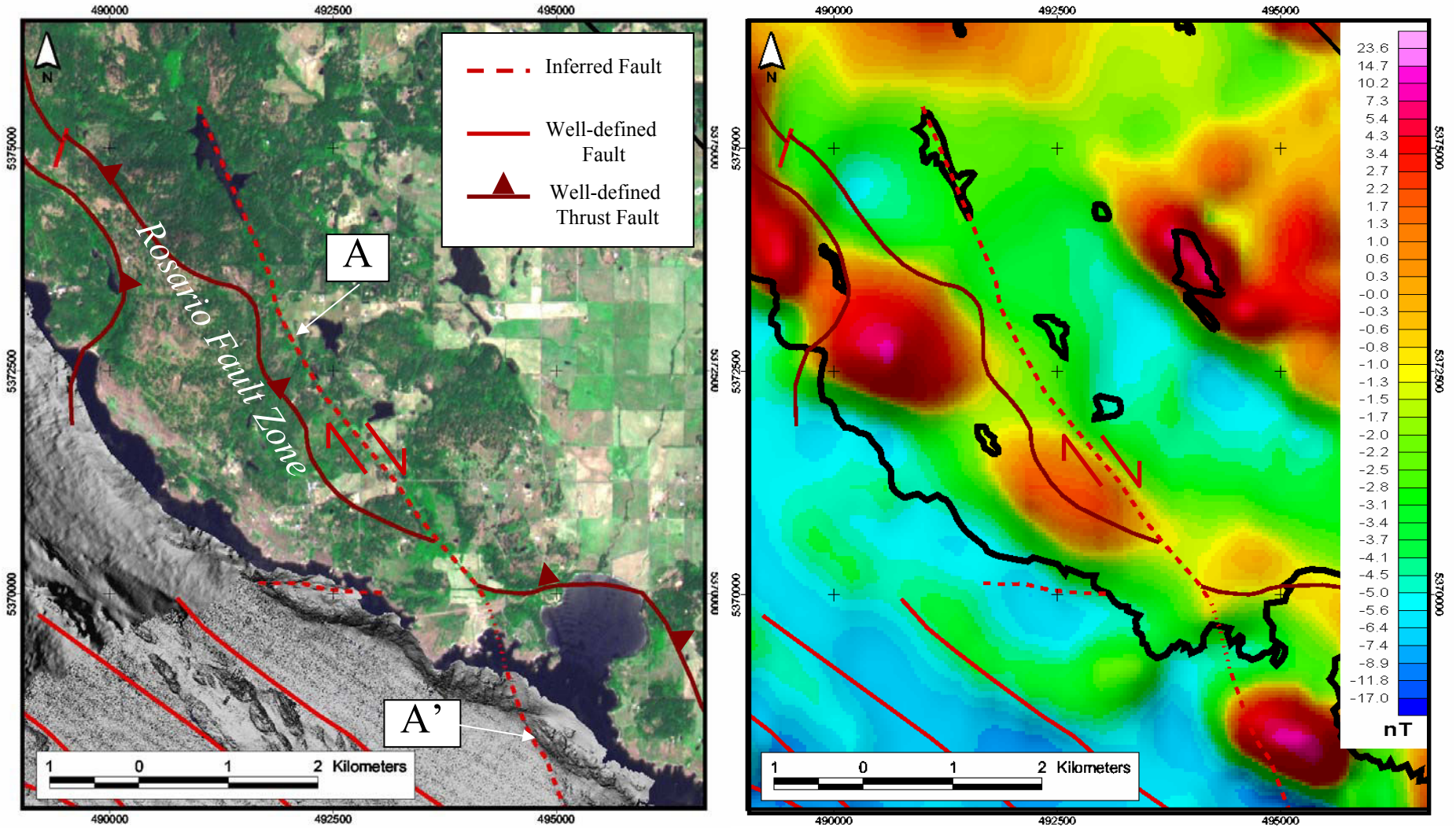

Figure 4.1. SPOT satellite image of southwestern San Juan Island is shown with Simrad EM1002 and Reson 8101 multibeam imagery (left). Onshore thrust faults, modified after Schuster (2000), are shown with interpreted structure (left). Inferred fault (A) follows a distinct NNW-SSE lineament visible in the satellite imagery beginning at Trout Lake in the north and continuing south where it offsets the Rosario fault zone. Right-lateral offset is visible in the residual aeromagnetic anomalies (right) as well. Fault (A') was mapped independtly offshore based on interpretation of multibeam imagery. The two faults (A & A') may be connected by a buried fault.

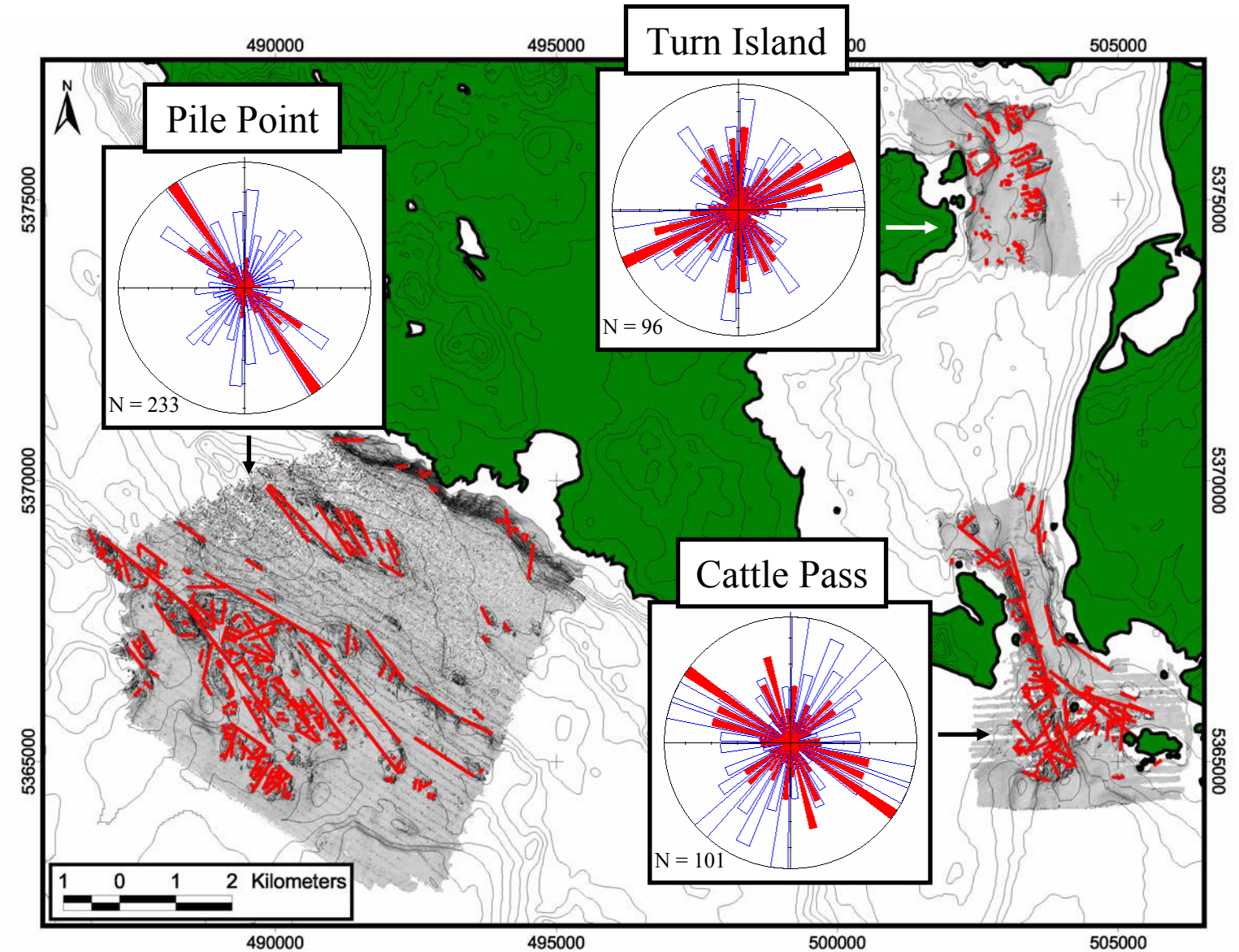

Figure 4.2. Lineation map of the study area with length-weighted (solid red) and frequency (blue outline) rose diagrams highlighting the predominant lineation orientations according to lineation length at Turn Island, Cattle Pass, and Pile Point. Lineation analyses were performed on 2 m resolution Reson 8101 multibeam imagery.

The distribution in Cattle Pass is much more widely dispersed than Pile Point with a 95% confidence of ±46° in Cattle Pass and a 95% confidence of ±9° in Pile Point (Table 4.1).

Statistic	Pile Point	Cattle Pass	Turn Island
Length-Azimuth Plot			
Maximum Length (%)	18923.2 (26.1%)	5238.7 (14.3%)	1501.3 (12.8%)
Total Length	72399.1	36511.2	11723.3
Mean Resultant Direction (95% confidence interval)	143°-323° (±9°)	138°-318° (±46°)	32°-212° (±77°)
Frequency-Azimuth Plot			
# of linear features at the Maximum frequency (% of total)	28 (12.0%)	9 (8.9%)	9 (9.4%)
Scale: the tick interval is a certain % of the total length of all linear features in that survey area Length = meters			

Table 4.1. Rose diagram statistics for each survey area for the Length-Azimuth plots and the Frequency-Azimuth plots.

Both the length-azimuth and frequency-azimuth plots for Turn Island have widely dispersed orientations. The length-weighted rose diagram for Pile Point shows a dominant NW-SE linear trend and a minor N-S trend. The length-azimuth plot for Cattle Pass shows a prevailing NW-SE trend, a less dominant NNW-SSE trend and a minor NE-SW trend. The linear features at Turn Island are distributed in predominantly NE-SW orientations and less significant N-S orientations.

Two bedrock highs offshore Pile Point have distinctive lineation patterns (Figure 4.3). Length-azimuth and frequency-azimuth rose diagrams were plotted for each bedrock high. The frequency-azimuth plots for each bedrock high are quite different (Figure 4.3A, B). The bedrock high closer to San Juan Island has a mean resultant direction of 152°/332° with a 95% confidence of ± 14° for the frequency-azimuth plot, indicating linear feature orientations are tightly grouped. In contrast, the bedrock high further offshore has a mean resultant direction of 169°/349° with a 95% confidence of ± 39° for the frequency-azimuth plot, demonstrating linear feature orientations are widely dispersed. The length-azimuth rose diagrams for both bedrock highs, on the other hand, are quite similar, indicating a predominant NW-SE lineation trend. The dissimilarity in linear feature orientations between the two bedrock highs may reflect different tectonic histories, but not necessarily different lithologies. Alternatively, two distinct lithologies

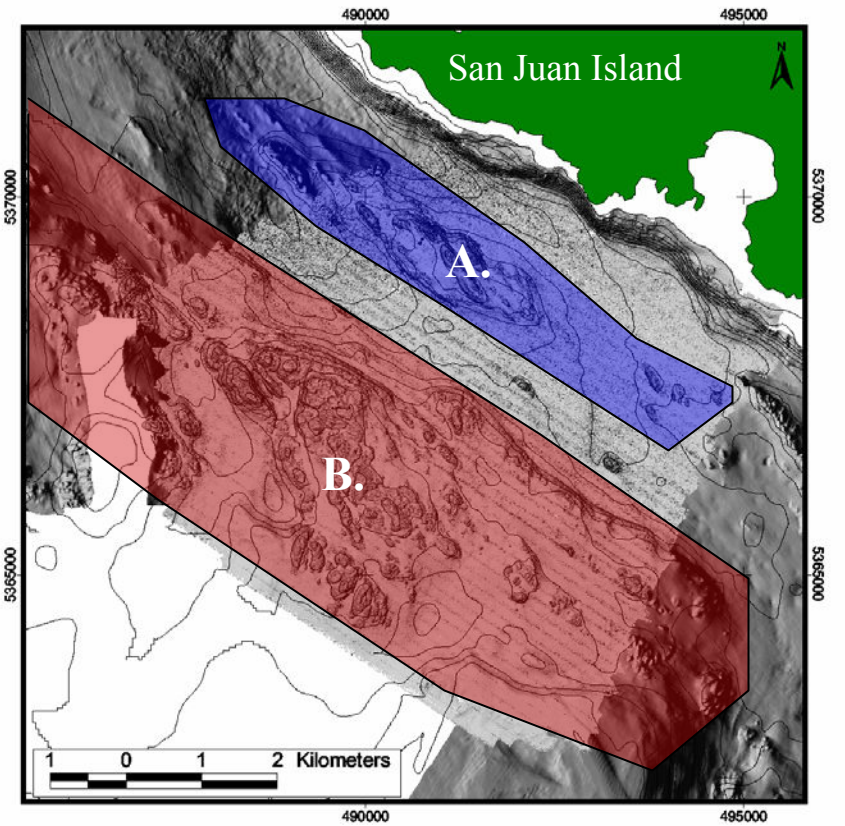

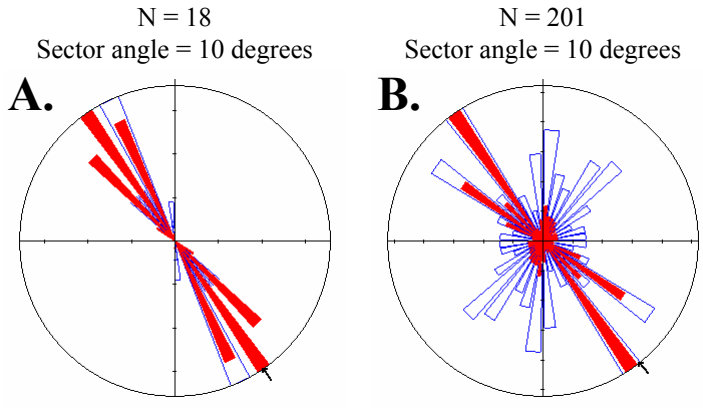

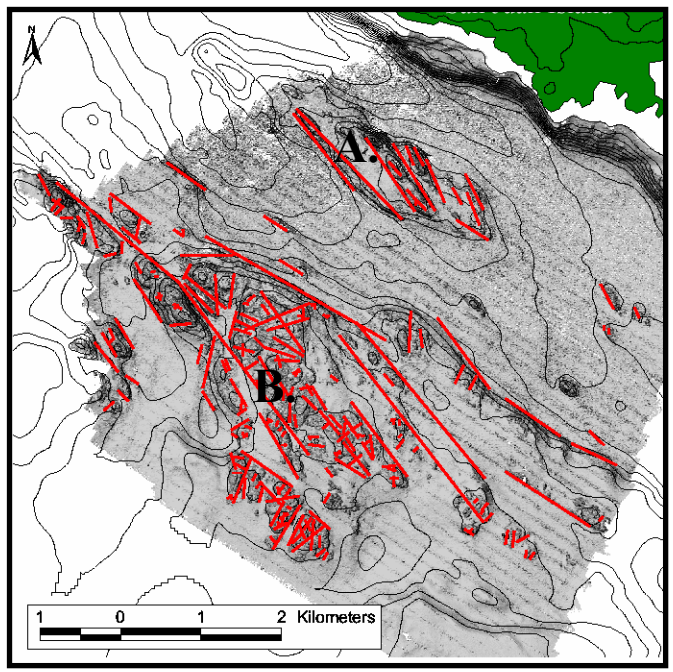

Figure 4.3. Multibeam bathymetry image (above) showing two distinct bedrock highs (shaded areas A. & B.) offshore southwestern San Juan Island separated by a saddle. The two bedrock highs exhibit different lineation patterns as seen in the rose diagrams (right). Blue = frequency-azimuth plot. Red = length-azimuth plot. Notice the length-azimuth plots are similar, but the frequency-azimuth plots are quite different among the two bedrock highs. Contour interval = 20 m.

may deform differently under similar tectonic stresses. Since the general trend for both bedrock highs is NW-SE and the length-weighted trends for each are distinctly different, I propose that similar tectonic stresses, which are likely reflected in the general NW-SE linear trend, were applied to different bedrock lithologies, which deform differently at the smaller outcrop scale.

4.3. TERRANE BOUNDARIES

The surface extents of two terrane boundaries within the southwestern SJI were constrained based on interpretation of aeromagnetic data and multibeam imagery; 1) the Buck Bay fault and 2) the boundary between the Deadman Bay terrane and Wrangellia, which is presumably a thrust fault. The Buck Bay fault juxtaposes the highly magnetic ultramafic rocks of the Decatur terrane and the less magnetic marine sedimentary rocks of the Constitution Formation along what Brandon (1980) describes as a shallow eastward-dipping thrust fault. The multibeam and single-beam imagery show no evidence of faulting on the seafloor within southern San Juan Channel or Griffin Bay. However, shallow-focused aeromagnetic data reveal anomalies radiating outward (westward) from the distinctive magnetic anomaly defining the Fidalgo ophiolite and volcanic-arc sequence (Figure 4.4). The magnetic field strength of these radiating anomalies decreases from 12 nT to ~ 6 nT coincident with the mapped extents of the Lummi Formation, a sedimentary unit overlying the Decatur terrane terrane. These distinctive anomalies disappear in Wasp Passage (Figure 4.4) and in southern San Juan Channel. The inferred Buck Bay fault trace is drawn along the western edge of this series of radiating anomalies. The trace of the Buck Bay fault is questionably extended across Mt. Finlayson based on a N-S magnetic anomaly in the area that corresponds to the previously mapped trace of the fault (Brandon, 1980). Alternatively, the Buck Bay fault bends southeastward across Cattle Point and merges with the Lopez Fault Zone. In Wasp Passage the trace of the Buck Bay fault was questionably inferred based on subtle differences in magnetic field strength on either side of the fault.

If the rocks of Wrangellia do not extend into the SJI, then the boundary between Wrangellia and the Deadman Bay terrane must lie within Haro Strait. The anomaly pattern west of Smallpox Bay on San Juan Island shows the intersection of a N-S oriented ~12 nT anomaly, presumably representing rocks of the Deadman Bay terrane, with a number of NW-SE trending anomalies (Figure 4.5). The NW-SE trending anomalies have an orientation similar to outcrop

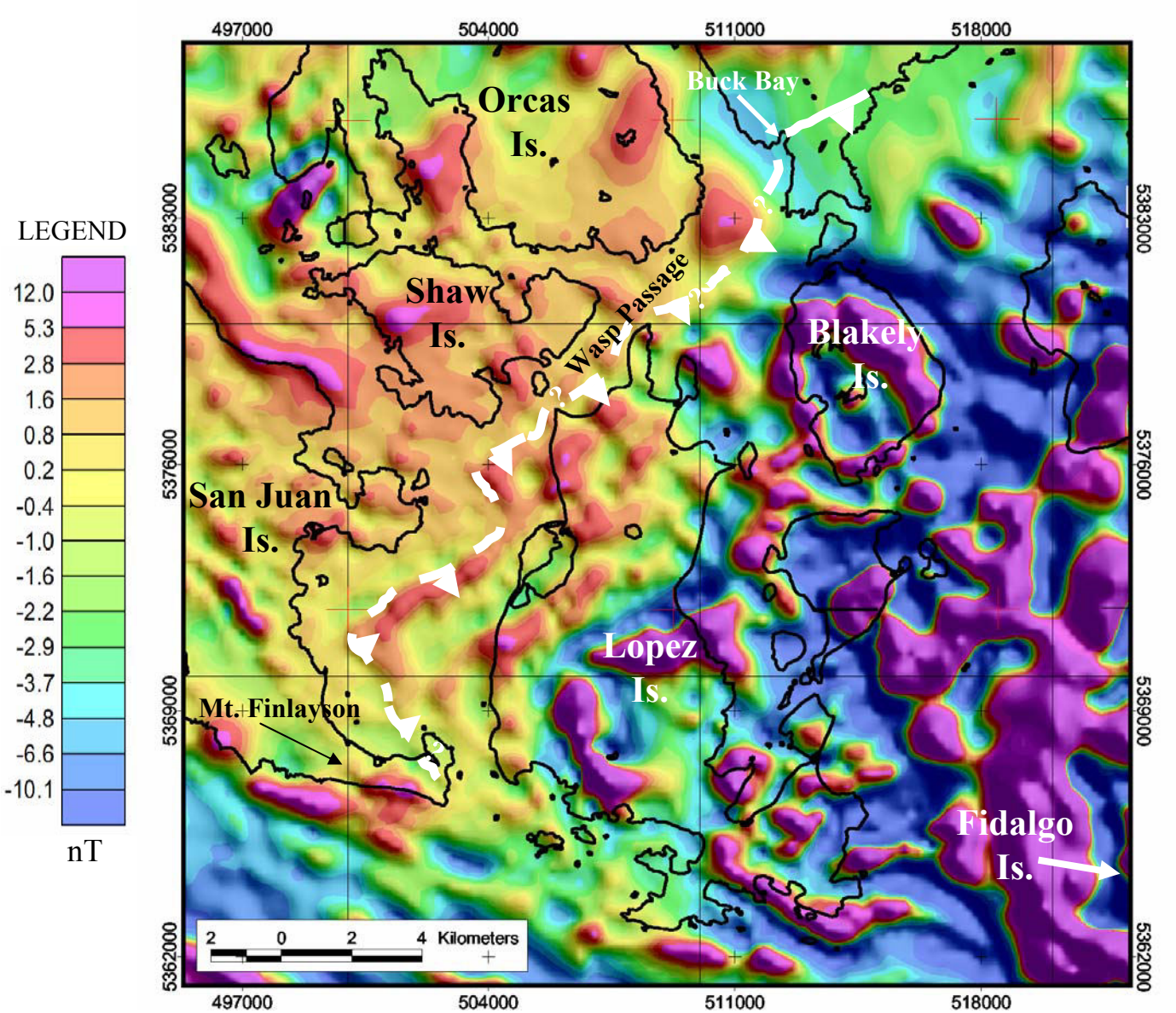

Figure 4.4. Residual aeromagnetic map highlighting short-wavelength magnetic anomalies associated with the Fidalgo Ophiolite. The inferred trace of the Buck Bay thrust fault is represented by a white dashed line. The fault is questionably inferred where dashed with question marks. The fault has been mapped onshore southeast Orcas Island (Brandon, 1980) near Buck Bay. The thick black line represents the shoreline of the islands. Aeromagnetic data supplied by R.J. Blakely at the U.S. Geological Survey.

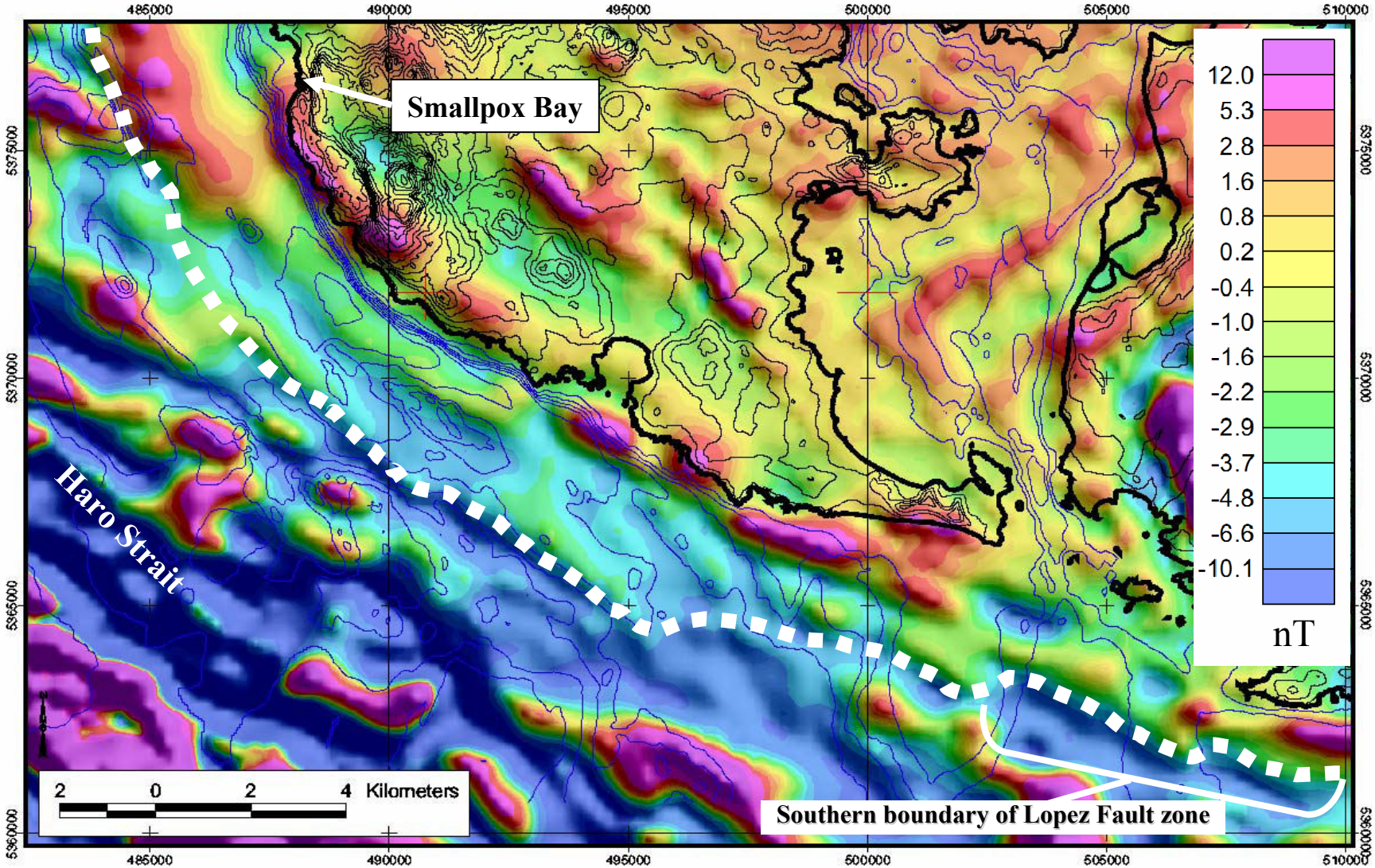

Figure 4.5. Shallow-focused aeromagnetic map of the southwestern SJI showing the inferred location of the Haro fault in Haro Strait (white dashed line). The shoreline is represented by a thick black line. Contour interval offshore = 50 m. Contour interval onshore = 20 m. Aeromagnetic data supplied by R.J. Blakely at the U.S. Geological Survey.

patterns on Vancouver Island (Muller, 1983) and are therefore interpreted as Wrangellian. The intersection of these two anomaly patterns is interpreted as the terrane boundary in this area. The boundary becomes obscured to the south and east due to a regional NW-SE orientation of magnetic anomalies exhibiting similar magnetic field strength. The elongate, NW-SE trending bedrock high visible in multibeam imagery ~2 km offshore Pile Point appears to be part of the San Juan thrust system based on the NW-SE outcrop trend, which corresponds to foliation and bedding orientations on San Juan Island. If this is the case, the terrane boundary must be outboard of this bedrock high. The inferred terrane boundary thus follows the general arc of southwest San Juan Island ~2.5–3 km offshore. South of Cattle Point, the boundary is characterized by a series of left-stepping elongate anomalies likely marking the southern edge of the Lopez Fault Zone.

4.4. SURFICIAL MARINE GEOLOGY

The marine geology of the southwestern San Juan Islands (Plate 1) involves a complex seafloor with fractured, faulted, and folded bedrock outcrops often separated by deep (100–320 m), current-swept channels. The seafloor imagery was characterized by 8 unconsolidated units and 10 bedrock geologic units based on their morphologic and/or acoustic character. The confidence with which I have identified the lithologies of the bedrock in the marine environment depends on proximity to mapped units onshore, and thus diminishes with distance from shore. Bedrock lithologies are questionably inferred for outcrops in San Juan Channel and off the southwestern coastline of San Juan Island. There was insufficient evidence to confidently define lithologies of outcrops ~1 km offshore San Juan Island in Haro Strait. Linear feature patterns appeared quite different among two bedrock highs >1 km offshore southwestern San Juan Island (labeled A and B in Figure 4.3). Tentatively, the inner bedrock high is mapped as San Juan Thrust system rock based on its proximity to San Juan Island and its NW-SE lineation pattern, which corresponds to NW-SE foliation mapped onshore (Muller, 1983 and Bergh, 2002; refer to Plate 1). The outer bedrock high is mapped as Wrangellian rock based on a lack of evidence linking it to the San Juan Islands. Unconsolidated marine sedimentary units were characterized as Holocene reworked sediment (Qs), Pleistocene continental glacial outwash (Qgom), Pleistocene glacial till (Qgt), Pleistocene glacial marine sediments (Qgm), Quaternary slumps (Qls), Sediment Waves (Qw), Chaotic Bedforms (Qc), or Current-scoured Seafloor (Qcs)

(Figures 4.6 and 4.7). Linear features that were associated with apparent horizontal or vertical offset of the seafloor were considered faults. All linear features exhibiting apparent seafloor offset were overlaid on the shallow-focused aeromagnetic anomalies to see if the surface offset corresponded with magnetic anomaly patterns and gradients, providing evidence for subsurface expressions of the faults. For a fault to be characterized as a well-defined rather than an inferred fault, more than one line of evidence supporting faulting needed to exist. If a linear feature appeared to offset the seafloor in multibeam imagery either horizontally or vertically and was also associated with either a gradient in aeromagnetic anomalies or a fault previously mapped based on interpretation of seismic reflection data, the feature was considered a well-defined fault. Linear features that were associated with apparent horizontal or vertical offset of the seafloor and had no apparent correlation to aeromagnetic anomalies or previously mapped structures were mapped as inferred faults.

Multibeam imagery, SPOT imagery, and residual aeromagnetic anomalies allowed for identification of 29 new fault traces and further constrained and/or extended 8 previously mapped faults and folds. When overlain on shallow-focused aeromagnetic data, a number of the new and/or extended structures correspond to 2 to 13 nT magnetic anomaly gradients (Figure 4.8). A number of onshore faults were extended offshore based on apparent bedrock offset(s) visible in multibeam imagery. In addition, two terrane boundaries have been constrained based on morphologic and geophysical evidence; 1) the western thrust edge of the Decatur terrane, defined by the Buck Bay fault, and 2) the boundary between the Deadman Bay and Wrangellia terranes.

4.5. MARINE BENTHIC HABITATS

Fifteen marine benthic habitat types were identified among the three areas surveyed (Figure 4.9A), and each of these has been assigned a corresponding habitat code (Figure 4.9B). The asterisk in the habitat code precedes a macro or micro-habitat classification based on ROV video review. All of the survey areas contained similar types of habitats including mainly hard, fractured, glacially scoured bedrock outcrops and subcrops with varying degrees of sediment cover; soft, unconsolidated, current winnowed sediment (cobbles, gravel, boulders, and sand); and marine and glacial terraces of varying morphologies. The most common habitat type among the three survey areas is gravel and sand sediment. Prior to the ROV survey, much of the smooth

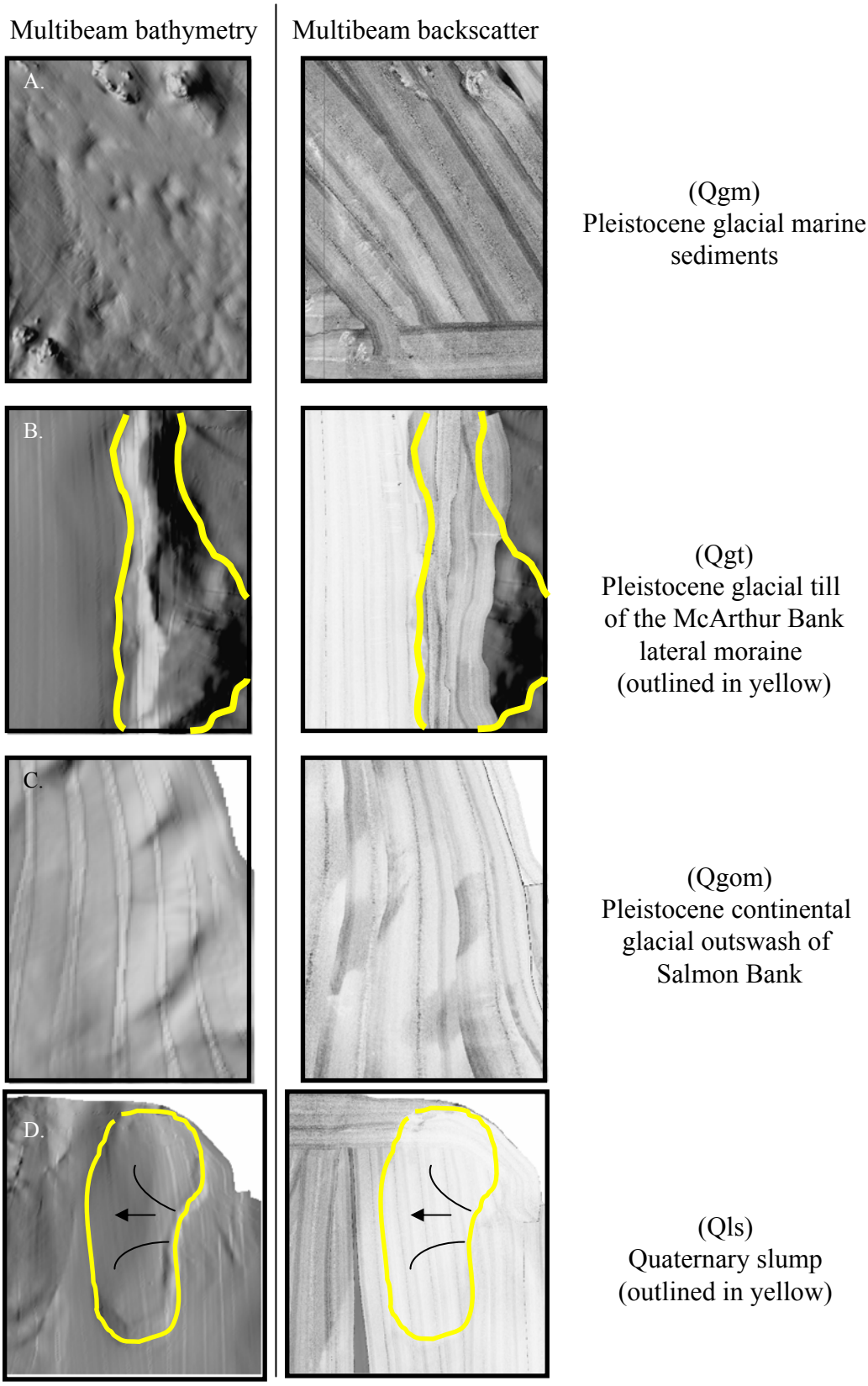

Figure 4.6. Examples showing multibeam bathymetry and multibeam backscatter images of unconsolidated Sediment types in the study area. Index map is Figure 3.1.

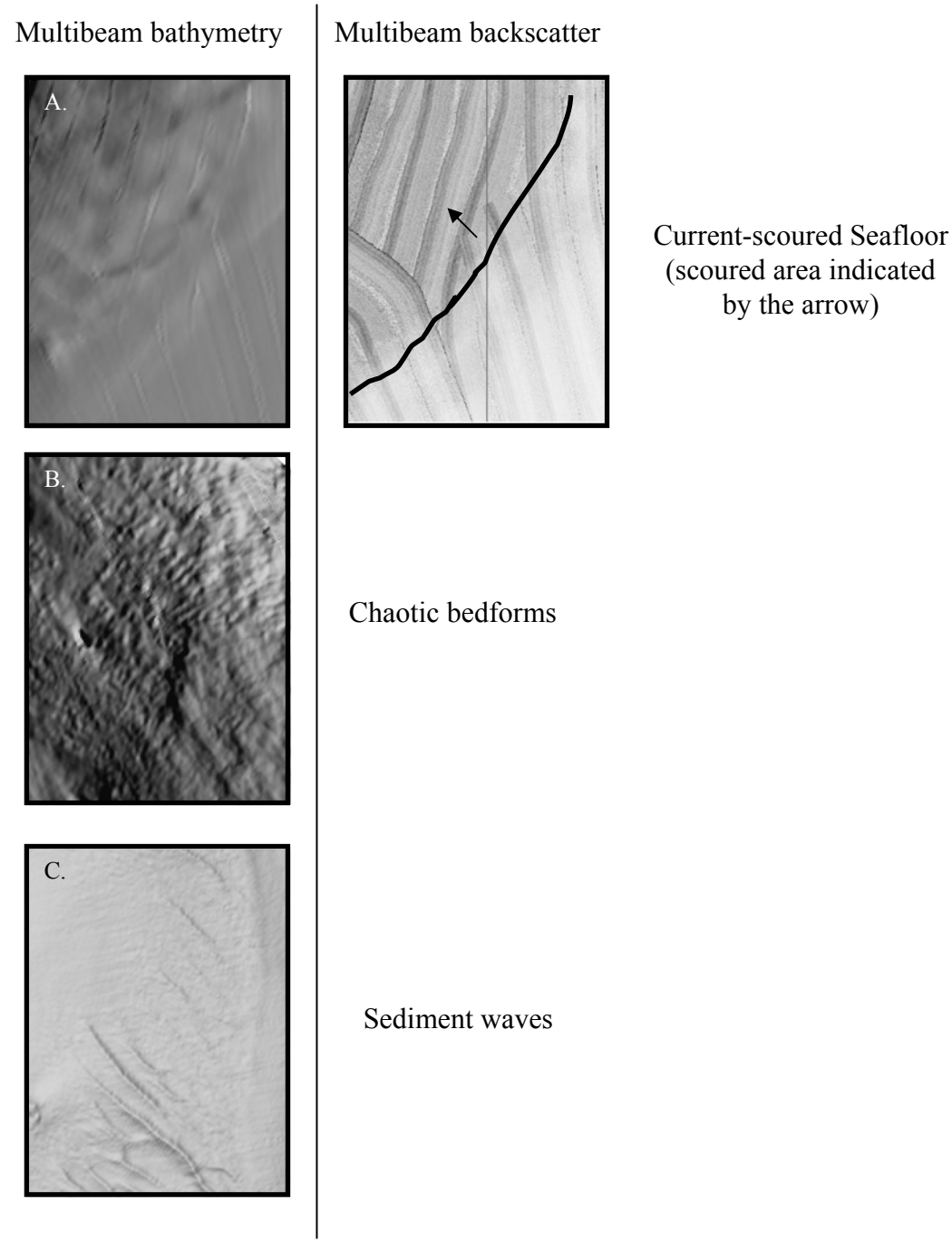

Figure 4.7. Examples showing multibeam bathymetry and multibeam backscatter images of unconsolidated sediment types in the study area. Index map is Figure 3.1.

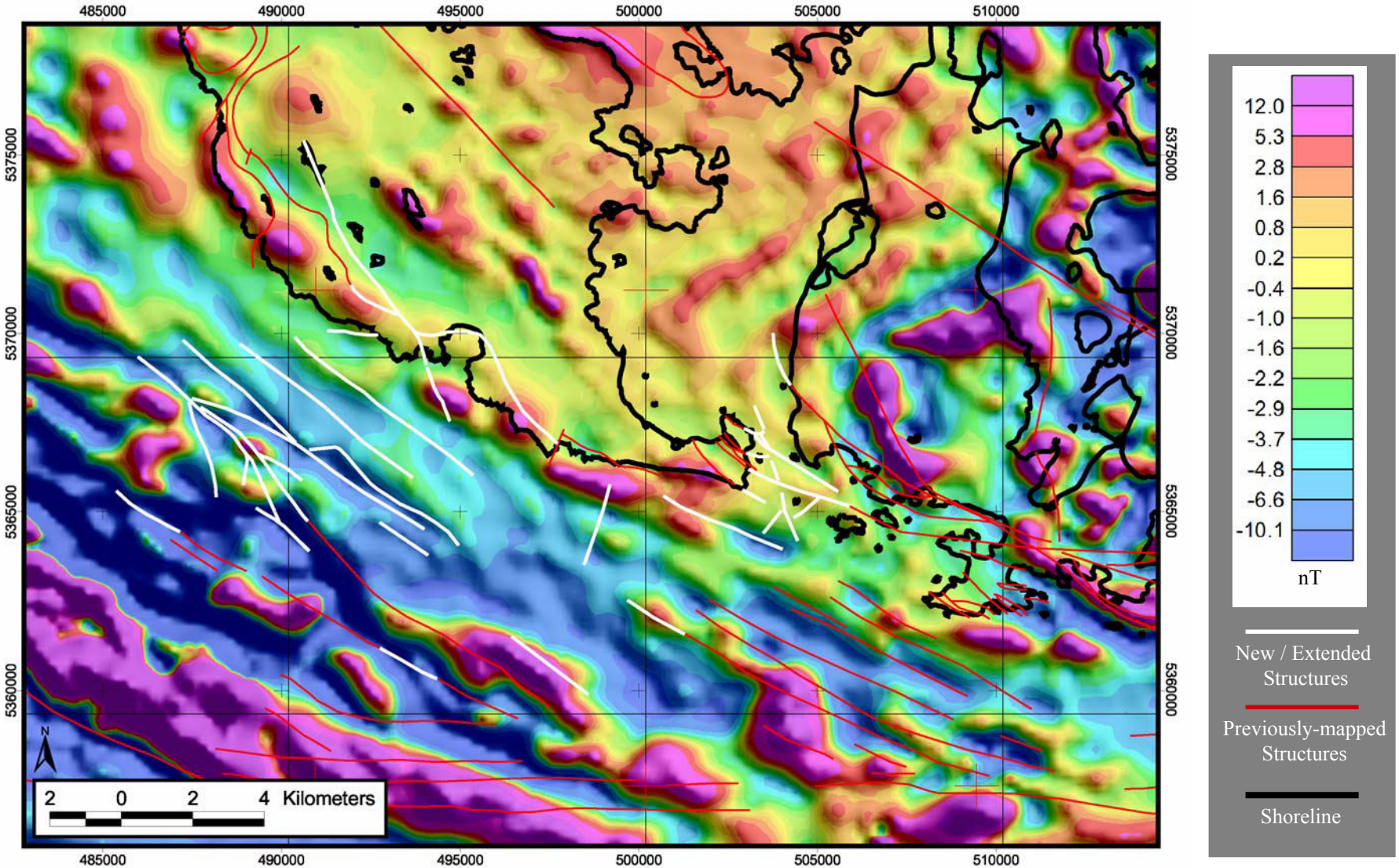

Figure 4.8. Map showing new and/or extended structures (white) and previously mapped structures (red) on top of shallow-focused aeromagnetic data (R.J. Blakely, written commun., 2003).

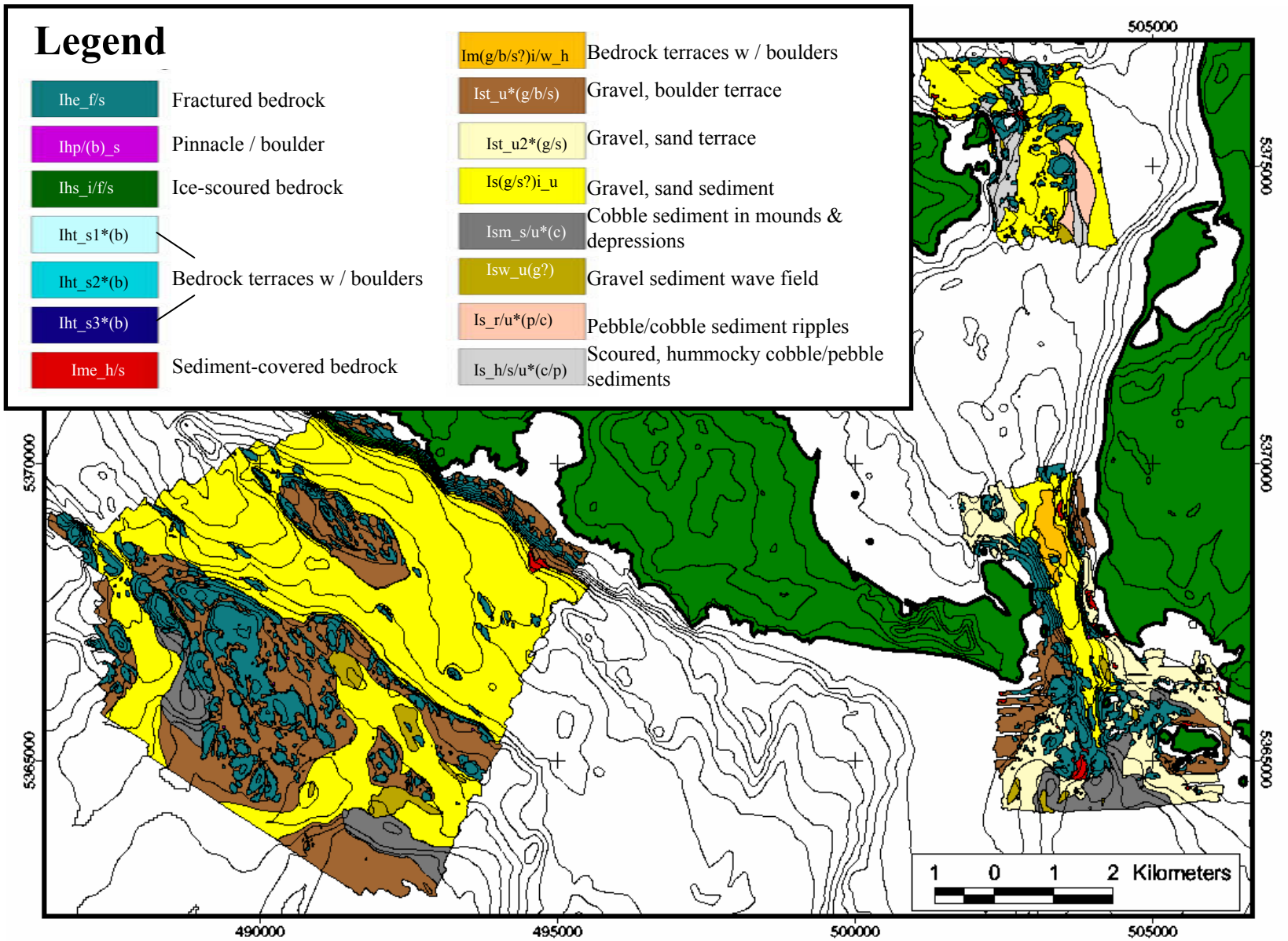

Figure 4.9A. Marine benthic habitat maps based on 2 m-resolution Reson 8101 multibeam imagery. Refer to Figure 4.6b. For explanation of habitat types. Marine contour interval = 40 m. Land contour interval = 20 m.

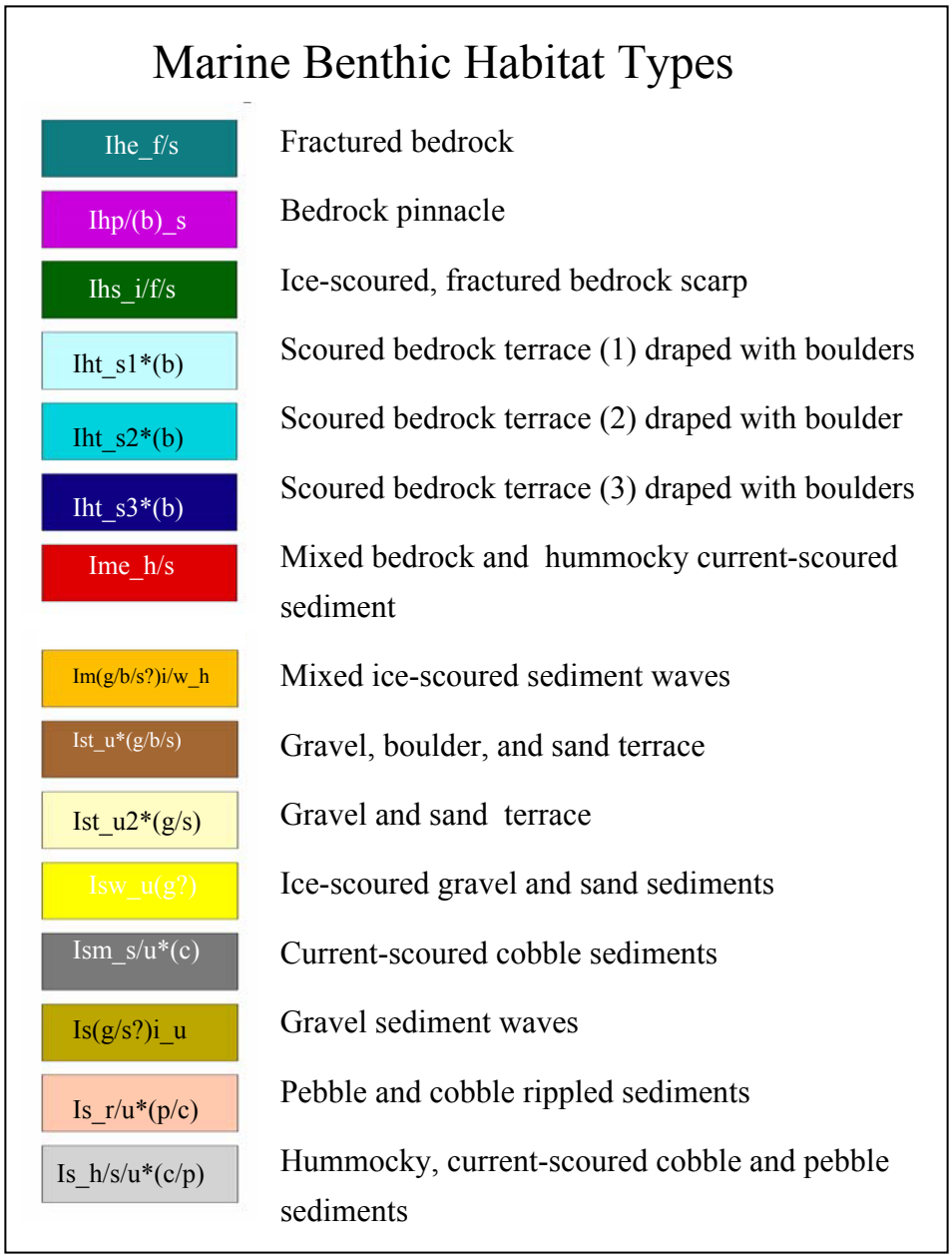

Figure 4.9B. Marine benthic habitat codes and explanations for Figure 4.6a. The asterisk in the code precedes a macro or micro-habitat classification. Refer to *Appendix A* for a more detailed explanation of the habitat codes.

flat seafloor was mapped as sand sediment. However, the ROV showed that these areas were covered with cobbles, pebbles, and small boulders in most cases.

Eight of the fifteen benthic habitats identified were considered potential adult rockfish habitat, representing 26 km^2 and accounting for 40.6% of the area surveyed. These potential habitats were characterized by bedrock exposures and mixed boulder sediment. Nearly 95% of adult rockfishes observed in ROV videos were on or within 10 m of areas mapped as potential rockfish habitats (Figure 4.10). Roughly 13% of the rockfishes were observed on mixed boulder habitat.

4.6. SEAFLOOR COMPLEXITY MAP

Based on the criteria listed in the methods, low complexity represents rugosity values between 1 and 1.020. Intermediate complexity contains rugosity values between 1.021 and 1.075. High complexity represents rugosity values > 1.075. Of the approximately 28 km^2 of seafloor surveyed, 16 km^2 were low complexity, 5 km^2 were intermediate complexity, and 7 km^2 were high complexity (Figure 4.11).

4.7. HABITAT UTILIZATION BY ADULT ROCKFISHES

In total, 17,629 data points were analyzed to determine seafloor complexities available along the thirteen ROV transects, and of those 17% were low complexity, 33% were intermediate complexity, and 50% were high complexity. In total, 164 adult rockfishes were observed during video analysis, with 10% observed on low complexity seafloor, 26% on intermediate complexity seafloor, and 64% on high complexity seafloor (Figure 4.12).

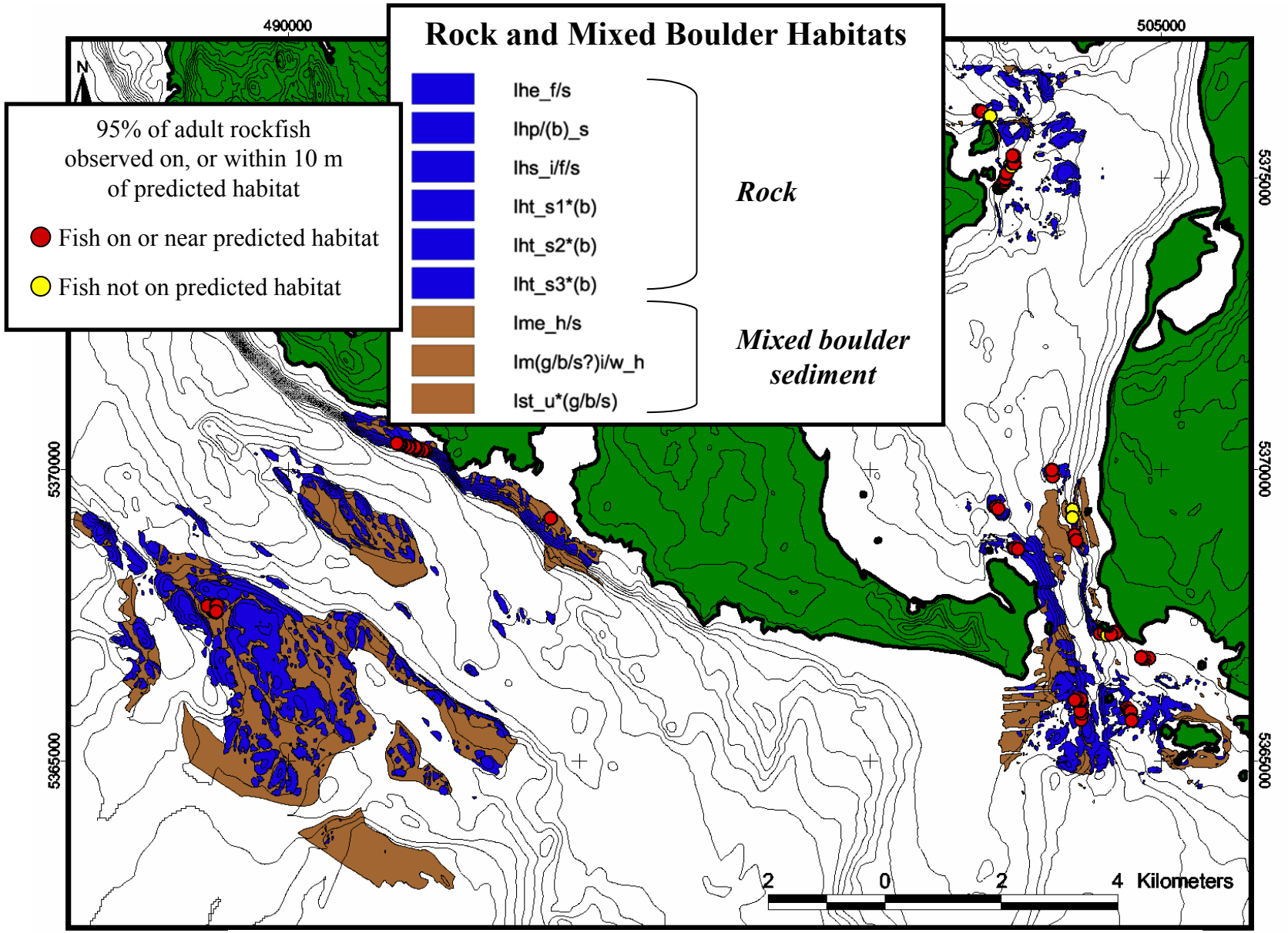

Figure 4.10. Map of potential adult rockfish habitats characterized according to the modified Greene et al. (1999) habitat classification methodology. Contour interval = 20 m. See *Appendix A* for explanation of habitat codes.

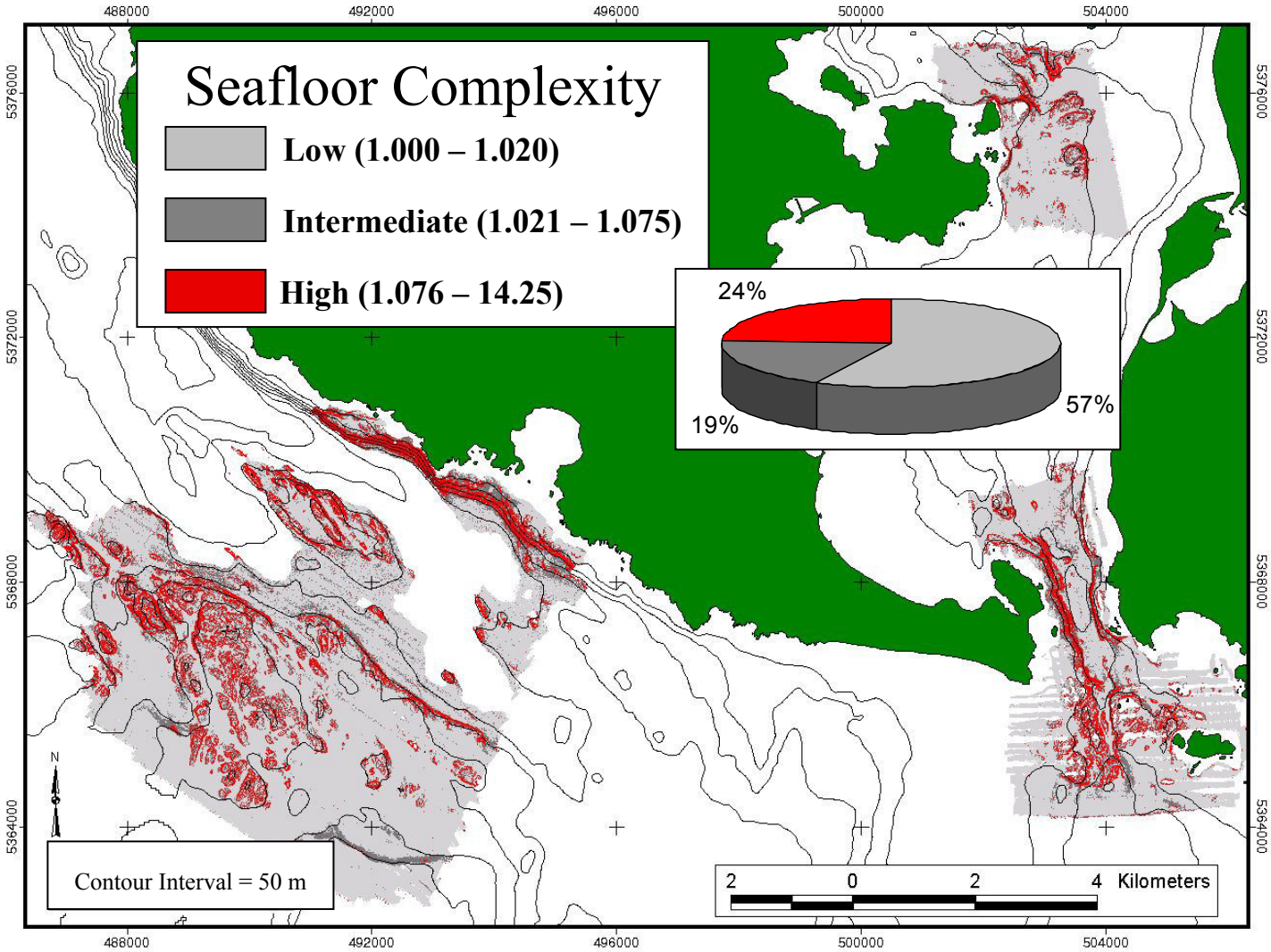

Figure 4.11. Seafloor complexity map of the southwestern SJI, where Reson 8101 multibeam bathymetry data were collected.

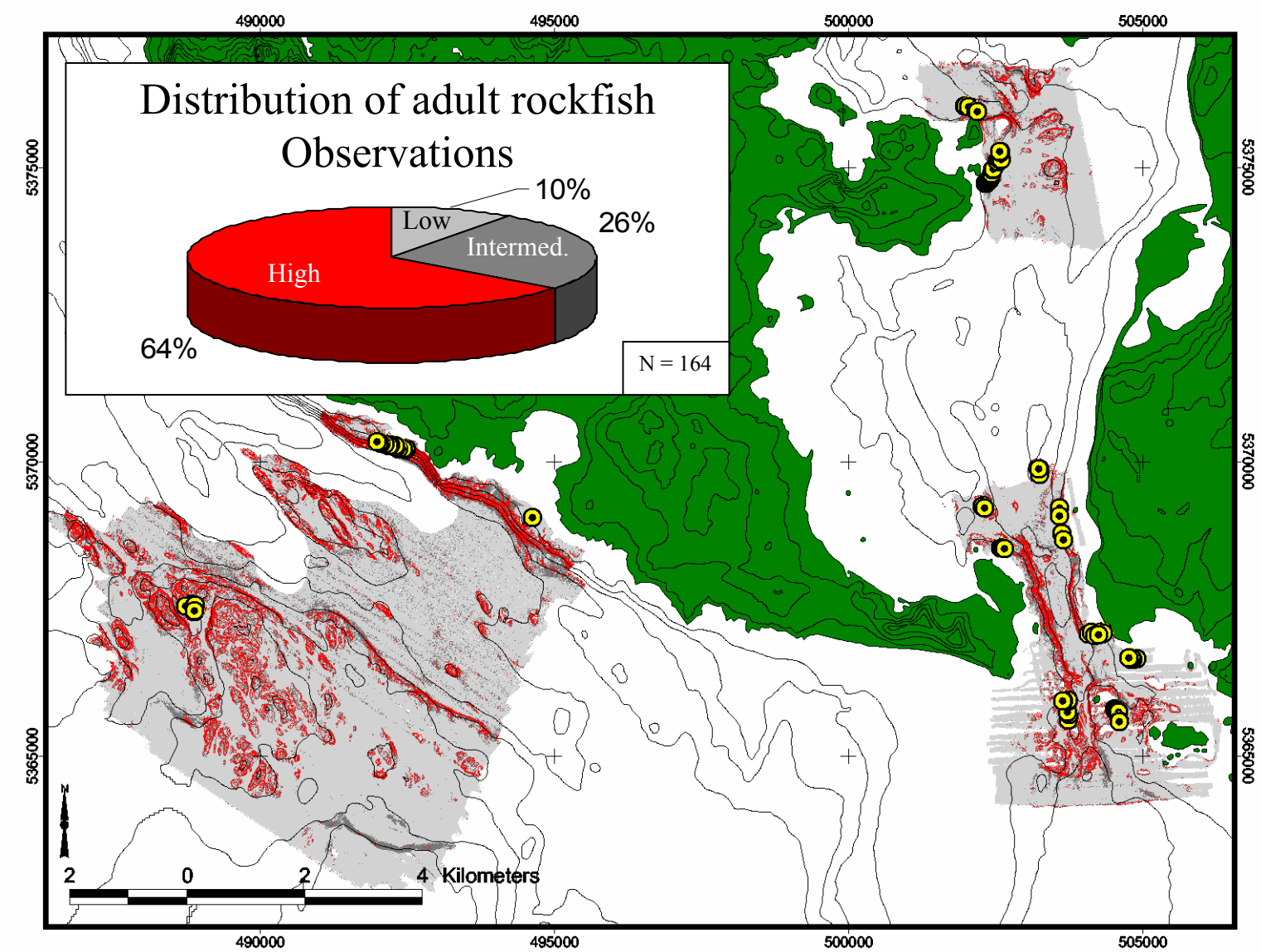

Figure 4.12. Pie chart and map showing the distribution of adult copper and quillback rockfishes (yellow circles) observed from ROV video on low, intermediate, and high complexity seafloor as measured from multibeam bathymetry. Bathymetry contour interval = 40 m and the topographic contour interval = 20 m.

Manly's selection index (Table 4.2) indicated that adult rockfishes utilized areas of seafloor that had both high and intermediate complexity (Manly's α = 0.475 and 0.390, respectively). Both were statistically significant because their respective α values exceeded 0.333, the value expected if utilization were equal among all complexity categories. Low complexity seafloor was not utilized much by adult rockfishes (α = 0.134).

MANLY'S alpha	Seafloor Complexity	Utilization Index
0.134	Low	Not Utilized
0.390	Intermediate	Utilized
0.475	High	Utilized

Table 4.2. Manly's alpha for each of the complexity categories and the corresponding utilization index.

Expected and observed proportions of fish are shown in Table 4.3, along with proportions of available seafloor complexities. The log likelihood chi-square analysis confirmed that adult

Habitat Type (Complexity Category)	Total Habitat (2 m cell)	Proportion of total habitat	# of rockfishes observed	Expected[a] # of rockfishes observed	Proportion of rockfishes observed in each category (p_o)	Proportion of rockfishes expected based on the proportion of habitat (p_e)	Confidence interval on proportion of occurrence (95% family confidence coefficient)
1	4676	0.265	16	44	0.098	0.265	$0.034 \le p_o \le 0.161$
2	4215	0.239	42	39	0.256	0.239	$0.162 \le p_o \le 0.350$
3	8738	0.496	106	81	0.646	0.496	$0.543 \le p_o \le 0.749$
Total	17629		164	164			

Table 4.3. Occurrence of rockfishes on low, intermediate, and high complexity seafloor. [a] Calculated by multiplying proportion p_o x n; i.e., 0.239 x 164 = 39

rockfish distributions were not independent of seafloor complexity distributions (P=0.05), meaning that rockfishes were not distributed evenly among the categories of complexity. The confidence intervals generated using Bonferroni normal statistics (Table 4.3) indicate significant differences between observed and expected proportions of rockfishes for low complexity and high complexity categories. The low complexity habitat was used significantly less than expected according to availability and high complexity habitat was used significantly more than expected. Because the expected proportion of rockfishes for the intermediate complexity category fell within the confidence interval for the proportion of rockfishes observed, there is no

significant difference between observed and expected. Rockfishes used intermediate complexity habitat in proportion to its availability. This can be seen graphically in Figure 4.13. The results of Manly's index for both low complexity and high complexity seafloor agreed with the results of the modified Neu et al. (1974) method. Manly's index established that intermediate complexity habitat was utilized by adult rockfishes, however, the modified Neu et al. (1974) technique showed that intermediate complexity habitat was used proportionately to its availability.

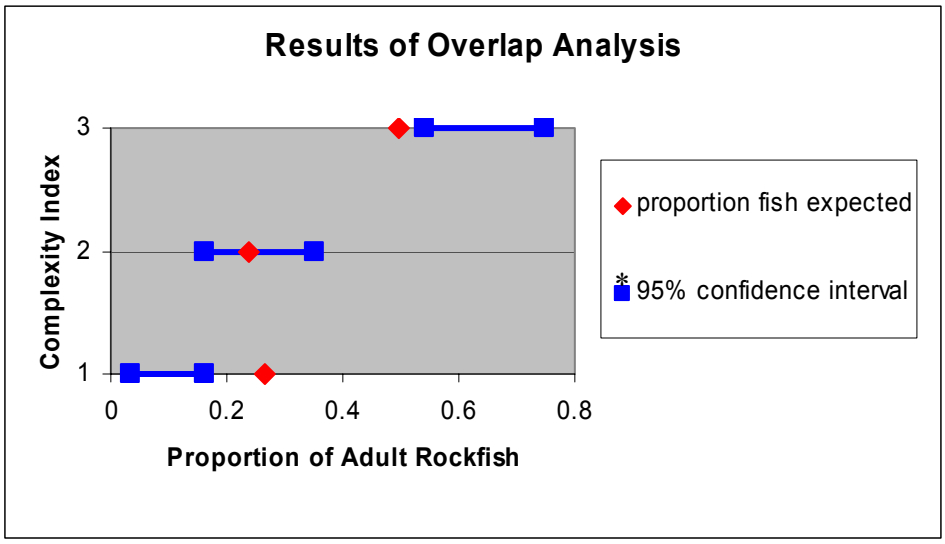

Figure 4.13. Graph showing the proportion of fish expected in each category (red triangle) from Table 4.3 plotted with the confidence interval (blue line) on the proportion of occurrence.
* Confidence interval on the proportion of fish observed (95% family confidence coefficient).

According to the combined results of the habitat utilization analysis, adult copper and quillback rockfishes within the southwestern SJI utilized high complexity habitat, and to a lesser degree intermediate complexity habitat. Adult rockfishes do not use low complexity habitat. Since adult rockfishes utilize intermediate complexity habitat, high seafloor complexity alone does not adequately define potential adult rockfish habitats in the southwestern SJI. The occurrence of intermediate complexity seafloor often corresponded to seafloor mapped as rock habitat, which is considered potential adult rockfish habitat for this study. To provide a more comprehensive view of potential rockfish habitats, complexity data should be integrated with marine benthic habitat maps to illustrate the overlap between intermediate complexity and rock substrate (Figure 4.14).

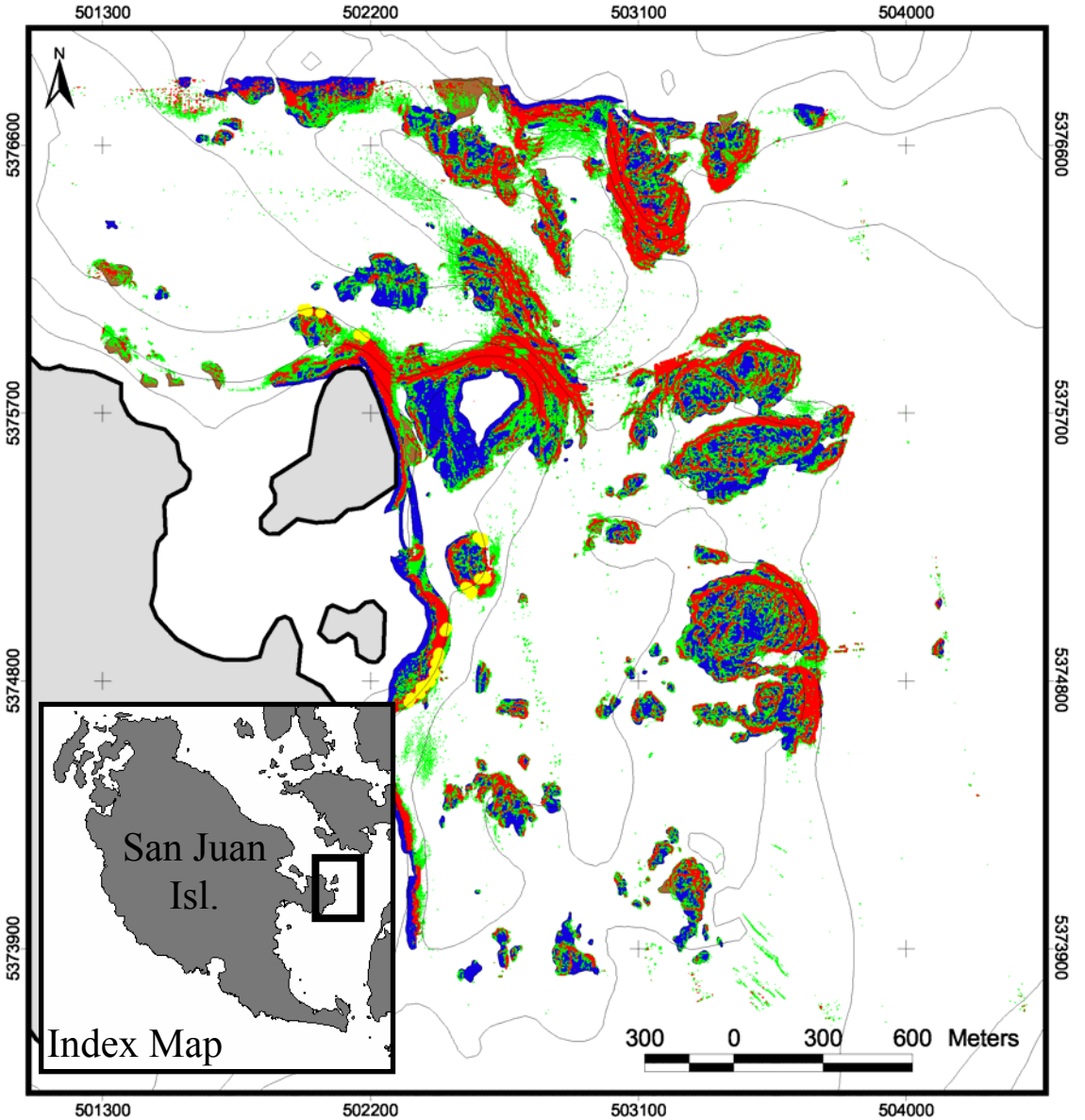

Potential Rockfish Habitats

Rock and mixed boulder (Meso-habitats)

- Ihe_f/s – fractured bedrock
- Ihp/(b)_s – bedrock pinnacle
- Ihs_i/f/s – bedrock scarp
- Ime_h/s – Mixed hummocky sediment
- Ist_u*(g/b/s) – gravel, boulder, and sand terrace

Complexity (Macro-habitats)

- Intermediate (1.021-1.075)
- High (>1.076)

- Observations of Adult Copper or Quillback Rockfish

Figure 4.14. Map of potential adult rockfish habitat at Turn Island. Rock and mixed boulder habitat identified qualitatively is overlain by high and intermediate complexity habitat identified quantitatively. Observations of adult copper and quillback rockfishes are shown with yellow circles. Contour interval = 20 m. See *Appendix A* for explanation of habitat codes.

5. DISCUSSION

5.1. GEOLOGY

For discussion purposes, the seamless onshore/offshore geologic map created for this study has been divided into three areas (Plate 1) with similar bedrock geology and structure. Area 1 includes the onshore and offshore areas of western and southwestern San Juan Island. Area 2 extends from southern San Juan Channel over Salmon Bank and the western margin of McArcthur Bank, including adjacent onshore areas of San Juan and Lopez islands. Area 3 covers central San Juan Channel and adjacent shorelines from Friday Harbor south to southern San Juan Channel.

5.1.1. Area 1

The bedrock geology of Area 1 (Plate 1) includes the oceanic volcanic island rocks of the Deadman Bay terrane and bedrock of unknown lithology offshore Pile Point. The bedrock from the shoreline of San Juan Island out to approximately 1 km offshore is likely comprised of Deadman Bay Volcanics (TRPMv(d) on Plate 1) in the north and primarily Orcas chert (JTRmct(o) on Plate 1) south of Deadman Bay. The morphology of the nearshore out to ~1 km is consistently characterized by an island shelf that drops off quickly to depths of 120–240 m (394-1,115 ft) in Area 1. This steep drop off may represent the location of a thrust fault, either within, or marking the western boundary of the Deadman Bay terrane of Brandon et al. (1988). Alternatively, this steep scarp may be the result of glacial scouring during the Pleistocene. The existence of an elongate, 5-12 nT, magnetic anomaly running along the southwestern shoreline of San Juan Island corresponds to the surface extents of the Deadman Bay Volcanics. The location and continuity of this anomaly indicates the possibility that the Deadman Bay pillow basalts cropping out onshore at Limekiln may follow the shoreline arc of San Juan Island to the south underneath the presumably less-magnetic Orcas chert (Figure 5.1). Detailed mapping by Brandon et al. (1988) showed fault slices of pillow basalt intermixed with ribbon chert and basaltic tuff at Eagle Point. If the magnetic anomaly described above is in fact representative of the Deadman Bay pillow basalts and the steep gradient associated with the anomaly offshore False Bay indicates the magnetic rock is at or near the surface, then the bedrock exposed offshore False Bay may be basalt rather than chert as it is mapped in Plate 1. Using the same

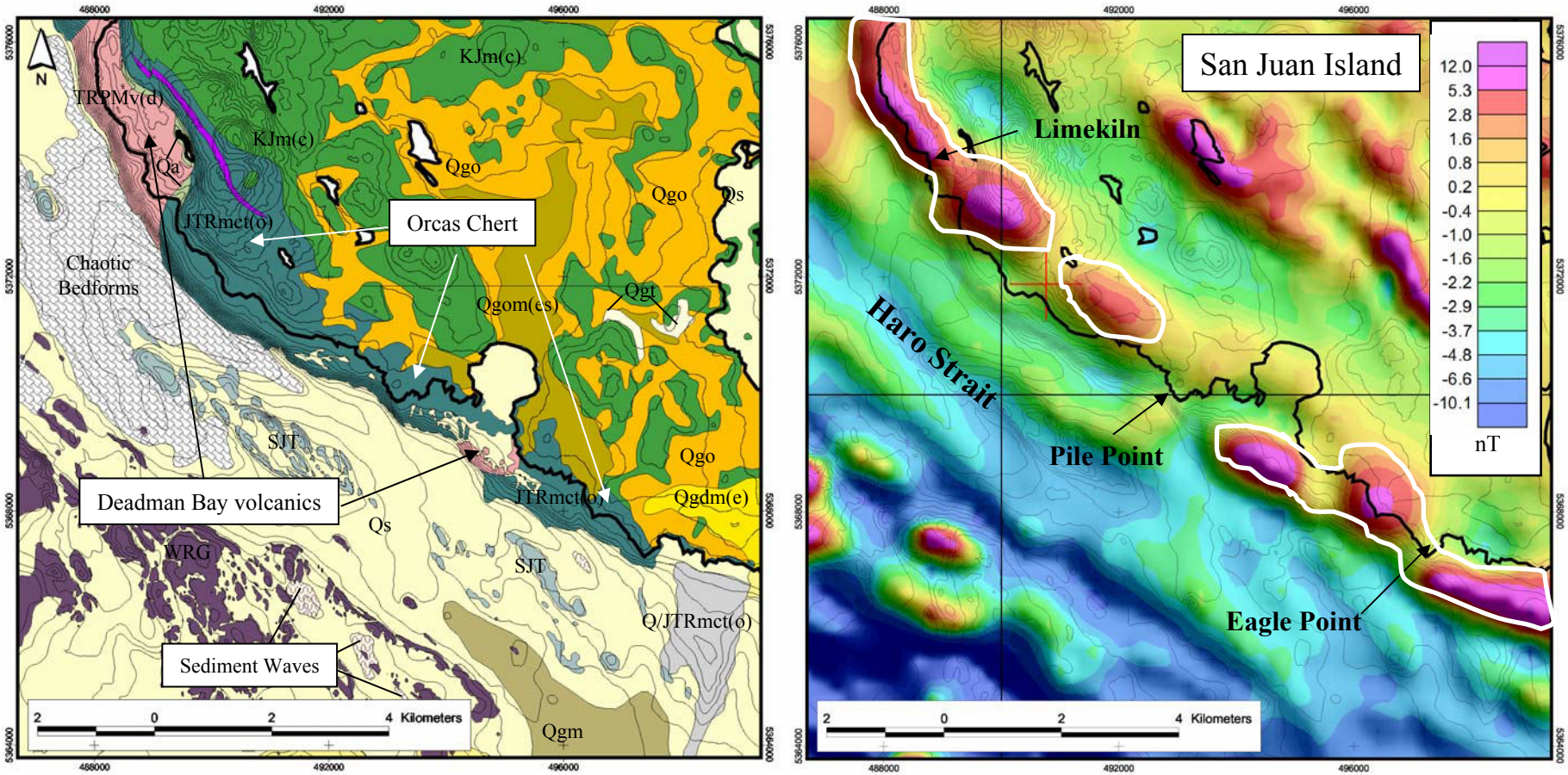

Figure 5.1. Seamless geologic map of southwestern San Juan Island (above left) and a derivative aeromagnetic map of southwestern San Juan Island accentuating shallow (< ~1 km) sources (above right). The magnetic anomaly outlined in white (above right) is interpreted to represent the Deadman Bay volcanic unit, which appears to dive under the Orcas chert and follow the arc of the shoreline of San Juan Island (thick black line) to San Juan Channel. Bathymetry contour interval = 50 m. Topographic contour interval = 20 m. Refer to Plate 1 for explanation of geologic symbology (left).

line of reasoning, the bedrock outcrop located just south and west of South Beach on San Juan Island may be basalt as well.

There are two distinct northwest-trending bedrock highs offshore southwest San Juan Island. One is ~2 km offshore, and will be referred to as the inner bedrock high, and the other is ~3 km offshore, and will be referred to as the outer bedrock high. The inner northwest-trending bedrock high is lithologically unknown, but has been interpreted to be part of the San Juan Thrust system based on similarities in structural and magnetic character between the onshore and offshore. What appears to be either bedding or foliation in the inner bedrock high is aligned with foliation and bedding orientations mapped onshore (Plate 1). Furthermore, the magnetic character of the inner bedrock high is similar to that of the Orcas chert onshore (Figure 5.1). However, interpretation of multibeam imagery and existing seismic reflection data (Johnson et al., 2000) suggest that the inner bedrock high may be fault-bounded, and therefore current bedding/foliation orientations may have been altered by deformation associated with movement on those faults. Differences in lineation pattern and magnetic character between the inner and outer bedrock highs suggest the outer bedrock high does not belong to the San Juan thrust system, but more likely the Wrangellia terrane, which crops out onshore southeastern Vancouver Island.

The predominant unconsolidated sediment type in Area 1 is Holocene reworked sediments (Qs on Plate 1). This sediment type is characterized by low to intermediate backscatter intensity and flat, sediment-covered seafloor. Two extensive glacial marine outwash deposits (Qgom on Plate 1) were imaged, one at Salmon Bank and the other at Middle Bank. The surface extents of the glacial marine outwash at Salmon Bank is mapped in detail based upon subtle changes in backscatter intensity along the margin of the deposit. Middle Bank, however, was not fully imaged and the western margin of the bank was denoted based on interpretation of NOAA single-beam imagery. An area just west of Salmon Bank is classified as glacial marine sediment (Qgm on Plate 1) based on the pockmark-like morphology and intermediate backscatter intensity (Figure 4.6A). Hewitt and Mosher (2000) also mapped this area as glacial marine sediment based on interpretation of seismic reflection profiles.

Multiple sediment wave fields and areas of chaotic bedforms were outlined in Area 1. A number of these sediment wave fields, particularly those imaged just south and west of Salmon Bank, were visible in the backscatter imagery, but not in the multibeam imagery (Figure 5.2).

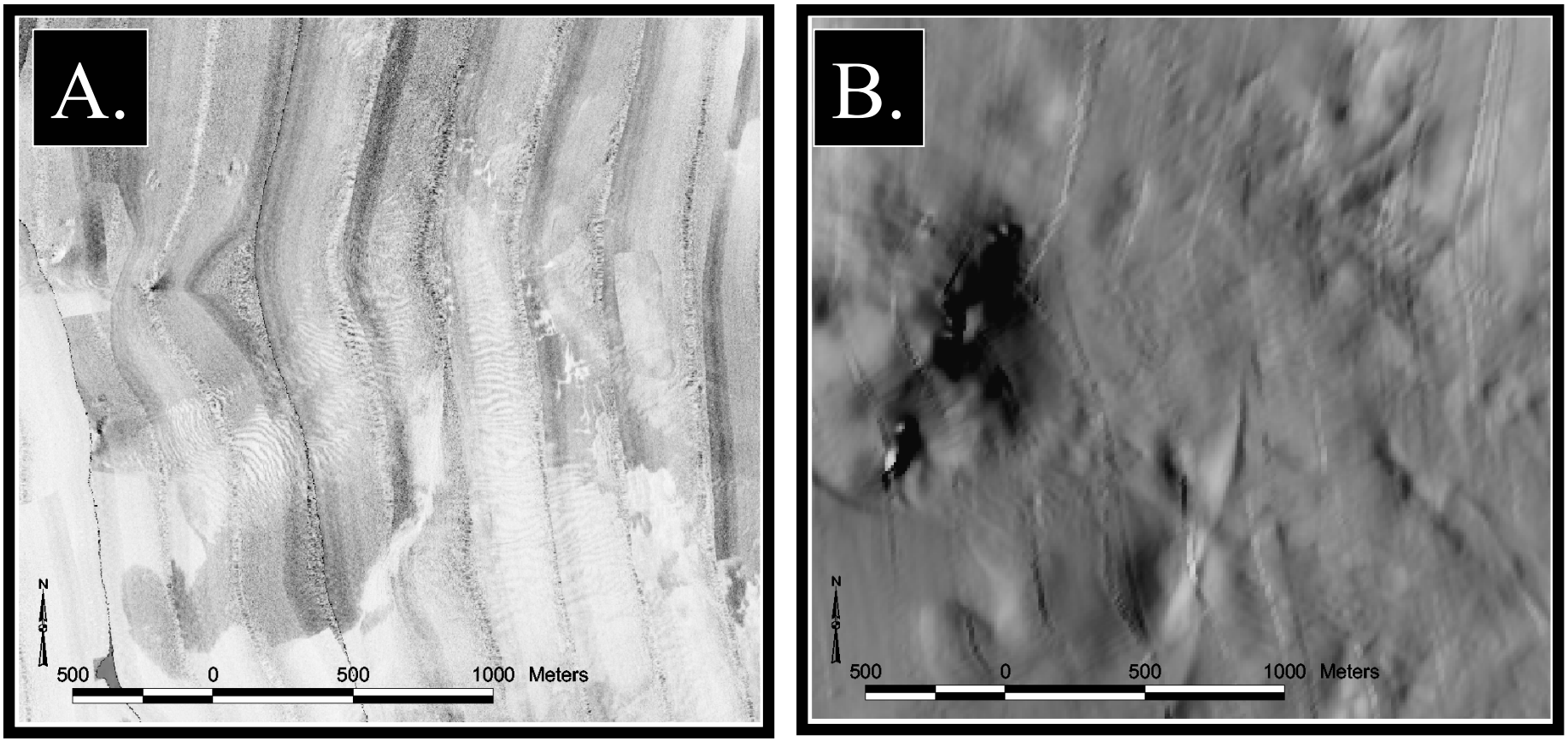

Figure 5.2. On the left (A.) is a multibeam backscatter image showing multiple interlaced sediment wave fields. On the right (B.) is a multibeam bathymetry image of the same area. Note that the sediment wave fields are not clearly defined in the multibeam image. Refer to Figure 3.1. as index map.

This implies that the sediment waves visible only in the backscatter imagery may have wavelengths smaller than the horizontal resolution of the gridded multibeam bathymetry (2 m). The Simrad backscatter imagery has a horizontal accuracy of 10's of centimeters. The chaotic bedforms are located in water depths between 260 and 320 m in an area where upwelling was observed in the form of large boils at the sea surface during the Reson 8101 multibeam survey.

The major structures mapped in this area include northwest-trending faults and folds. A number of the northwest-trending faults, as well as anticlinal and synclinal axes offshore are related to structures mapped by Johnson et al. (2001). The surface traces of Quaternary faults located by Johnson et al. (2001) were relocated and/or extended based on interpretation of the detailed bathymetric and shallow-focused aeromagnetic data. The northwest-trending, S-shaped fold axis in Area 1 is consistent with structural geometries predicted in a left-lateral wrench fault environment (Wilcox et al., 1973) (Figure 5.3 below).

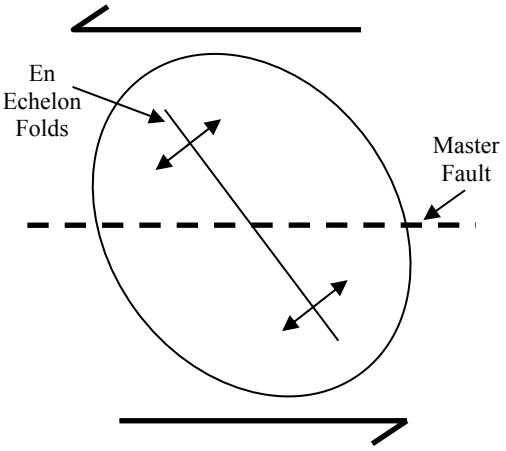

Figure 5.3. Strain ellipse illustrating the predicted structural geometries resulting from the stresses within a left-lateral wrench fault system (modified after Wilcox et al., 1973).

As illustrated in the strain ellipse above in Figure 5.3, NW-SE folds form within an EW trending left-lateral system. The bedrock highs in Area 1 were possibly uplifted and elongated in a NW-SE direction due to wrench fault tectonics along the DMF.

5.1.2. Area 2

The bedrock as imaged with multibeam in Area 2 (Plate 1) is highly faulted and deformed. The predominant lithology here is marine sedimentary rock of the Lopez Structural Complex that has been mapped as KJm(ll) on Plate 1 onshore San Juan Island and Lopez Island

in Cattle Pass (Schuster, 2000). Bedrock exposures off the southeastern tip of Cattle Point are mapped as clastic material of the Constitution Formation. The exotic fault slice of pre-Devonian tonalite (pDi(t) in Plate 1) mapped onshore at the northern tip of Cattle Point is extended offshore to the north and west surrounding Harbor Rock to encompass the bedrock exposure shown in multibeam bathymetric imagery (Figure 5.4).

Unconsolidated sediment in Area 2 was mapped as Holocene reworked sediment (Qs) in areas with low to intermediate backscatter intensity and/or in areas with flat, featureless seafloor as visible in multibeam imagery. An area of high backscatter intensity associated with a plunge pool identified in multibeam imagery at the mouth of San Juan Channel was mapped as "Current-scoured" (Figure 4.7A.). Currents appear to have eroded the eastern slope of Salmon Bank along the 80-m-isobath. The western margin of Salmon Bank has a gentle slope with an irregular shape that fans outward to approximately the 140-m-isobath with hummocky morphology in some areas. Morgan (1996) identified a number of slope failures in seismic reflection profiles from the western and southern margins of Salmon Bank. Numerous sediment wave fields were identified from multibeam bathymetry and backscatter imagery within or at the margins of the heavily scoured region east of Salmon Bank and in the deepest part of Cattle Pass at the northern end of Area 2. Within a region of low backscatter intensity just east of the current-scoured seafloor described above, there is an area that appears to be a slump and is mapped as a landslide (Qls in Plate 1; Figure 3.1, 4.6D). One reason for calling this feature a slump rather than a scour depression, which would have a similar morphology, is that a scoured area would likely have higher backscatter intensity due to coarser sediment. Bathymetric profiles across the slump (Figure 5.5) show characteristic slope failure morphologies. Both a headscarp and slump deposit is visible in more than one profile. Erosion due to current scouring at the mouth of San Juan Channel downslope could cause a failure upslope.

The structures identified in Area 2 are the result of numerous deformational events that occurred since the mid-Cretaceous. The first of these events, described as D2 by Bergh (2002), involved combined strike-slip motion and northwest-directed thrusting as a result of oblique convergence. This deformational event affected the Lopez Structural Complex rocks of Area 2, and is characterized by the existence of distinct lineations within and among marine bedrock outcrops (Figure 5.4). The NW-SE oriented faults mapped in Cattle Pass cut the Lopez Structural Complex. The majority of these faults are extended offshore from faults previously mapped

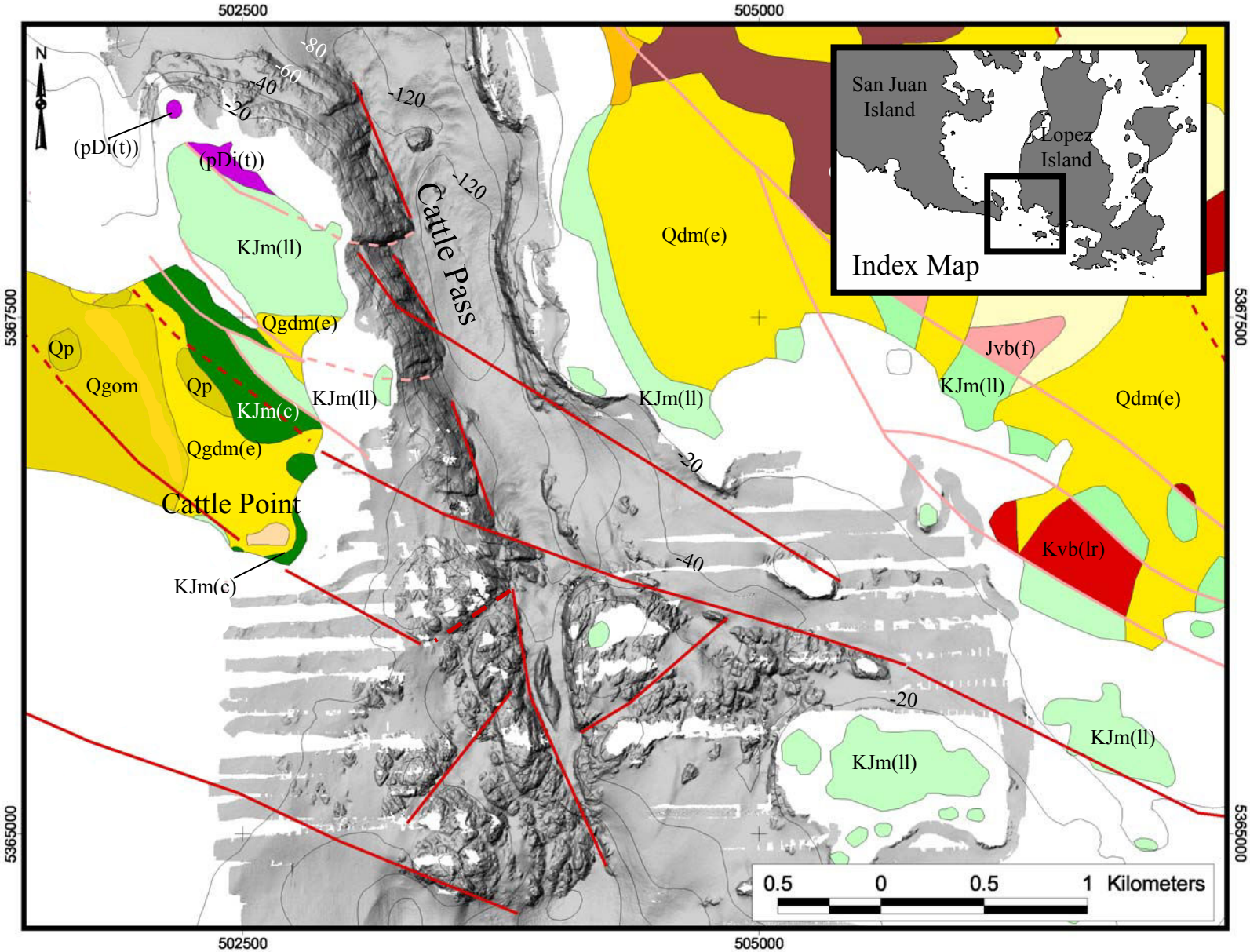

Figure 5.4. Map showing the offshore Reson 8101 multibeam bathymetry, onshore geology of Cattle Pass, and faults of the Lopez Structual Complex. Note the thrust faults (pink) extending offshore Cattle Point into Cattle Pass along distinct bedrock scarps. Contour interval = 20 m. Refer to Plate 1 for explanations of geologic symbology.

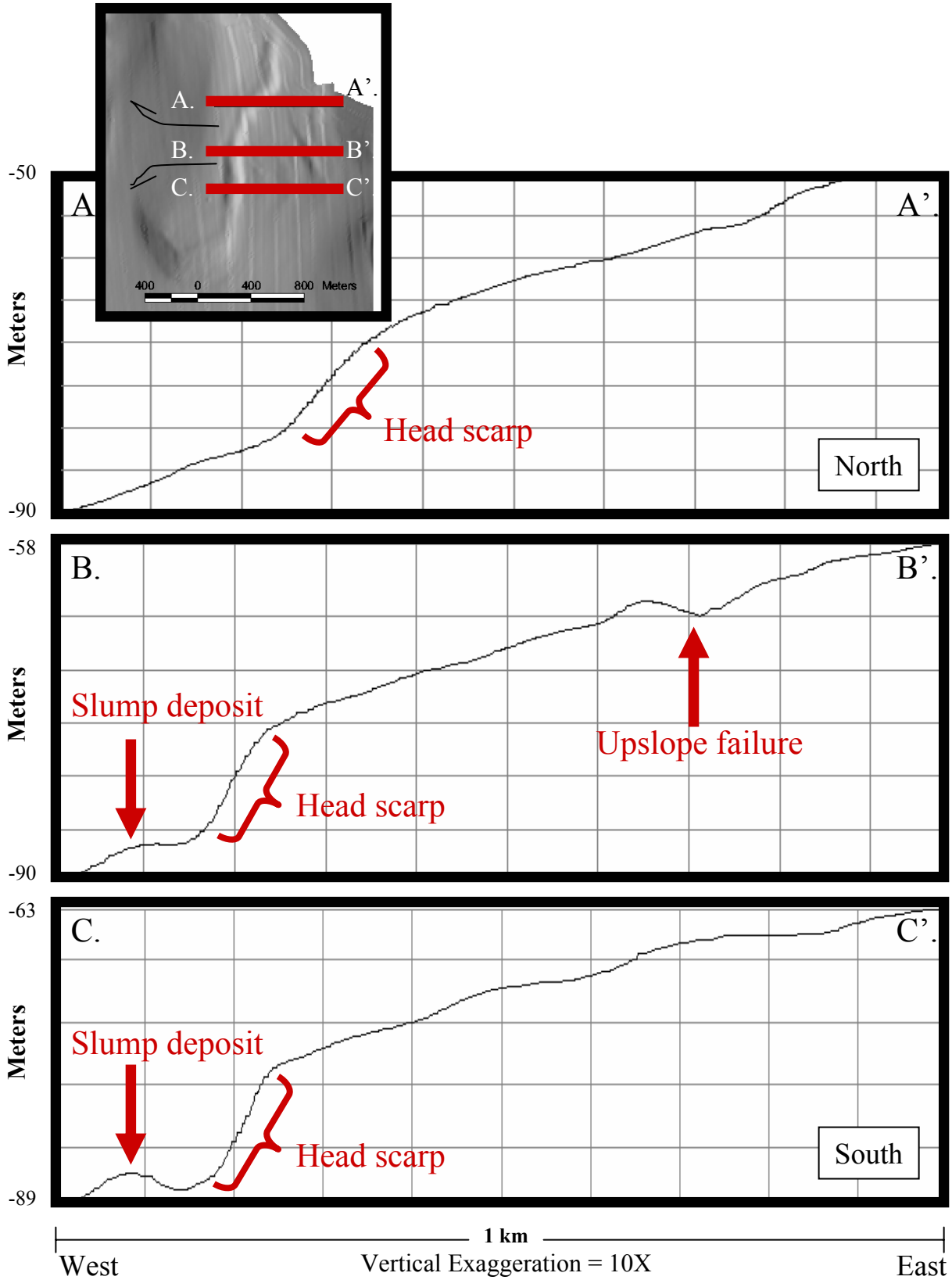

Figure 5.5. East-west cross-sections of the slump at the mouth of San Juan Channel, highlighting characteristic slope failure morphologies. Reference Figure 3.1 as an index map.

onshore. These extensions were based on the existence of distinct lineations within and among bedrock outcrops. The NW-SE trending structures in Cattle Pass correspond to weak NW-SE trending magnetic anomalies. There is no apparent correlation between the NE-SW trending structures in Cattle Pass and shallow magnetic anomalies. The NE-SW trending faults and the NNE-SSW trending faults appear conjugate to the dominant NW-SE fault trend. This relationship is illustrated in Figure 4.2 by the frequency-azimuth rose diagram representing linear features in Cattle Pass. The Lopez Thrust fault is extended offshore along the northern boundary of a bedrock outcrop mapped as marine sedimentary rock of the Lopez Structural Complex. Thrust faults mapped on Cattle Point are extended offshore through the western wall of San Juan Channel along distinct bedrock offsets visible in multibeam bathymetric imagery (Figure 5.4). The fault trace cutting across northern Salmon Bank was inferred based on a linear gradient visible in shallow-focused aeromagnetic data that connects to a distinct lineation in bedrock on the eastern end of the fault.

The most recent of the deformational events in Area 2 involves active left-lateral transpression that occurred and is occurring along the Devils Mountain fault zone. Fault traces identified south of the Reson 8101 multibeam bathymetry coverage in Cattle Pass are mapped as active structures by Johnson et al. (2000) and are associated with the DMF system (Figure 5.6). The fault trace proposed across southern Salmon Bank is based on deformational features within unconsolidated sediment visible on the eastern and western margins of the bank from multibeam bathymetric imagery, as well as a linear magnetic anomaly extending across the bank (Figure 5.7). This fault was extended from a fault mapped by Johnson et al. (2000) based on seismic reflection data. The locations of anticlinal and synclinal axes previously mapped by Johnson et al. (2000) in Area 2 could neither be confirmed nor denied based on multibeam and backscatter imagery.

5.1.3. Area 3

The bedrock exposures in Area 3 (Plate 1) are composed of the Constitution and Lummi Formations and the Turtleback Complex. The clastic rocks of the Constitution Formation line the northern and western shorelines of Area 3, and therefore bedrock exposure identified offshore were also mapped as the Constitution Formation. The bedrock exposures located just north of the Area 2/Area 3 boundary in the middle of San Juan Channel may either be Lummi Formation

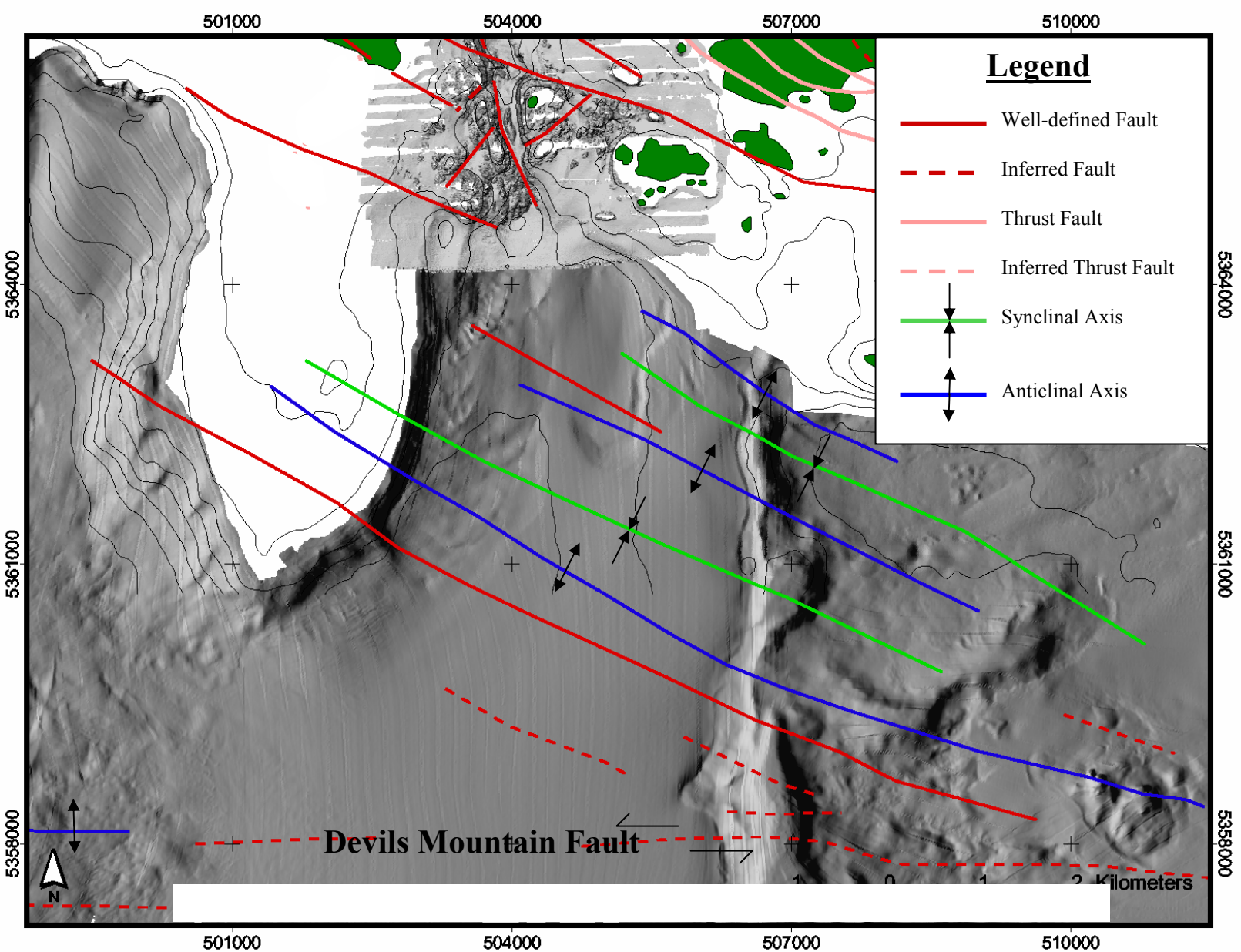

Figure 5.6. Map highlighting the NW-SE oriented geologic structures south of San Juan Channel that Johnson et al. (2000) mapped as active structures associated with the Devils Mountain fault (Structures modified after Johnson et al., 2000).

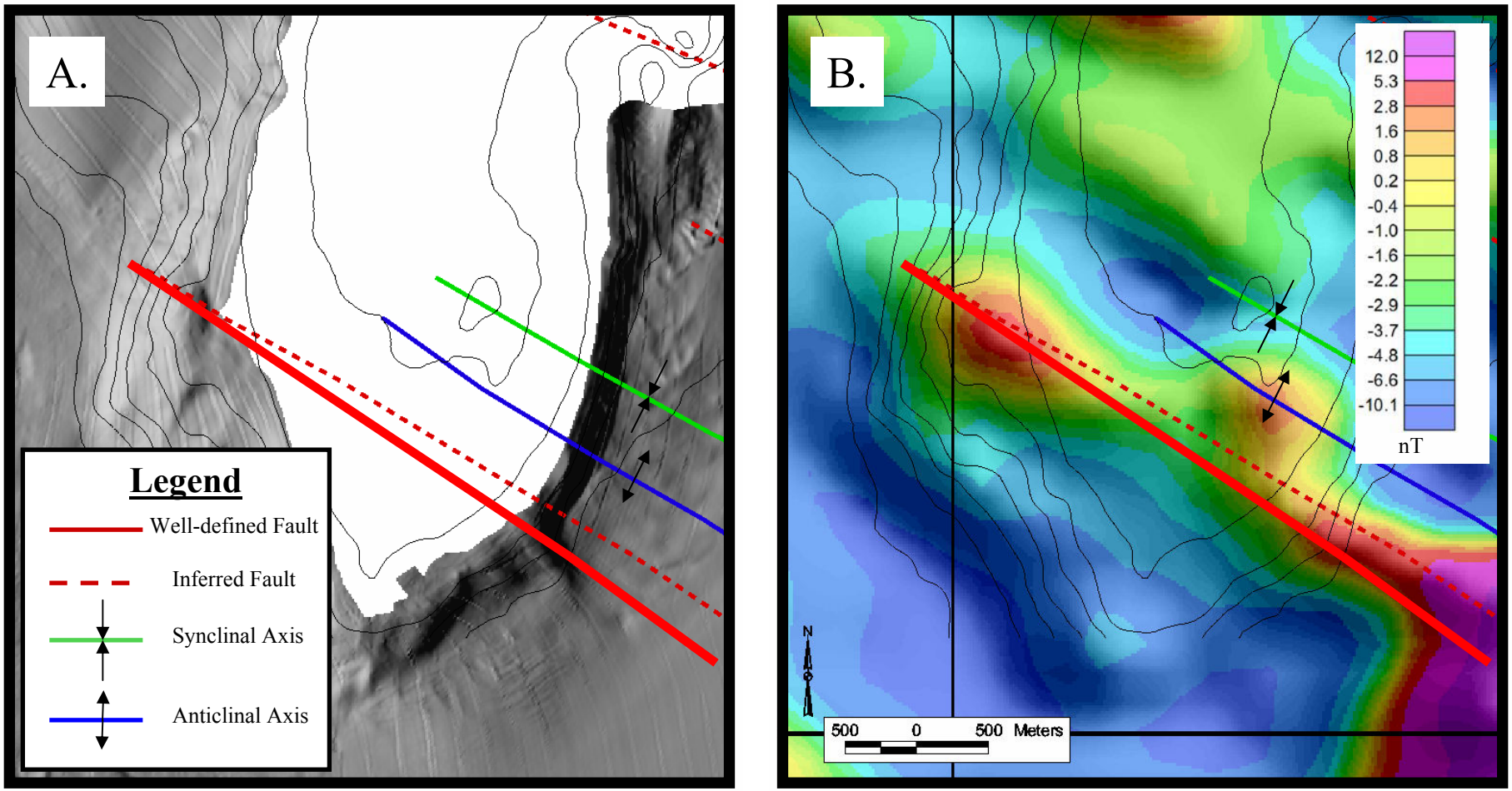

Figure 5.7. Sun-shaded 10 m-resolution Simrad EM1002 multibeam imagery (A.) and sun-shaded shallow-focused aeromagnetic anomalies (B.) at Salmon Bank shown with interpreted structure (thick red solid line = altered trace of previously mapped fault). The proposed fault (thin red dashed line) coincides with apparent sediment deformation in the multibeam imagery and a NW-SE oriented magnetic anomaly. Structure modified after Johnson et al. (2000).

rocks from the Lopez Structural Complex or marine sedimentary rocks of the Lopez Structural Complex. Because a distinction between the two rock types could not be made, these outcrops were tentatively mapped as Lopez Structural Complex rocks (LSC in Plate 1). In Area 3 the Lummi Formation crops out along the shoreline of the peninsula separating San Juan Channel and Fisherman's Bay and therefore the bedrock in the nearshore has been mapped as marine sedimentary rock of the Lummi Formation (Plate 1). No backscatter data were available for this area, and as a result unconsolidated sediment is characterized as either Holocene reworked sediment or sediment waves. Two sediment wave fields were identified from multibeam imagery in Area 3 (Figure 5.8). Both fields are located in the middle of San Juan Channel southeast of Turn Island.

There are only two major structures mapped in Area 3. One is the Buck Bay fault, described by Brandon (1980) as a low angle thrust juxtaposing the Lopez Structural complex and Decatur terrane with the Constitution Formation and older terranes. The other structure is a synclinal axis (Schuster, 2000) onshore San Juan Island (Plate 1). The widely dispersed linear feature orientations plotted for Area 3 likely reflect the convergence of two terranes along the Buck Bay fault followed by regional folding along NW-SE axes. Interpretation of shallow-focused aeromagnetic data in central and southern San Juan Channel suggests that the Buck Bay fault meanders through San Juan Channel to southern Griffin Bay, where the fault trace becomes questionably inferred (Figure 4.4). The meanders in the trace of the fault make sense based on the regional NE-SW folding of the islands and the shallow dip of the fault, as mapped onshore Orcas Island. I have mapped the leading edge of the Buck Bay thrust along the western edge of a weak magnetic anomaly forming a semi-continuous band in central and southern San Juan Channel. The location of the fault trace in southern Griffin Bay is highly speculative because the magnetic anomaly clearly visible to the north becomes indistinguishable near the mouth of San Juan Channel, likely because of the lack of magnetic structure within the highly deformed, relatively non-magnetic rocks of the Lopez Structural Complex.

5.2. POTENTIAL BENTHIC HABITATS BASED ON GEOLOGY

Discussions of habitat require a corresponding discussion of scale, including the scale at which data were collected, the scale at which the data were analyzed, and the scale at which the individual (species) is operating (i.e. home range). According to Sale (1998), in a multi-scalar

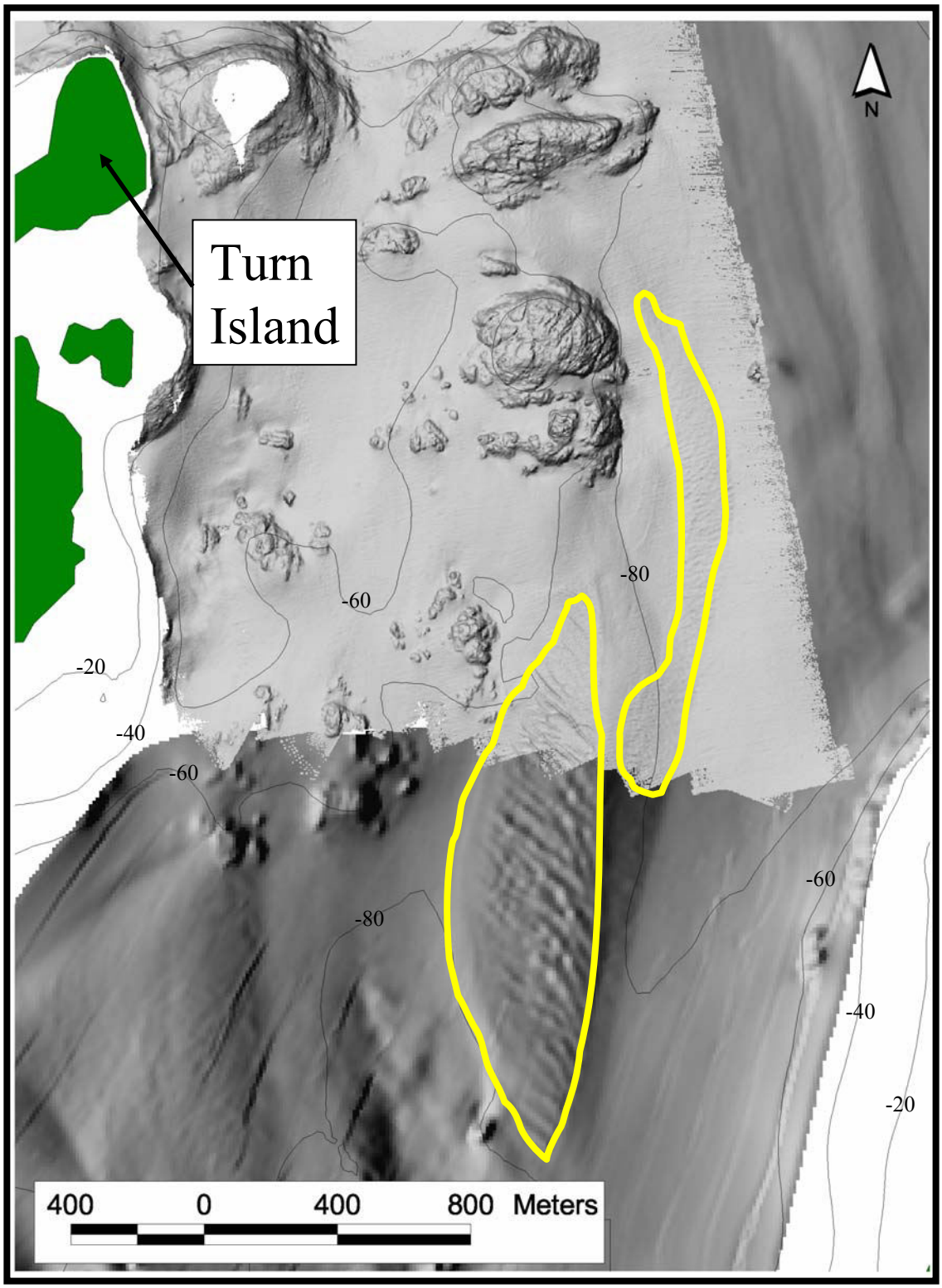

Figure 5.8. Reson 8101 and Simrad EM1002 multibeam imagery showing sediment waves in central San Juan Channel (outlined in yellow). Contour interval = 20 m.

system no one scale is sufficient for sampling, and scale-dependence must be carefully considered when interpreting results. In addition, the accuracy of GPS equipment needs to be taken into consideration in relation to the scale of the data upon which location points are being overlaid. For this study, the horizontal accuracy of the acoustic Trackpoint system used to locate the ROV is approximately 4 m. The cell size of the complexity grid is 2 m. Because the accuracy of the GPS system used in this survey is less than the scale of the data with which the GPS data are being compared, error is introduced. I did not relate fish location to micro-habitat (<1 m) visible on the ROV video, and instead took those fish locations and overlaid them on an independent dataset (complexity grid).

Adult rockfishes are associated with macro-habitat features (e.g. boulders and fractures) within the larger meso-habitats (e.g. rock outcrops > 10 meters in diameter) (Pacunski and Palsson, 2001), meaning the distribution of macro-habitats can affect the use by rockfishes of meso-habitats. The rugosity grid that represents complexity for this study is 2 m-resolution, with each 2 m x 2 m cell having a rugosity value. Therefore, macro-habitats can be identified from this dataset, but the dataset is confounded by the fact that rugosity calculations involved meso-habitat scale neighborhood analysis. It is likely that adult rockfishes are operating on a macro or micro-habitat scale, which is beyond the resolution of the data. For instance, boulder fields, an important macro-habitat for adult rockfishes, were not identifiable using 2 m-gridded multibeam bathymetry data. Boulder fields were visible in the ROV data, but these data represent a small fraction of the area covered by the multibeam survey. Boulder habitats are prevalent offshore the southwestern SJI, likely because of glacial erosion of the bedrock and the resultant deposition of eroded material during retreat of the glacier. Because boulder habitats were utilized by adult and sub-adult rockfishes, these habitats need to be mapped in more detail in the future. Habitat mapping of boulder fields can be achieved using side scan sonar technology (Greene et al., 1995; Yoklavich et al., 1999, 2002;) A side-scan sonar towfish is capable of imaging boulder fields and other benthic macro-habitats. Therefore, integration of side-scan sonar data would likely improve the methodology behind categorizing seafloor complexity.

5.2.1. Seafloor Complexity as a quantitative method

Multibeam bathymetry data reveal a seafloor with numerous outcrops of highly fractured and faulted bedrock, the surfaces of which can be described as complex or rugose. It is the

surface geometry created in part by the tectonic and glacial processes described previously that likely plays a key role in determining the distribution of adult rockfishes in the SJI. The seafloor complexity analysis carried out in this study is quantitative and thus mathematically reproducible, unlike the Greene et al. (1999) method used to map the marine benthic habitats. While area analyses can be applied to marine benthic habitat maps created according to the Greene et al. (1999) method, the interpretation process itself is not quantitative, but qualitative and therefore not mathematically reproducible. The seafloor complexity analysis uses area analysis, which provides a more comprehensive estimation of seafloor complexity compared to two-dimensional methods employed using SCUBA. However, seafloor complexity is merely one component of benthic habitat for adult rockfishes. While it may be a relatively important component, it cannot stand alone as a predictor of potential rockfish habitat.

According to the results of the habitat utilization analysis, adult copper and quillback rockfishes within the southwestern SJI utilize high complexity habitats, and to a lesser degree intermediate complexity habitats. That adult rockfishes also utilize intermediate complexity habitats is not surprising based on the findings of Pacunski and Palsson (2001). These authors observed adult copper and quillback rockfishes in both intermediate and high complexity habitats. In this case, complexity was characterized by the amount of vertical relief and the number of crevices (void space) large enough to accommodate sub-adult to adult rockfishes within the camera's viewing area (~8 to 10 m in diameter).

As a comparison, our study characterized complexity by taking into account vertical relief on the macro-habitat scale, but not void spaces. Both the resolution and down-looking nature of multibeam technology prevents imaging of small voids (i.e. between large boulders) and overhangs. It is also likely that a portion of the rockfishes observed on intermediate complexity macro-habitat were also observed on rock meso-habitat. While a number of rockfishes observed in the ROV video were utilizing a range of rugosity ratios within the intermediate complexity category, mapping both intermediate and high complexity as potential rockfish habitat would be an over-estimation and a misrepresentation of potential rockfish habitat. Instead, complexity data should be integrated with marine benthic habitat maps to map potential rockfish habitats. Marine benthic habitat mapping still needs to be completed in other portions of my study area and throughout the SJI. Once basic habitat mapping is completed, the next step in mapping potential rockfish habitats should involve integrating seafloor

characterization with analyses of other factors that may control the distribution of adult rockfishes; including depth, current speed, and nutrient supply.

Adult copper rockfish have been associated with shallow boulder habitats in central California (Yoklavich et al., 2002), and adult and sub-adult copper and quillback rockfish often utilize boulder habitats within Puget Sound (Pacunski and Palsson, 2001). The same general trend was observed in this study from review of ROV videos. Because the resolution of the multibeam bathymetric imagery is insufficient to distinguish boulder habitats from other habitats, it is not surprising that complexity measured from multibeam bathymetric data does not fully describe the potential habitats of these fishes. Difficulty in navigating the ROV in open water with strong currents resulted in transects preferentially following along either the base or top edge of rock walls where a distinct morphologic boundary could be followed. Boulder habitats were often observed at the base of these rock walls. Because the analysis area for measuring complexity was 36 m^2, boulder habitats were often included with adjacent rock walls, making the boulder habitats spatially indistinguishable from the rock walls. Rock walls always exhibited high complexity. Therefore, adult rockfishes utilization of high complexity macro-habitat may have been overestimated due to the planar (map view) proximity of boulder and rock wall habitats.

5.2.2. Habitat Mapping and MPAs

Studies comparing habitat use of copper and quillback rockfishes with movement patterns in central Puget Sound indicate that adults on high relief rock outcrops, such as are prevalent in the SJI, have significantly smaller home ranges (<30 m^2) than those on low relief rock outcrops (<4000 m^2; Matthews, 1990a, 1990b, c). However, telemetry work done by Eisenhardt (2003) offshore Pile Point on San Juan Island showed that adult copper rockfish can have larger home ranges than originally thought when continuous rocky high relief habitat is present. Similarly, considerable short-term variation in the movements of greenspotted rockfish was observed in central California (Starr et al., 2001) with excursions as large as 1.6 km^2. Starr et al. (2001) attributed these large short-term movements to foraging activity along the canyon ledge, a habitat for which this species may have an affinity.

The distribution of potential rockfish habitat may affect the direction and extent of large horizontal and vertical movements of rockfishes. Thus, the distribution of potential rockfish

habitat relative to MPA boundaries may affect the potential for adult spillover from reserve to non-reserve. For instance, adult rockfishes may move in and out of an MPA more readily if continuous complex rocky habitat spans the MPA boundary, as is the case offshore Pile Point (Figure 5.9). Fisherman directly benefit from an MPA when adult fish travel outside the reserve boundaries, where they can legally be caught. However, prolific adult spillover of long-lived and slow-growing species such as rockfishes would negate the benefits accrued inside the reserve. Thus, the potential for adult spillover from reserve to non-reserve is an important factor in balancing fishing opportunity with continued conservation and recovery efforts. The possible variation in home range size depending on the continuity of essential habitats implies that MPAs with continuous rocky complex habitats extending outward from reserve boundaries would have greater potential for adult spillover. Hence, identifying and mapping the spatial distribution of adult rockfish habitats in the southern SJI may provide important baseline information for developing management plans which include MPAs. Marine benthic habitat maps and seafloor complexity maps can also provide a foundation for scientific research aimed at developing more quantitative habitat models.

6. CONCLUSIONS

The integration of existing geologic and geophysical datasets with new multibeam bathymetry and backscatter interpretations has resulted in a seamless onshore-offshore geologic map of the southwestern SJI. Sun-shaded images of processed multibeam bathymetry and multibeam backscatter data reveal a complex network of faulted and fractured bedrock outcrops, glaciated channels, Pleistocene glacial deposits, and dynamic bedforms. The tectonics, past and present, within the SJI region have produced faulted and fractured bedrock surfaces. Three areas within the southwestern SJI have distinctive bedrock patterns and structural character. Strong NW-SE trending linear features within Areas 1 and 2 likely reflect compression during late Cretaceous thrusting, subsequent movement along late Cretaceous strike-slip faults in the Lopez Structural Complex, and recent oblique left-lateral convergence along the DMF. The widely dispersed orientations of linear features in Area 3 likely reflect the NW-SE convergence of two terranes along the Buck Bay thrust fault and regional folding along NW-SE axes. Multibeam backscatter imagery was especially useful in delineating the surface extents of a number of glacial sedimentary deposits throughout the study area, including the surface extents of Middle,

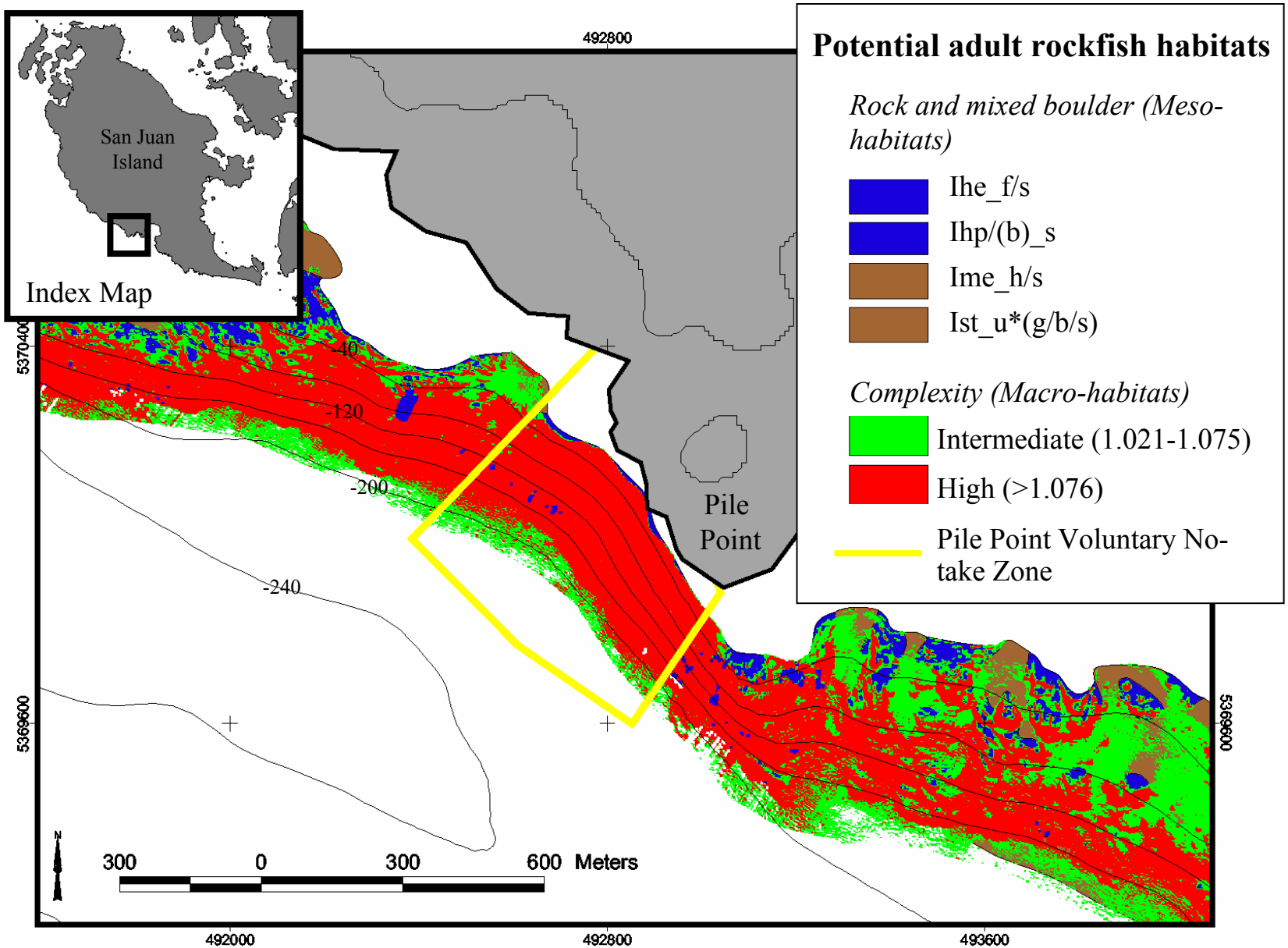

Figure 5.9. Map showing continuous rocky complex habitat extended outward from the Pile Point Voluntary No-take Zone (yellow). Contour interval onshore = 20 m, offshore = 40 m.

Salmon, and McArthur banks. The numerous sediment wave fields identified in multibeam bathymetry and backscatter imagery reflect the funneling of large amounts of water through deep, narrow channels during tidal cycling. In addition, distinct slump morphologies in multibeam bathymetry and backscatter imagery suggest recent slumping of Holocene sediments at the mouth of San Juan Channel.

Shallow-focused aeromagnetic data within the SJI reveal a number of areas with distinct anomaly patterns, which likely reflect regional tectonic features. Gradients in magnetic anomalies often corresponded with fault traces identified in high-resolution multibeam bathymetric imagery and may reflect slight magnetic susceptibility contrasts across fault contacts. Aeromagnetic data constrained two terrane boundaries not identified in multibeam imagery: 1) the Buck Bay fault, which separates the Lopez Structural Complex and Decatur terrane from the underlying Constitution Formation, and 2) the Haro fault separating the Deadman Bay terrane of the San Juan Thrust system from the Wrangellia terrane on Vancouver Island. Structural analysis using multibeam and aeromagnetic data allowed identification of numerous faults and other tectonic landforms, expanding the knowledge of fault networks within and adjacent to the active Devils Mountain fault. This new information will be useful for regional seismic hazard assessment.

Mid-Cretaceous thrusting and resultant uplift of the SJI has resulted in a local bedrock high within the larger Puget lowland. Likely as a result of post-Oligocene oblique left-lateral convergence along the EW-trending DMF, a NW-SE-trending bedrock high developed approximately 4 km offshore of southwestern San Juan Island. The glaciers that moved through the northern Puget Lowland scoured deep channels in the SJI and deposited large amounts of glacial sediment where the glaciers paused during retreat. The glacial scouring and tectonic uplift, combined with the daily tidal flushing that occurs throughout the islands, has left much of the seafloor devoid of recent sediments and bedrock exposed over large areas. The faulted and fractured bedrock and prevalent mixed boulder substrate represent marine benthic habitats for a number of marine species including adult copper and quillback rockfishes. The geologic information described above provided a framework for classifying marine benthic habitats. In total, fifteen marine benthic habitats were identified within the study site, eight of which were considered potential adult rockfish habitats based on having classifications that included rock or mixed boulder substrate.

In an attempt to create a quantitative tool for assessing habitat and improve the predictive capabilities of marine benthic habitat mapping, a unique seafloor complexity index was developed based on a quantitative and reproducible methodology involving computerized analysis of gridded multibeam data. Seafloor complexity utilization by rockfishes suggests adult copper and quillback rockfishes utilize high complexity seafloor, and to a lesser degree intermediate complexity seafloor as identified from multibeam bathymetry. Since adult rockfishes utilized intermediate complexity habitats, high seafloor complexity alone does not adequately define potential adult rockfish benthic habitats in the southwestern SJI. The resolution of multibeam bathymetry data in this study (2 m) was insufficient for identifying boulder substrate, a habitat type highly associated with copper and quillback rockfishes. Multibeam bathymetry may be inadequate for pinpointing threshold complexities that accurately characterize boulder habitats. Collection of quality high-resolution backscatter and/or side-scan sonar data, having horizontal resolutions of 10's of centimeters, could allow for identification of boulder field habitat. Potential adult rockfish habitats were identified within the study site by characterizing and mapping seafloor complexity and integrating these data with marine benthic habitat maps. The seafloor complexity data overlain on marine benthic habitat maps illustrates the regional distribution of rocky complex habitat. Integrating these two datasets illustrates intermediate complexity seafloor that corresponds to rock macro and meso-habitats. These data can be used by fisheries scientists and resource managers to make scientifically based decisions about conservation, particularly in regards to the establishment of MPAs. This study helps bridge the gap in scale between traditional fisheries surveys (e.g. SCUBA, video, or trawl) and regional mapping efforts using remote sensing. Collecting and integrating data at a number of scales will likely provide the most in-depth view of the ecosystem(s) being studied. GIS provides a useful platform for integrating and analyzing such multi-scalar datasets.

ACKNOWLEDGEMENTS

This research was made possible by funding from a variety of sources, including the Dickinson Foundation; the Marine Ecosystem Health Program (SeaDoc) of the University of California Davis; NOAA's National Undersea Research Program, West Coast and Polar Regions Undersea Research Center, University of Alaska Fairbanks; the NOAA Coastal Services Center; and the Dr. Earl H. Myers and Ethel M. Myers Oceanographic and Marine Biology Trust. A special thanks for the support and encouragement given by Kathy and Ron McDowell. I would like to thank the captains and crews of the *R/V MacGinitie*, *R/V Vector*, and *R/V Molluscan* for providing research platforms for the multibeam surveys and the ROV survey. Thanks to the University of Washington's Friday Harbor Laboratories , especially David Duggins, for the use of their ROV. Also, thank you Lance Horn for your expertise in navigating and in teaching others to navigate an ROV in the high-current conditions of the San Juan Islands. I would like to thank Bob Pacunski and Eric Eisenhardt of the Washington Department of Fish and Wildlife. Thanks to the Geological Survey of Canada and the Canadian Hydrographic Service for their continued support and cooperation in collecting geophysical data in the San Juan Islands/southwestern Vancouver Island region. I would also like to thank Rick Blakely at the U.S. Geological Survey for supplying aeromagnetic anomaly maps. Special thanks to my major advisor, Gary Greene and committee members Ivano Aiello, Gregor Caillet, and Wayne Palsson. Joe Bizzarro and Jeff Field, I thank you both for your help with statistics and video analysis. Thank you Holly Lopez for processing the multibeam backscatter I used for my research. Thanks Norman Maher for creating the shaded relief grid of the NOAA single-beam bathymetry data. In addition, I would like to thank Tracy Vallier, Casey Moore, Sam Johnson, and the Geophysics Unit of Menlo Park (GUMP) for their conversations, suggestions, and comments that greatly improved the quality of this work. Special thanks to Steve Watt for all his patience and support.

LITERATURE CITED

Atwater, B.F. and Moore, A.L., 1992. A tsunami about 1000 years ago in Puget Sound, Washington. Science, 258: 1614-1617.

Beaumont, E.A. and Foster, N.H., 1989. *Geophysics IV: Gravity, Magnetic, and Magnetotelluric Methods*, Treatise of Petroleum Geology Reprint Series, No. 15, The American Association of Petroleum Geologists: Tulsa, Oklahoma, 1533p.

Bergh, S.G., 2002. Linked thrust and strike-slip faulting during Late Cretaceous terrane accretion in the San Juan thrust system, Northwest Cascades orogen, Washington. Geological Society of America Bulletin, 114: 934-949.

Blais-Stevens, A. and Clague, J.J., 2001. Paleoseismic signature in late Holocene sediment cores from Saanich Inlet, British Columbia. Marine Geology, 175: 131-148.

Blakely, R.J., 1996. Potential Theory in Gravity & Magnetic Applications. Cambridge Univ. Press, New York: 441 pp.

Blakely, R.J.; Langenheim, V.E.; Ponce, D.A.; and Dixon, G.L., 2000. Aeromagnetic survey of the Amargosa Desert, Nevada and California: a tool for understanding near-surface geology and hydrology: U.S. Geological Survey Open-File Report 00-188, 32 p., 2 plates. http://geopubs.wr.usgs.gov/open-file/of00-188

Bogue, S.W.; Cowan, D.S.; and Garver, J.I., 1989. Paleomagnetic evidence for poleward transport of Upper Jurassic rocks in the Decatur terrane, San Juan Islands, Washington, Journal of geophysical research, 94: B8, 10415-10427.

Booth, D.B. and Goldstein, B., 1994. Patterns and processes of landscape development by the Puget Lobe ice sheet. Washington Division of Geology and Earth Resources Bulletin, 80, 207-218.

Brandon, M.T., 1980. Structural geology of middle Cretaceous thrust faulting on southern San Juan Island, Washington. M.S. thesis: Seattle, University of Washington, 130 p.

Brandon, M.T., 1985. Mesozoic mélange of the Pacific Rim Complex, western Vancouver Island, *in* Tempelman-Kluit, D., ed. Field guides to geology and mineral deposits in the southern Canadian Cordillera, Geological Society of America Cordilleran section meeting: Vancouver, British Columbia, Geological Survey of Canada, 7.1-7.28.

Brandon, M.T.; Cowan, D.S.; Muller, J.E.; and Vance, J.A., 1983. Fieldtrip Guidebook: Pre-Tertiary geology of San Juan Islands, Washington and southeast Vancouver Island, British Columbia. Geological Association of Canada, Victoria Section, 65p.

Brandon, M.T.; Cowan, D.S.; and Vance, J.A., 1988. The Late Cretaceous San Juan thrust system. Geological Society of America Special Paper 221, 81p.

Brandon, M.T.; Cowan, D.S.; and Feehan, J.G., 1993. Kinematic analysis of the San Juan thrust system, Washington: Discussion. Geological Society of America Bulletin, 105: 839-841.

Brown, E.H., 1987. Structural geology and accretionary history of the Northwest Cascades system, Washington and British Columbia. Geological Society of America Bulletin, 99: 201-214.

Burmester, R.F., Blake Jr., M.C., and Engebretson, D.C., 2000. Remagnetization during Cretaceous Normal Supercron in Eastern San Juan Islands, WA: implications for tectonic history. Tectonophysics, 326: 73-92.

Danner, W.R., 1977. Paleozoic rocks of northwest Washington and adjacent parts of British Columbia, in Stewart, J.H., Steven, C.H., and Fritsche, A.E., Eds., Paleozoic paleogeography of the western United States: Society of Economic Paleontologists and Mineralogists, Pacific Section, 481-502.

Dethier, D.P.; Pessl, Jr., F.; Keuler, R.F.; Balzarini, M.A.; and Pevear, D.R., 1995. Late Wisconsinan glaciomarine deposition and isostatic rebound, northern Puget Lowland, Washington. GSA Bulletin, 107: 11, 1288-1303.

Easterbrook, D.J., 1992. Advance and retreat of Cordilleran ice sheets in Washington, U.S.A. *Géographie physique et Quaternaire*, 46: 1, 51-68.

Easterbrook, D.J., 1994. Chronology of Pre-Late Wisconsin Pleistocene sediments in the Puget Lowland, Washington. Washington Division of Geology and Earth Resources Bulletin, 80: 191-206.

Eisenhardt, E.P., 2003. San Juan County Bottomfish Recovery Program, 2002 Acoustic Telemetry Project Final Report. 34pp.

Eschmeyer, W.N., Herald, E.S., and Hammann, H., 1983. A field guide to Pacific coast fishes of North America. Houghton Mifflin Company: Boston, U.S.A. 336p.

Feehan, J.G. and Brandon, M.T., 1999. Contribution of ductile flow to exhumation of low-temperature, high-pressure metamorphic rocks: San Juan-Cascade nappes, NW Washington State. Journal of Geophysical Research, 104: B5, 10883-10902.

Fox, D.; Amend, M.; and Merems, A., 1999. 1999 Nearshore Rocky Reef Assessment. Coastal Zone Management Section 309 Grant Final Report, Contract No. 99-072, 32p.

García-Charton, J.A. and Pérez-Ruzafa, Á., 2001. Spatial pattern and the habitat structure of a Mediterranean rocky reef fish local assemblage, Marine Biology, 138: 917-934.

Glassley, W.E., Whetten, J.T.; Cowan, D.S.; and Vance, J.A., 1976. Significance of coexisting lawsonite, prehnite, and aragonite in the San Juan Islands, Washington. Geology, 4: 301-302.

Gower, H.D.; Yount, J.C.; and Crosson, R.S.; 1985. Seismotectonic map of the Puget Sound region, Washington. U.S. Geological Survey Miscellaneous Investigations Series Map I-1613, scale 1:250,000.

Greene, H.G., Yoklavich, M.M., Sullivan, D., and Caillet, G.M., 1995, A geophysical approach to classifying marine benthic habitats: Monterey Bay as a model, in: O'Connell, T., and Wakefield, W. (Eds.), Applications of side-scan sonar and laser-line systems in fisheries research, Alaska Dept. Fish and Game Sp. Publ. No. 9, pp. 50.

Greene, H.G.; Yoklavich, M.M.; Starr, R.M.; O'Connell, V.M.; Wakefield, W.W.; Sullivan, D.E.; McRea Jr., J.E.; and Cailliet, G.M., 1999. A classification scheme for deep seafloor habitats. Oceanologica Acta, 22: 6, 663-678.

Greene, H.G. and Tilden, J.E., 2002. Using Multibeam bathymetry to characterize rockfish habitat in San Juan County, Washinton marine reserves, USA, MEHP final report, Marine Ecosystem Health Program, University of California Davis, 5 plates, 21p.

Hart, J.L., 1973. Pacific fishes of Canada. Fish. Res. Board Can. Bull. 180, 740p.

Hewitt, A.T. and Mosher, D.C., 2001. Late Quaternary stratigraphy and seafloor geology of eastern Juan de Fuca Strait, British Columbia and Washington, Marine Geology, 177: 295-316.

Hirshfeld, M.A., 1996. Inside a lastest Pleistocene ice-contact submarine fan, Northern Puget Lowland, Washington, Undergraduate Thesis, Williams College, 121p.

Housen, B.A. and Beck, Jr., M.E., 1999. Testing terrane transport: an inclusive approach to the Baja B.C. controversy. Geology, 27: 4, 1143-1146.

Irving, E., 1985. Whence British Columbia? Nature, 314: 673-674.

Jenness, J., 2001. Surface Areas and Ratios Extension. ArcView 3.x extension and readme documentation.

Johnson, D.H., 1980. The comparison of usage and availability measurements for evaluating resource preference. Ecology, 81: 1, 65-71.

Johnson, S.Y., 1999. Neotectonics of the Devils Mountain Fault and Northern Whidbey Island Fault, Eastern Strait of Juan de Fuca and Northern Puget Lowland, Washington. Seismological Research Letters, 70: 2, 220.

Johnson, S.Y.; Mosher, D.C.; Dadisman, J.R.; Childs, J.R.; and Rhea, S.B., 2000. Tertiary and Quaternary structure of the eastern Juan de Fuca Strait: interpreted map, *in*: Mosher, D.C. and Johnson, S.Y. (Eds.), Rathwell, G.J., Kung, R.B., and Rhea, S.B. (Compilers), Neotectonics of the eastern Juan de Fuca Strait; a digital geological and geophysical atlas. Geological Survey of Canada Open File Report 3931.

Johnson, S.Y.; Dadisman, S.V; Mosher, D.C; Blakely, R.J.; and Childs, J.R., 2001. Active tectonics of the Devils Mountain fault and related structures, Northern Puget Lowland and Eastern Strait of Juan de Fuca region, Pacific Northwest. U.S. Geological Survey Professional Paper 1643, 45p.

Jones, D.L.; Howell, D.G.; Coney, P.J.; and Monger, J.W.H., 1983. Recognition, character, and analysis of tectonostratigraphic terranes in western North America, in Hashimoto, M. and Uyeda, S., (Eds.) Accretion tectonics in the circum-Pacific regions: Tokyo, Terra Scientific Publishing Company, 21-35.

Jones, M.A., 1999. Geologic Framework for the Puget Sound Aquifer System, Washington and British Columbia. U.S. Geological Survey Professional Paper #1424-C, 31p.

Kovanen, D.J. and Easterbrook, D.J., 1997. Two re-advances of the Cordilleran ice sheet in the northern Puget Lowland, WA, during the Sumas stade between 10,000 and 11,500 C-yrs B.P. ABTRACT: Geological Society of America annual meeting, 29: 6, 109.

Kovanen, D.J. and Easterbrook, D.J., 2001. Late Pleistocene, post-Vashon, alpine glaciation of the Nooksack drainage, North Cascades, Wasington. Geological Society of America Bulletin, 113: 2, 274-288.

Krebs, C.J., 1999. Ecological Methodology, 2nd Ed., Addison-Welsey Educational Publishers, Inc., Menlo Park, CA, 620pp.

Lapen, T.J., 2000. Geologic Map of the Bellingham 1:100,000 Quadrangle, Washington. Washington Division of Geology and Earth Resources, Open File Report #2000-5, 36p., 2 plates.

Loveseth, T.P., 1975. The Devils Mountain fault zone, northwestern Washington: Seattle, Wash., University of Washington M.S. thesis, 29p.

Maekawa, H. and Brown, E.H., 1991. Kinematic analysis of the San Juan thrust system, Washington. Geological Society of America Bulletin, 103: 1007-1016.

Maekawa, H. and Brown, E.H., 1993. Kinematic analysis of the San Juan thrust system, Washington: Reply. Geological Society of America Bulletin, 105: 841-844.

Mahoney, J.B.; Mustard, P.S.; Haggart, J.W.; Friedman, R.M.; Fanning, C.M.; and McNicoll, V.J., 1999. Archean zircons in Cretaceous strata of the western Canadian Cordillera: The "Baja B.C." hypothesis fails a "crucial test", Geology, 27: 27-95.

Manly, B.F.J.; McDonaly, L.L.; Thomas, D.L.; McDonald, T.L.; and Erikson, W.P., 2002. Resource Selection by Animals, 2nd Ed., Kluwer Academic Publishers, Dordrecht, The Netherlands, 221pp.

Matthews, K.R., 1990a. A comparative study of habitat use by young-of-the-year, subadult, and adult rockfishes on four habitat types in Central Puget Sound. Fishery Bulletin, 88: 223-239.

Matthews, K.R., 1990b. A telemetric study of the home ranges and homing routes of copper and quillback rockfishes on shallow rocky reefs. Canadian Journal of Zoology, 68: 2243-2250.

Matthews, K.R., 1990c. An experimental study of the habitat preferences and movement patterns of copper, quillback, and brown rockfishes (*Sebastes* spp.). Environmental Biology of Fishes, 29: 161-178.

Mazzoti, S.; Dragert, H.; Hyndman, R.D.; Miller, M.M.; and Henton, J.A., 2002. GPS deformation in a region of high crustal seismicity: N. Cascadia forearc, Earth and Planetary Science Letters, 198: 41-48.

Mathewes, R.W. and Clague, J.J., 1994. Detection of large prehistoric earthquakes in the Pacific Northwest by microfossil analysis. Science, 264: 688-691.

McClellan, R.D., 1927. The geology of the San Juan Islands. Washington Univ. Publ. *in:* Geology 2: 185pp.

McGroder, M.F., 1991. Reconciliation of two-sided thrusting, burial metamorphism, and diachronous uplift in the Cascades of Washington and British Columbia. Geological Society of America Bulletin, 103: 189-209.

Monger, J.W.H.; Price, R.A.; and Tempelman-Kluit, J.D., 1982. Tectonic accretion and the origin of the two major metamorphic and plutonic belts in the Canadian Cordillera. Geology, 10: 70-75.

Morgan, W.S., 1996. Terrestrial and marine evidence for changing ice regime during latest Pleistocene ice recession, Northern Puget Lowland, Washington. Undergraduate Thesis, Williams College, 136p.

Mosher, D.C. and Johnson, S.Y. (Eds.), Rathwell, G.J.; Kung, R.B.; and Rhea, S.B. (Compilers), 2000. Neotectonics of the eastern Juan de Fuca Strait; a digital geological and geophysical atlas. Geological Survey of Canada Open File Report 3931.

Muller, J.E., 1980. The Paleozoic Sicker Group of Vancouver Island, British Columbia: Geological Survey of Canada Paper 79-30, 23 p.

Muller, J.E., 1983. Geology, Victoria, British Columbia: Geological Survey of Canada Map 1553A, scale 1:100,000.

Neu, C.W.; Byers, C.R.; and Peek, J.M., 1974. A technique for analysis of utilization availability data. Journal of Wildlife Management, 38: 541-545.

O'Connell, V.M. and Carlile, D.W., 1993. Habitat-specific density of adult yelloweye rockfish *Sebastes ruberrimus* in the eastern Gulf of Alaska. Fishery Bulletin, 91: 304-309.

Oldow, J.S., 2000. Fault Characterization and assessment of slip on the Devil's Mountain and North Whidbey Island fault systems, northwestern Washington. U.S. Geological Survey Final Technical Report, 10p.

Oldow, J.S., Bally, A.W., and Avé Lallement, H.G., 1990. Transpression, orogenic float, and lithospheric balance. Geology, 18: 991-994.

Pacific Fishery Management Council, 1999. Status of the Pacific coast groundfish fishery through 1999 and recommended accepFigure biological catches for 2000: stock assessment and fishery evaluation. Pacific Fishery Management Council, Portland, OR.

Pacunski, R.E. and Palsson, W.A., 2001. Macro- and micro-habitat relationships of adult and sub-adult rockfish, lingcod, and kelp greenling in Puget Sound. Proceedings of the Puget Sound Research Conference: Bellvue, WA, 11p.

Palsson, W.A. and Pacunski, R.E., 1995. The response of rocky reef fishes to harvest refugia in Puget Sound. In: Puget Sound Research, 1: 224-234, Puget Sound Water Quality Authority, Olympia, Washington.

Palsson, W.A.; Northrup, T.J.; and Barker, M.W., 1998. Puget Sound Groundfish Management Plan, Washington Department of Fish and Wildlife Fish Program Marine Resources Division, 43p.

Porter, S.C. and Swanson, T.W., 1998. Radiocarbon age constraints on rates of advance and retreat of the Puget Lobe of the Cordilleran ice Sheet during the last glaciation. Quaternary Research, 50: 205-213.

Price, R.A. and Charmichael, D.M., 1986. Geometric test for Late Cretaceous-Paleogene intracontinental transform faulting in the Canadian Cordillera, Geology, 14, 468-471.

Puget Sound Water Quality Action Team, 2000. Puget Sound Update: Seventh report of the Puget Sound Ambient Monitoring Program, 127pp.

Ramachandran, K., 2003. Structure of the Cascadia subduction zone below Vancouver Island: Juan de Fuca plate and forearc mantle. Geological Society of America annual meeting abstract, Washington State Convention and Trade Center, Seattle: paper no. 127-8.

Rubin, C.M.; Saleeby, J.B.; Cowan, D.S.; Brandon, M.T.; and McGroder, M.F., 1990. Regionally extensive mid-Cretaceous west-vergent thrust system in the northwestern Cordillera: Implications for continent-margin tectonism. Geology, 18: 276-280.

Russell, R.H., Ed., 1975. *Geology and Water Resources of the San Juan Islands, San Juan County Washington.* Washington Department of Ecology Water Supply Bulletin #46, 56p.

San Juan Nature Institute, 1998. *Marine Reserve: Bottomfish Recovery Program, San Juan County Marine Resources Committee* (pamphlet, reprinted by Washington Sea Grant Program.

Sale, P.F., 1998. Appropriate spatial scales for studies of reef-fish ecology. Australian Journal of Ecology, 23: 202-208.

Schuster, J.E., 2000. Digital Geology of Washington State. Washington State Department of Natural Resources Division of Geology and Earth Resources, scale 1:100,000.

Starr, R.M.; Heine, J.N.; Felton, J.M.; and Caillet, G.M., 2002. Movements of bocaccio (*Sebastes paucispinis*) and greenspotted (*S. chlorostictus*) rockfishes in a Monterey submarine canyon: implications for the design of marine reserves. Fish. Bull., 100: 324-337.

Thorson, R.M., 1980. Ice-Sheet glaciation on the Puget Lowland, Washington, during the Vashon Stade (Late Pleistocene), Quaternary Research, 13: 303-321.

Thorson, R.M., 1989. Glacio-isostatic response of the Puget Sound area, Washington: Geological Society of America Bulletin, 101: 1163-1174.

Todd, B.J.; Pickrill, R.A.; Valentine, P.C.; Snow-Carter, S.; and Noji, T., 2002. Mapping the Gulf of Maine: Building the link between marine geology and benthic habitats to improve ocean management. Abstract, GEOHAB: Marine Geological Habitat Mapping Conference, Moss Landing Marine Laboratories, CA, p. 40.

Vance, J.A., 1968. Metamorphic aragonite in the prehnite-pumpellyite facies, northwest Washington: American Journal of Science, 266: 299-315.

Vance, J.A., 1977. The stratigraphy and structure of Orcas Island, San Juan Islands. *In:* Geological Excursions in the Pacific Northwest, Eds. E.H. Brown & R.C. Ellis, Geological Society of America 1977 Annual Meeting, Seattle, 170-203.

Vance, J.A.; Dungan, M.A.; Blanchard, D.P.; and Rhodes, J.A., 1980. Tectonic setting and trace element geochemistry of Mesozoic ophiolitic rocks in western Washington: American Journal of Science, 280-A: 359-388.

West, J.E.; Buckley, R.M.; Doty, D.C.; and Bookheim, B.E., 1997. Ecology and habitat use of juvenile rockfishes (Sebastes spp.) associated with artificial nursery habitats in Puget Sound, Washington, 191-202, *In:* Puget Sound Research 1995, Puget Sound Water Quality Authority, Olympia, WA.

Wells, R.E., Blakely, R.J., and Weaver, C.S., 2002. Cascadia microplate models and within-slab earthquakes. *in:* The Cascadia Subduction Zone and Related Subduction Systems, U.S. Geological Survey Open File Report, ?????, 17-22.

Wilcox, R.E.; Harding, T.P.; and Seely, D.R., 1973, Basic wrench tectonics. *in*: Sylvester, A.G., 1984. *Wrench Fault Tectonics: Selected papers reprinted from the AAPG Bulletin and other geological journals*, AAPG Reprint Series No. 28, American Association of Petroleum Geologists, Tulsa, Oaklahoma: 291-313.

Wilson, D.S., 2002. The Juan de Fuca plate and slab: Isochron structure and Cenozoic plate motions, *in:* The Cascadia Subduction Zone and Related Subduction Systems, U.S. Geological Survey Open File Report, ?????, 9-12.

Yoklavich, M., ed., 1998. Marine harvest refugia for West Coast rockfish: A workshop, NOAA Technical Memorandum NMFS, NOAA-TM-NMFS-SWFSC-255, 159pp.

Yoklavich, M.M., de Marignac, J., Field, J.M., Lea, R.N., Caillet, G.M., and Starr, R.M., 2000, Deepwater benthic fish and habitats associated with a marine reserve off central California. Abstract in 11th Western Groundfish Conference, Sitka, Alaska.

Yoklavich, M.M.; Greene, H. G.;Cailliet, G.M.; Sullivan, D.E; Lea, R.N.; and Love, M.S., 2000. Habitat associations of deep-water rockfishes in a submarine canyon: an example of a natural refuge. Fish. Bull., 98: 625-641.

Yoklavich, M.M.; Caillet, G.M.; Lea, R.N.; Greene, H.G.; Starr, R.; De Marignac, J.; and Field, J., 2002. Deepwater habitat and fish resources associated with the Big Creek Ecological Reserve. CalCOFI Report, 43: 120-140.

Yoklavich, M.M.; Grimes, C.B.; and Wakefield, W.W., 2003. Using laser line scan imaging technology to assess deepwater habitats in the Monterey Bay National Marine Sanctuary. Marine Technology Society Journal, 37: 18-25.

Zar, J.H., 1996, *Biostatistical Analysis*, 3rd Ed., Prentice Hall, 662pp.

APPENDIX A

Deep-Water Marine Benthic Habitat Classification Scheme

Explanation for Habitat Classification Code

(modified after Greene et al., 1999)

Habitat Classification Code

A habitat classification code, based on the deep-water habitat characterization scheme developed by Greene et al. (1999), was created to easily distinguish marine benthic habitats and to facilitate ease of use and queries within GIS (e.g., ArcView®, TNT Mips®, and ArcGIS®) and database (e.g., Microsoft Access® or Excel®) programs. The code is derived from several categories and can be subdivided based on the spatial scale of the data. The following categories apply directly to habitat interpretations determined from remote sensing imagery collected at the scale of 10s of kilometers to 1 meter: Megahabitat, Seafloor Induration, Meso/Macrohabitat, Modifier, Seafloor Slope, and Geologic Unit. Additional categories of Macro/Microhabitat and Seafloor Slope apply to areas at the scale of 10 meters to centimeters and are determined from video, still photos, or direct observations. These two components can be used in conjunction to define a habitat across spatial scales or separately for comparisons between large and small-scale habitat types. Categories are explained in detail below. Not all categories may be required or possible given the study objectives, data availability, or data quality. In these cases the categories used may be selected to best accommodate the needs of the user.

Explanation of Attribute Categories and their Use

Determined from Remote Sensing Imagery (for creation of large-scale habitat maps)

1) Megahabitat – This category is based on depth and general physiographic boundaries and is used to distinguish regions and features on a scale of 10s of kilometers to kilometers. Depth ranges listed for category attributes in the key are given as generalized examples. This category is listed first in the code and denoted with a capital letter.

2) Seafloor Induration – Seafloor induration refers to substrate hardness and is depicted by the second letter (a lower-case letter) in the code. Designations of hard, mixed, and soft substrate may be further subdivided into distinct sediment types, which are then listed immediately afterwards in parentheses either in alphabetical order or in order of relative abundance.

3) Meso/Macrohabitat – This distinction is related to the scale of the habitat and consists of seafloor features ranging from 1 kilometer to 1 meter in size. Meso/Macrohabitats are noted as the third letter (a lower-case letter) in the code. If necessary, several Meso/Macrohabitats can be included either alphabetically or in order of relative abundance and separated by a backslash.

4) Modifier – The fourth letter in the code, a modifier, is noted with a lower-case subscript letter or separated by an underline in some GIS programs (e.g., ArcView®). Modifiers describe the texture or lithology of the seafloor. If necessary, several modifiers can be included alphabetically or in order of relative abundance and separated by a backslash.

5) Seafloor Slope – The fifth category, represented by a number following the modifier subscript, denotes slope. Slope is typically calculated for a survey area from x-y-z multibeam data and category values can be modified based on characteristics of the study region.

6) Geologic Unit – When possible, the geologic unit is determined and listed subsequent to the habitat classification code in parentheses.

Determined from video, still photos, or direct observation (for designation of small-scale habitat types)

7) Macro/Microhabitat –Macro/Microhabitats are noted by the eighth letter in the code (or first letter, if used separately) and preceded by an asterisk. This category is subdivided between geologic (surrounded by parentheses) and biologic (surrounded by brackets) attributes. Dynamic segmentation can be used to plot macroscale habitat patches on Mega/Mesoscale habitat interpretations (Nasby 2000).

8) Seafloor Slope – The ninth category (or second category, if used separately), listed by a number denotes slope. Unlike the previous slope designation (#5), the clarity of this estimate can be made at smaller scales and groundtruthed or compared with category #5. Category values can be modified based on characteristics of the study region.

Habitat Key (Code)

Deep-Water Marine Benthic Habitat Classification Scheme

Key to Habitat Classification Code for Mapping and use with GIS programs

(modified after Greene et al., 1999)

Interpreted from remote sensing imagery for mapping purposes

Megahabitat – Use capital letters (based on depth and general physiographic boundaries; depth ranges approximate and specific to study area).

A = Aprons, continental rise, deep fans and bajadas (3000-5000 m)
B = Basin floors, Borderland types (floors at 1000-2500 m)
F = Flanks, continental slope, basin/island-atoll flanks (200-3000 m)
I = Inland seas, fiords (0-200 m)
P = Plains, abyssal (>5000 m)
R = Ridges, banks and seamounts (crests at 200-2500 m)
S = Shelf, continental and island shelves (0-200 m)

Seafloor Induration-Use lower-case letters (based on substrate hardness).

h = hard substrate, rock outcrop, relic beach rock or sediment pavement
m = mixed (hard & soft substrate)
s = soft substrate, sediment covered

Sediment types (for above indurations)-Use parentheses.
(b) = boulder

(c) = cobble
(g) = gravel
(h) = halimeda sediment, carbonate
(m) = mud, silt, clay
(p) = pebble
(s) = sand

Meso/Macrohabitat-Use lower-case letters (based on scale).

a = atoll
b = beach, relic
c = canyon
d = deformed, tilted and folded bedrock
e = exposure, bedrock
f = flats, floors
g = gully, channel
i = ice-formed feature or deposit, moraine, drop-stone depression
k = karst, solution pit, sink
l = landslide
m = mound, depression
n = enclosed waters, lagoon
o = overbank deposit (levee)
p = pinnacle (Note: Pinnacles are often difficult to distinguish from boulders. Therefore, these features may be used in conjunction [as (b)/p] to designate a meso/macrohabitat.
r = rill
s = scarp, cliff, fault or slump
t = terrace
w = sediment waves
y = delta, fan
$z_{\#}$ = zooxanthellae hosting structure, carbonate reef
1 = barrier reef
2 = fringing reef
3 = head, bommie
4 = patch reef

Modifier-Use lower-case subscript letters or underscore for GIS programs (textural and lithologic relationship).

$_a$ = anthropogenic (artificial reef/breakwall/shipwreck)
$_b$ = bimodal (conglomeratic, mixed [includes gravel, cobbles and pebbles])
$_c$ = consolidated sediment (includes claystone, mudstone, siltstone, sandstone, breccia, or conglomerate)
$_d$ = differentially eroded
$_f$ = fracture, joints-faulted
$_g$ = granite
$_h$ = hummocky, irregular relief
$_i$ = interface, lithologic contact
$_k$ = kelp

$_l$ = limestone or carbonate
$_m$ = massive sedimentary bedrock
$_o$ = outwash
$_p$ = pavement
$_r$ = ripples
$_s$ = scour (current or ice, direction noted)
$_u$ = unconsolidated sediment
$_v$ = volcanic rock

Seafloor Slope-Use category numbers. Typically calculated for survey area from x-y-z multibeam data.

1 Flat (0-1º)
2 Sloping (1-30º)
3 Steeply Sloping (30-60º)
4 Vertical (60-90º)
5 Overhang (> 90º)

Geologic Unit – When possible, the associated geologic unit is identified for each habitat type and follows the habitat designation in parentheses.

Examples: Shp_d1(Q/R)-Continental shelf megahabitat; flat, hard seafloor with pinnacles differentially eroded. Geologic unit = Quartenary/Recent.

Fhd_d2 (Tmm)-Continental slope megahabitat; sloping hard seafloor of deformed (tilted, faulted, folded), differentially eroded bedrock exposure forming overhangs and caves. Geologic unit = Tertiary Miocene Monterey Formation.

Determined from video, still photos, or direct observation.

Macro/Microhabitat – Preceeded by an asterisk. Use parentheses for geologic attributes, brackets for biologic attributes. Based on observed small-scale seafloor features.

Geologic attributes (note percent grain sizes when possible)
(b) = boulder
(c) = cobble
(d) = deformed, faulted, or folded
(e) = exposure, bedrock (sedimentary, igneous, or metamorphic)
(f) = fans
(g) = gravel
(h) = halimeda sediment, carbonate slates or mounds
(i) = interface
(j) = joints, cracks, and crevices
(m) = mud, silt, or clay
(p) = pebble
(q) = coquina (shell hash)
(r) = rubble

(s) = sand
(t) = terrace-like seafloor including sedimentary pavements
(w) = wall, scarp, or cliff

Biologic attributes
[a] = algae
[b] = bryozoans
[c] = corals
[d] = detritus, drift algae
[g] = gorgonians
[n] = anemones
[o] = other sessile organisms
[s] = sponges
[t] = tracks, trails, or trace fossils
[u] = unusual organisms, or chemosynthetic communities
[w] = worm tubes

Seafloor Slope-Use category numbers. Estimated from video, still photos, or direct observation.

1 Flat (0-1º)
2 Sloping (1-30º)
3 Steeply Sloping (30-60º)
4 Vertical (60-90°)
5 Overhang (90°+)

Examples: *(m)[w]1-Flat or nearly flat mud (100%) bottom with worm tubes.

*(s/c)1-Sand bottom (>50%) with cobbles. Flat or nearly flat with very.

*(h)[c]1-Coral reef on flat bottom with halimeda sediment.

Shp_d1(Q/R)*(m)[w]1C -*Large-scale habitat type:* Continental shelf megahabitat; flat, hard seafloor with pinnacles differentially eroded. Geologic unit = Quaternary/Recent. *Small-scale habitat type:* Flat or nearly flat mud (100%) bottom with worm tubes.

Geology of the Southwestern San Juan Islands, Washington

By: Janet E. Tilden
Moss Landing Marine Laboratories

Index Map

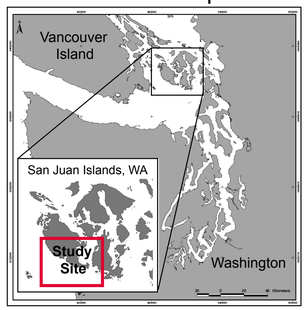

Inset A. Index map of the northwest Washington southwest British Columbia, Canada area. The study site is outlined in red.

Existing Data Coverage Map

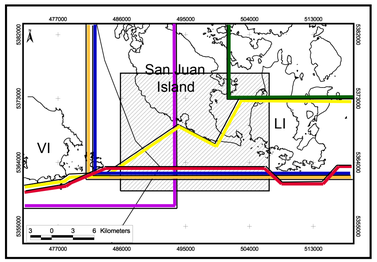

- Late Quaternary stratigraphy and seafloor geology of eastern Juan de Fuca Strait (Hewitt and Mosher, 2001)
- Digital Geology of Washington State (Schuster, J.E., 2000)
- Tertiary and Quaternary structure of the eastern Strait of Juan de Fuca (Johnson et al., 2000)
- Geologic Map of the Bellingham 1:100,000 Quadrangle (Lapen, T.J., 2000)
- Geology of the San Juan Islands (Brandon et al., 1988)
- Geology of Victoria, British Columbia, Canada 1:100,000 (Muller, 1983)

Inset B. Map showing existing data coverage of the study area. The black lines mark the data coverage borders, while the colored lines are drawn within the data coverage area. VI = Vancouver Island, LI = Lopez Island

Multibeam Bathymetry / Backscatter and ROV Data Coverage Map

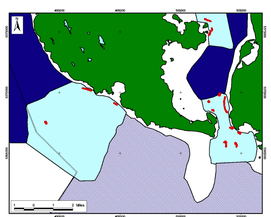

Inset C. Map showing where 2 m resolution Reson 8101 multibeam bathymetry data (light blue), 10 m resolution Simrad EM1002 multibeam bathymetry (dark blue), 0.2 m resolution Simrad EM1002 backscatter (dark blue pattern), and ROV video data (red dots) where collected.

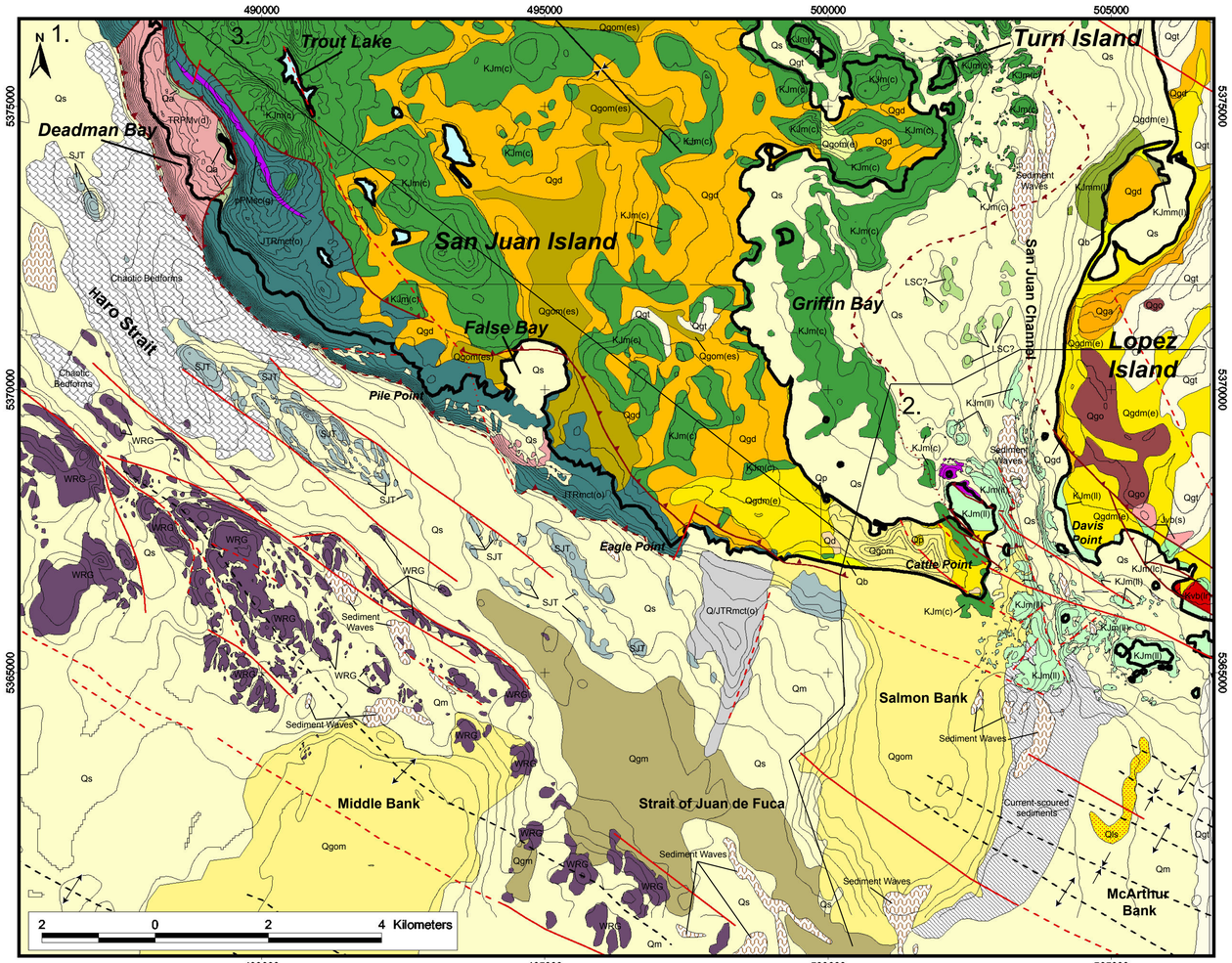

Scale: 1:50,000
Contour Interval = 20 meters
Projection: UTM, Zone 10
Datum: WGS 84

*Funding for this research was provided by the Dickinson Foundation, the Marine Ecosystem Health Program (MEHP) at the University of California, Davis; the Canadian Geological Survey; NOAA's National Undersea Research Program (NURP) West Coast and Polar Regions Undersea Research Center, University of Alaska, Fairbanks; the NOAA Coastal Services Center; and the Dr. Earl H. Myers & Ethel M. Myers Oceanographic and Marine Biology Trust.

LEGEND

*Symbology after Schuster (2000) and Muller (1983)

Qa	Alluvium
Qb	Beach deposits
Qd	Dune deposits
Qp	Peat deposits
Qga	Pleistocene advance continental glacial outwash
Qgd	Pleistocene continental glacial drift
Qgdm(e)	EVERSON GLACIOMARINE DRIFT
Qgm	Pleistocene glacial marine sediments
Qgo	Pleistocene continental glacial outwash
Qgom	Pleistocene glacial marine outwash
Qgom(e)	EVERSON glacial marine outwash
Qgt	Pleistocene continental glacial till
Qls	Quaternary Slump
Qs	Recent sediments
Kvb(r)	Richardson basalt flows, Lopez Island
KJm(c)	CONSTITUTION FORMATION, marine sedimentary rocks
KJm(lc)	LOPEZ STRUCTURAL COMPLEX, marine sedimentary rocks, Constitution Formation derivatives
KJm(ll)	LOPEZ STRUCTURAL COMPLEX, marine sedimentary rocks, Lummi Formation derivatives
KJmm(l)	LUMMI FORMATION, metagreywacke
LSC?	LOPEZ STRUCTURAL COMPLEX rocks?
Jvb(f)	FIDALGO OPHIOLITE, basalt flows
JTRmct(o)	ORCAS FORMATION, chert-rich marine sedimentary rocks
TRPMv(d)	DEADMAN BAY VOLCANICS, volcanic rocks
pPMsc(g)	GARRISON SCHIST, high-grade schist
pDit(t)	TURTLEBACK COMPLEX, intrusive rocks
SJT	San Juan thrust system rocks
Q/SJT	Recent sediments covering San Juan thrust system rocks
WRG	Wrangellia terrane rocks
	Current-scoured sediments
	Sediment Waves
	Chaotic Bedforms
	Fault; solid where well-defined, dashed where inferred, queried where questionably inferred, dotted where concealed
	Thrust fault; solid where well-defined, dashed where inferred, queried where questionably inferred, dotted where concealed
	Anticline; solid where well-defined, dashed where inferred
	Syncline; solid where well-defined, dashed where inferred
	Area boundaries 1., 2., and 3. for geologic discussion

Plate 1. Geologic map of the southwestern San Juan Islands, WA including information on surficial geology, bedrock geology, geohazards, and dynamic bedforms. Inset A provides an index map of the study area, Inset B illustrates the extents of existing geologic and geophysical data within the study area, and Inset C shows where Reson 8101, Simrad EM1002, and ROV video data were collected. A number of faults and all fold axes mapped offshore are modified from Johnson et al., 2000 (Refer to Figure 4.9 in text for a map of previously mapped geologic structures offshore). Onshore geologic structures were modified after Brandon et al. (1988) and Schuster, J.E. (2000).